

# **FLOW INSTABILITY AND ITS MITIGATION IN SUPERCRITICAL CO<sub>2</sub> BASED NATURAL CIRCULATION LOOPS: NUMERICAL AND EXPERIMENTAL STUDY**

Thesis

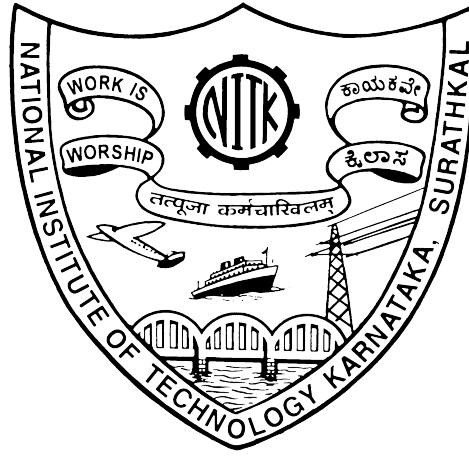
Submitted in partial fulfillment of the requirements of the degree of

**DOCTOR OF PHILOSOPHY**

by

**TABISH WAHIDI**

(158036 ME15F26)



DEPARTMENT OF MECHANICAL ENGINEERING  
NATIONAL INSTITUTE OF TECHNOLOGY KARNATAKA,  
SURATHKAL, MANGALORE - 575 025

DECEMBER, 2021

**FLOW INSTABILITY AND ITS MITIGATION IN SUPERCRITICAL  
CO<sub>2</sub> BASED NATURAL CIRCULATION LOOPS: NUMERICAL  
AND EXPERIMENTAL STUDY**

Thesis

Submitted in partial fulfillment of the requirements of the degree of

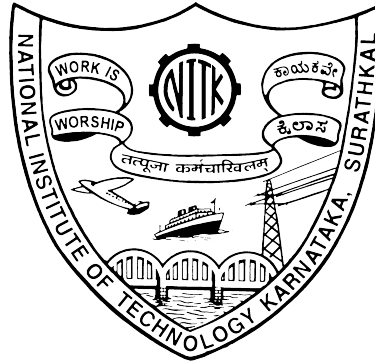
**DOCTOR OF PHILOSOPHY**

by

**TABISH WAHIDI**

(158036 ME15F26)

Under the guidance of  
**Dr. AJAY KUMAR YADAV**



DEPARTMENT OF MECHANICAL ENGINEERING  
NATIONAL INSTITUTE OF TECHNOLOGY KARNATAKA,  
SURATHKAL, MANGALORE - 575 025

DECEMBER, 2021

## DECLARATION

I hereby *declare* that the Research Thesis entitled “**Flow instability and its mitigation in supercritical CO<sub>2</sub> based natural circulation loops: Numerical and experimental study**” which is being submitted to the **National Institute of Technology Karnataka, Surathkal** in partial fulfillment of the requirements for the award of the **Doctor of Philosophy** in **Department of Mechanical Engineering** is a *bonafide report of the research work carried out by me*. The material contained in this Research Thesis has not been submitted to any University or Institution for the award of any degree.

TABISH WAHIDI  
158036 ME15F26  
Department of Mechanical Engineering  
NITK, Surathkal - 575 025  
(Signature with date)

Place: NITK-Surathkal

Date:





## C E R T I F I C A T E

This is to *certify* that the Research Thesis entitled “**Flow instability and its mitigation in supercritical CO<sub>2</sub> based natural circulation loops: Numerical and experimental study**” submitted by Tabish Wahidi (Register Number: 158036 ME15F26) as the record of research work carried out by him, *is accepted as the Research Thesis submission* in partial fulfillment of the requirements for the award of the degree of Doctor of Philosophy.

Dr. AJAY KUMAR YADAV

Assistant Professor

Research Supervisor

Department of Mechanical Engineering

NITK, Surathkal - 575 025

(Signature with date & Seal)

Chairman - DRPC

(Signature with date & Seal)



*DEDICATED TO*

**MY FAMILY MEMBERS  
WHOSE LOVE AND SUPPORT  
SUSTAINED ME THROUGHOUT**



## ACKNOWLEDGMENT

The journey of completing my PhD has been head over heels, with failures and successes. But amid all the lows, few people stood by me and kept motivating to step further. This thesis will be incomplete without expressing my gratitude towards all those who have been my strength and left an affirmative mark in this journey.

I would like to begin my warmest thanks and acknowledgment to my supervisor, **Dr. Ajay Kumar Yadav**, for his patience, guidance, and support. I have benefited greatly from his wealth of knowledge and meticulous editing. I am extremely grateful that he took me as a student and continued to have faith in me over the years that I will never forget. His brilliant, skillful supervision enriched this study higher than my expectation.

I am thankful to **Dr. Satyabodh M. Kulkarni**, Professor and Head, Department of Mechanical Engineering, for the support and providing facilities required to complete this research work successfully. Furthermore, I take this opportunity to acknowledge the former HODs, Mechanical engineering, **Dr. Gangadharan K.V., Dr. Narendranath S., and Dr. Shrikantha S. Rao**, for their support and encouragement. I would also wish to express my gratitude to my RPAC members, **Dr. Arumuga D. Perumal** and **Dr. Vishwanath K. P.**, for their extended discussions and valuable suggestions, which have contributed greatly to the improvement of the thesis.

A very special word of thanks goes to my father, **Sarware Islam**, and my mother, **Shahnaz Sarwer**, for their endless supports and unwavering belief in me. Mummy, thank you for making number of untold sacrifices for the entire family. Dady, you are a great inspiration to me; thank you for all of your love, and without you, I would not be the person I am today. Deepest thanks to my elder siblings, **Faisal Wahidi, Sharique Wahidi**, and their wives, who keep me grounded, remind me of what is important in life, and always supported my educational journey. Thank you to my younger siblings, **Nazish Wahidi** and sister **Amber**, for letting me be vulnerable about sharing my dark and damaged past and leaving such wonderful, heartfelt comments. My thanks are extended to my in-laws for their unconditional love with patience. Last but not least, my cousin **Ammar Wahidi** providing me with immediate assistance in any computer problems I encountered and taking care of my home in my absence. I hope that I have made all of them proud.

Special thanks to my wife and love of life, **Yusha Rahman**, for his continuous support, motivation, and understanding, especially when things went haywire. She has stood by me through all my travails, absences, fits of pique and impatience. She gave me support and help, discussed ideas, and prevented several wrong turns. But most of

all, thank you for being my best friend. I owe you everything.

Two persons deserve a very special word of gratitude: one is **Dr. Thippeswamy L. R.**, the other is **Mr. Srivatsa Thimmaiah**, they always given me a hand to deal with the practicalities of working in the research laboratory and offered me wise counsel at opportune times.

A warm word for my colleague and great friend **Shankar Kodate** always made me feel special and shared moments of deep anxiety and immense excitement. I would like to thank all my Ph.D. colleagues, Madagonda Biradar, Nidhul, Sangappa, Addisu, Anteneh, Vasista, Dr. Libin, Jagadish, Rudramoorthy, Jayashish Pandey, Kishore Babu, Mithun Kumar, Dr. Preveen T. R., Dr. Abdul Buradi, Ravi list seems to be endless.

Many others have been instrumental in this process. I would like to appreciate the generous assistance of B. Tech and M. Tech graduates Rajat A. C, Siva, Pranay, Dheeraj, Shambu, Pavan Karki, Abhay, and Anil roles at various stages in the completion of my work. Finally, I also want to thank Yogesh Suvarna and Late Ravi Anna, mess managers of my college, to ensure I never had to work with an empty stomach.

I am grateful to have had the privilege of attending the prestigious National Institute of Technology Karnataka. I am extremely grateful to the Mechanical Engineering department NITK, the faculty and the non-teaching staff for providing all the facilities for my research work.

I earnestly regret to numerous others whom I forget to cite. However, their contributions are also equally significant to me for completing my thesis successfully.

TABISH WAHIDI  
DECEMBER, 2021  
NITK, SURATHKAL

# ABSTRACT

A natural circulation loop (NCL) is a thermal energy transport system in which circulation solely occurs due to density gradient from a high-temperature source to a low-temperature sink without using any prime mover. Due to thermal imbalance in NCL, fluid flow oftenly subjects to instability in the form of oscillatory behaviour and flow reversal which may lead to catastrophic incidences. The underlying physics of instability for supercritical CO<sub>2</sub> based NCL is complex. Hence, numerical and experimental investigations are carried out for supercritical CO<sub>2</sub> based NCLs focus on the flow instability and its mitigation.

Three-dimensional computational fluid dynamics (CFD) simulation for supercritical CO<sub>2</sub> based NCL is carried out to explore the effects of pressure and heat inputs on instability and determine the possible cause of its occurrence. Investigation shows that for supercritical CO<sub>2</sub>, there is a threshold point that decides the nature of flow. A heat input lower than a threshold value causes repetitive-reversal flow, while at higher heat input, the flow changes to stable or unidirectional flow. With an increase in heat input, the system attains stability for a given operating pressure. In addition, a possible mechanism for continuous flow oscillation and measurement of instability with different pressure in unstable loops is also proposed.

The novelty of this investigation emphasizes the design of a modified Tesla type valve and its integration in the loop to assist the unidirectional flow of loop fluid, and in turn, reduces the instability. Results show that the use of a single modified Tesla valve leads to better stabilization for all supercritical pressures and heat inputs. It is also found that a loop with a single Tesla mitigates the temperature and velocity oscillations with a marginal reduction (8%) in the heat transfer performance. However, the use of a single modified Tesla type valve in NCL is not capable of mitigating the instability in the case of low heat inputs with operating pressures far away from the pseudocritical point.

NCL integrated with two modified Tesla type valves is used to promote the uni-

directional circulatory movement of loop fluid and to decrease the magnitude of instability. Results are obtained with supercritical CO<sub>2</sub> based twin Tesla-NCL and compared with regular-NCL and single Tesla NCL at different heat inputs and operating pressures. It is found that an increase in the number of Tesla valves, mitigates the instabilities in the NCL operated away from pseudo-critical region at lower heat inputs. However, the use of twin Tesla type valves in NCL drops the heat transfer capability by 15% compared to regular NCL.

To validate the simulation results and check the practical feasibility, an experimental setup of NCL integrated with a modified Tesla valve is designed and developed. Experiments are carried out to comprehend the instability in supercritical CO<sub>2</sub> based NCL. Experimental results show that the unidirectional fluid flow circulation can be achieved in the loop with the Tesla valve, which makes it an efficient technique to combat instability.

**Key words:** Natural circulation loop, Supercritical CO<sub>2</sub>, Instability, Heat Transfer, CFD, Tesla type valve.



# TABLE OF CONTENTS

<b>LIST OF TABLES</b>	<b>iv</b>
<b>LIST OF FIGURES</b>	<b>viii</b>
<b>LIST OF SYMBOLS</b>	<b>ix</b>
<b>1 Introduction</b>	<b>1</b>
1.1 Natural circulation loop . . . . .	1
1.2 Mechanism of NCL . . . . .	2
1.3 Different configurations of NCLs . . . . .	4
1.4 Advantages of NCL . . . . .	8
1.5 Disadvantages of NCL . . . . .	8
1.6 Selection of CO <sub>2</sub> as working fluid . . . . .	9
1.7 Instability in NCL . . . . .	12
1.8 Classification of instability . . . . .	14
1.8.1 Propagation method . . . . .	15
1.8.2 Nature of the oscillations . . . . .	15
1.8.3 Flow direction . . . . .	16
1.9 Tesla valve . . . . .	17
1.10 Structure of the thesis . . . . .	19
<b>2 Literature Review</b>	<b>21</b>
2.1 Natural circulation loop . . . . .	21
2.2 Instability in various NCLs . . . . .	23
2.3 Instability in rectangular NCL . . . . .	26
2.4 Instability in supercritical CO <sub>2</sub> based NCL . . . . .	31
2.5 Mitigation techniques for instability . . . . .	33
2.6 Tesla valve applications . . . . .	36
2.7 Research gap . . . . .	37
2.8 Thesis objectives . . . . .	38
<b>3 Supercritical CO<sub>2</sub> Flow Instability in Natural Circulation Loop</b>	<b>39</b>
3.1 Physical Model of NCL . . . . .	39
3.2 Mathematical formulations . . . . .	43
3.3 Simulation detail . . . . .	47

3.4	Validation	49
3.5	Results and discussion	50
3.5.1	Effect of heat input	51
3.5.2	Temperature variation	56
3.5.3	Effect of operating pressure	58
3.5.4	Nusselt number	63
3.6	Summary	63
<b>4</b>	<b>Stability Enhancement of Supercritical CO<sub>2</sub> based Natural Circulation Loop using a Modified Tesla Valve</b>	<b>65</b>
4.1	Physical model of NCL	65
4.2	Modified Tesla valve for NCL	67
4.3	Mathematical Formulation	71
4.4	Simulation detail	73
4.5	Grid independence study	75
4.6	Validation	75
4.7	Results and discussion	77
4.7.1	Transient variation of loop fluid temperature	77
4.7.2	Transient variation of fluid flow	79
4.7.3	Parametric study on heat input and loop operating pressure	83
4.7.4	Nusselt number variation	87
4.8	Summary	88
<b>5</b>	<b>Instability Mitigation by Integrating Twin Tesla Type Valves in Supercritical Carbon dioxide-based Natural Circulation Loop</b>	<b>89</b>
5.1	Twin Tesla model design for NCL	89
5.2	Simulation details and mathematical formulation	91
5.3	Grid independence study	91
5.4	Validation	93
5.5	Results and discussion	94
5.5.1	Feasibility of twin Tesla in NCL	94
5.5.2	Flow behaviour	96
5.5.3	Transient variation of temperature	100
5.5.4	Transient variation of mass flow rate	101
5.5.5	Effect of operating pressure on flow instability	105
5.5.6	Nusselt number	106
5.6	Summary	107

<b>6</b>	<b>An Experimental Study with Supercritical CO<sub>2</sub> based Natural Circulation Loops</b>	<b>109</b>
6.1	Design of regular natural circulation loop setup . . . . .	109
6.2	Design of Tesla natural circulation loop setup . . . . .	112
6.3	Fabrication of modified Tesla valve . . . . .	115
6.4	Data collection and instrumentation for R-NCL and T-NCL . . . . .	117
6.5	Experimental procedure . . . . .	120
6.6	Uncertainty analysis . . . . .	121
6.7	Results and discussion . . . . .	123
6.7.1	Mass flow rate variations . . . . .	123
6.7.2	Temperature variations . . . . .	127
6.7.3	Pressure variation . . . . .	130
6.8	Validation . . . . .	132
6.9	Summary . . . . .	134
<b>7</b>	<b>Conclusions and Scope of Future Work</b>	<b>135</b>
7.1	Conclusions . . . . .	135
7.1.1	Supercritical CO <sub>2</sub> flow instability in natural circulation loop . . . . .	135
7.1.2	Instability mitigation by integrating modified Tesla type valve . . . . .	136
7.1.3	Instability mitigation by integrating twin Tesla type valves in NCL . . . . .	136
7.1.4	Experimental investigation . . . . .	137
7.2	Scope for future work . . . . .	138
	<b>REFERENCES</b>	<b>139</b>
	<b>List of Publications</b>	<b>155</b>



## List of Tables

1.1	Comparison of properties for different secondary fluids. . . . .	10
3.1	Geometrical specification of loop used in present study. . . . .	40
4.1	Geometrical specification of loop used in present study . . . . .	67
4.2	Geometrical parameters of Tesla valve used in the study. . . . .	69
5.1	Repetitive oscillation or unidirectional start time for regular natural circulation (R-NCL) and twin Tesla circulation loop (Twin Tesla-NCL). . .	104
6.1	The geometrical dimensions of R-NCL. . . . .	111
6.2	The geometrical dimensions of T-NCL. . . . .	114
6.3	Equipment details used for experimentation. . . . .	119



## List of Figures

1.1	Schematic of natural circulation loop. . . . .	3
1.2	Classification of NCL (Vijayan and Nayak 2010). . . . .	5
1.3	Various geometrical configurations of natural circulation loop (Vijayan and Nayak 2010). . . . .	7
1.4	Phase diagram (NIST 2013). . . . .	11
1.5	A transient flow behaviour in NCL. . . . .	13
1.6	Types of instability (Vijayan and Nayak 2005). . . . .	13
1.7	Nature of oscillation (a) Uni-direction flow (b) Bi-directional flow (c) Chaotic oscillations with flow reversal. . . . .	16
1.8	Cross-section of Tesla valve (Nikola 1920). . . . .	17
1.9	Geometry of Tesla valve (Truong and Nguyen 2003). . . . .	18
1.10	Plot of the single-phase (a) diodicity and (b) Pressure difference against the Reynolds number (Vries et al. 2017). . . . .	19
2.1	Natural circulation loop in nuclear power plants. . . . .	22
3.1	Schematic of NCL analyzed in the present study. . . . .	40
3.2	Mesh generated at cross section of a heat exchanger. . . . .	42
3.3	Grid independence study at 90 bar and heat exchanger inlet temperature of 305 K for 1500 W heat input. . . . .	42
3.4	Time independent study. . . . .	43
3.5	Validation of the obtained result with correlations (a) $\ln Re$ and $\ln(Gr_{md}/L_t)$ (b) friction factor with Reynolds number. . . . .	50
3.6	Variations of mass flow rate for different operating pressures of 80, 90 and 100 bar for supercritical CO <sub>2</sub> based natural circulation loop for different heat inputs (a) 250 W (b) 500 W (c) 1000 W (d) 1500 W (e) 2000 W and (f) 2500 W. . . . .	52
3.7	Mass flow rate variation at (a) 500 W and (b) 2000 W and density variation at (c) 500 W and (d) 2000 W heat input at 90 bar. . . . .	55
3.8	Temperature contour in a central vertical plane at different time instances for 500 W at operating pressure of 90 bar. . . . .	56
3.9	Temperature variation at (a) 500 W and (b) 2000 W and density variation at (c) 500 W and (d) 2000 W heat input at 90 bar. . . . .	58

3.10	Transient Temperature variation for various operating pressures for 500 W. . . . .	59
3.11	Temperature contours at 500 W at various operating pressures of (a) 80 bar, (b) 90 bar and (c) 100 bar at different time intervals. . . . .	60
3.12	Variation of $C_p$ with temperature for various operating pressures (NIST 2013). . . . .	61
3.13	Measure of Instability. . . . .	62
3.14	Variation of Nusselt number at different heat inputs and operating pressures. . . . .	63
4.1	Schematic of (a) Regular natural circulation loop (scCO <sub>2</sub> R-NCL) (b) Tesla valve natural circulation loop (scCO <sub>2</sub> T-NCL). . . . .	66
4.2	(a) Design of scaled model of Tesla valve Vries et al. (2017) used in present study (dimensions are given in Table 4.2). (b) Forward and reverse flow directions are indicated and channel junctions 1 and 2 (J1, J2) are shown by black region. Inlet and outlet for the valve are indicated with I/O. . . . .	68
4.3	Diodicity of Tesla valve design for supercritical CO <sub>2</sub> at 90 bar with different Reynolds numbers. . . . .	68
4.4	Streamlines of the flow field in Tesla valve design for a Reynolds number of 100,000 (a) Forward flow (b) Reverse flow. . . . .	70
4.5	Pressure contour in Tesla valve design for a Reynolds number of 100,000 (a) Forward flow (b) Reverse flow. . . . .	70
4.6	Grid independence study with CO <sub>2</sub> at 90 bar and a sink temperature of 305 K for Regular natural circulation loop (scCO <sub>2</sub> R-NCL) and Tesla natural circulation loop (scCO <sub>2</sub> T-NCL) . . . . .	75
4.7	Validation plot of obtained results with steady-state Reynolds number $Re_{ss}$ and modified Grashof number ( $Gr_{md}/L_t$ ) correlation for supercritical CO <sub>2</sub> flow. . . . .	76
4.8	Transient variation of temperature at 90 bar of CO <sub>2</sub> for Regular natural circulation loop (scCO <sub>2</sub> R-NCL) and Tesla natural circulation loop (scCO <sub>2</sub> T-NCL) with different heat inputs (a) 500 W, (b) 750 W, (c) 1800 W and (d) 2000 W. . . . .	77
4.9	Velocity variation at 90 bar of CO <sub>2</sub> for Regular natural circulation loop (scCO <sub>2</sub> R-NCL) and Tesla natural circulation loop (scCO <sub>2</sub> T-NCL) with different heat inputs (a) 500 W and (b) 1800 W. . . . .	79



4.10	Temperature distribution for supercritical CO <sub>2</sub> based regular natural circulation loop for different time steps at 90 bar and 500 W (a) 200 s, (b) 203 s, (c) 204 s and (d) 207 s. . . . .	81
4.11	Temperature distribution in the 500 W at 90 bar of CO <sub>2</sub> for Tesla natural circulation loop (scCO <sub>2</sub> T-NCL) at different time steps from 195 s to 205 s. 82	82
4.12	Transient variation of velocity with a different operating pressure of CO <sub>2</sub> for regular natural circulation loop (scCO <sub>2</sub> R-NCL) and Tesla natural circulation (scCO <sub>2</sub> T-NCL) loop at different heat inputs (a) 500 W scCO <sub>2</sub> R-NCL, (b) 500 W scCO <sub>2</sub> T-NCL, (c) 750 W scCO <sub>2</sub> R-NCL, (d) 750 W scCO <sub>2</sub> T-NCL, (e) 1200 W scCO <sub>2</sub> R-NCL, (f) 1200 W scCO <sub>2</sub> T-NCL, (g) 1800 W scCO <sub>2</sub> R-NCL, (h) 1800 W scCO <sub>2</sub> T-NCL (i) 2000 W scCO <sub>2</sub> R-NCL and (j) 2000 W scCO <sub>2</sub> T-NCL. . . . .	86
4.13	Variation of Nusselt number ( $Nu$ ) with different heat inputs at 90 bar for Regular natural circulation loop (scCO <sub>2</sub> R-NCL) and Tesla natural circulation loop (scCO <sub>2</sub> T-NCL). . . . .	87
5.1	Schematic of (a) Regular natural circulation loop (R-NCL) (b) Twin Tesla valve natural circulation loop (Twin Tesla-NCL). . . . .	90
5.2	Grid independence study for supercritical CO <sub>2</sub> based Regular natural circulation loop and Twin Tesla natural circulation loop at 90 bar and sink temperature of 305 K at 1000 W heat input. . . . .	92
5.3	Mesh at heater section. . . . .	93
5.4	Validation plot of obtained results with steady-state Reynolds number ( $Re_{ss}$ ) and modified Grashof number ( $Gr_m d/L_t$ ) correlation for supercritical CO <sub>2</sub> flow. . . . .	94
5.5	Transient variations of (a) velocity at 90 bar for a heat input of 500 W (b) mass flow rate at 100 bar for heat input of 500 W for R-NCL, T-NCL and Twin Tesla-NCL. . . . .	96
5.6	Variations of (a) velocity and (b) temperature at 100 bar at a heat input of 500 W for R-NCL and twin Tesla-NCL . . . . .	97
5.7	Velocity and pressure variation oscillations at 100 bar at a heat input of 500 W for (a) R-NCL and (b) Twin Tesla NCL. . . . .	99
5.8	Variation of temperature at 100 bar for R-NCL and twin Tesla NCL cases with different heat fluxes of (a) 500 W, (b) 1000 W, (c) 1500 W and (d) 2000 W . . . . .	101

5.9	Mass flow rate of CO <sub>2</sub> for R-NCL and twin Tesla-NCL cases at 100 bar with different heat inputs of (a) 500 W, (b) 750 W, (c) 1000 W, (d) 1200 W, (e) 1500 W, and (f) 2000 W. . . . .	103
5.10	Variation of mass flow rate with different operating pressure at different heat inputs of (a) 500 W, (b) 1000 W, (c) 1500 W, and (d) 2000 W for twin Tesla NCL. . . . .	105
5.11	Variation of Nusselt number (Nu) with different heat inputs at 90 bar of supercritical CO <sub>2</sub> for regular natural circulation loop (R-NCL), single Tesla NCL and twin Tesla NCL (twin Tesla NCL). . . . .	106
6.1	Schematic of the regular NCL (R-NCL) with instruments used in the experiment. . . . .	109
6.2	Design of fabricated regular natural circulation loop. . . . .	110
6.3	Photographic view of the experimental setup (a) Without insulation and (b) With one layer insulation (asbestos rope). . . . .	112
6.4	Schematic of the Tesla NCL with heater and heat exchanger. . . . .	113
6.5	Design of fabricated Tesla natural circulation loop. . . . .	113
6.6	(a) Photographic view of the experimental setup (b) Modified Tesla valve inner view. . . . .	114
6.7	Photographic view of modified Tesla valve. . . . .	116
6.8	Equipment used for test facility (a) Rotameter (b) Safety valve (c) Differential Pressure transducer (d) Dimmerstat (e) Thermocouple. . . . .	118
6.9	Equipment used for test facility (a) Thermostatic bath (b) Data acquisition system (c) Vacuum pump (d) Mass flow meter. . . . .	118
6.10	Experimental setup of regular natural circulation loop. . . . .	119
6.11	Experimental setup of Tesla natural circulation loop. . . . .	120
6.12	Mass flow rate variation at 90 bar with different heat inputs at (a) 250 W, (b) 500 W, (c) 750 W and (d) 1000 W. . . . .	126
6.13	Variation of temperature at 90 bar for R-NCL and T-NCL cases with different heat inputs at (a) 250 W, (b) 500 W, (c) 750 W and (d) 1000 W. . . . .	129
6.14	Variation of differential pressure across heater at 90 bar for R-NCL and T-NCL cases with different heat inputs at (a) 250 W, (b) 500 W, (c) 750 W and (d) 1000 W. . . . .	131
6.15	Validation of simulation data with experimental results and available correlation. . . . .	132
6.16	Validation of simulation data with experimental results in terms of mass flow rate. . . . .	134

## LIST OF SYMBOLS

### Acronyms

$\bar{h}$	Heat transfer coefficient, W/m <sup>2</sup> .K
$A$	Area, m <sup>2</sup>
$C_p$	Specific heat at constant pressure, J/kg.K
$d$	diameter, m
$D_H$	Hydrullic diameter, m
$g$	accelaration due to gravity, m/s <sup>2</sup>
$h$	Enthalpy, J/kg
$m$	Mass flow rate, kg/m <sup>2</sup>
$P$	Pressure, Pa
$P_c$	Critical pressure, MPa
$Pr$	Prandtl number, $Pr = \frac{\mu C_p}{\lambda}$
$Q$	Heat input, W
$R$	Hydraulic resistance
$Re$	Reynolds number, $Re = \frac{\rho V d}{\mu}$
$T$	Temperature, K
$t$	time, s
$T_c$	Critical temperature, °C
$u$	Velocity in X- direction, m/s
$V$	Velocity, m/s
$v$	Velocity in Y- direction, m/s
$h_L$	Local heat transfer coefficient, W/m <sup>2</sup> .K

GWP	Global warming potential
ODP	Ozone depletion potential
scCO <sub>2</sub>	supercritical carbon-dioxide.

## **Greek Symbols**

$\beta$	Volume expansion coefficient, 1/K
$\kappa$	Turbulent Kinetic energy, m <sup>2</sup> /s <sup>2</sup>
$\lambda$	Thermal conductivity, W/m.K
$\mu_T$	Turbulent viscosity, Pa.s
$\mu$	Viscosity, Pa.s
$\rho_r$	local density along the radial direction.
$\rho$	Density, kg/m <sup>3</sup>
$\varepsilon$	Turbulent Kinetic energy dissipation rate, m <sup>2</sup> /s <sup>3</sup>
$\varphi$	Viscous dissipation function, W/ m <sup>3</sup>
$f$	frequency, 1/s
$G$	Rate of generation of turbulent kinetic energy, kg/m.s <sup>3</sup>

## **Subscripts**

$r$	radial direction
$ss$	steady state

# CHAPTER 1

## Introduction

Many nuclear disasters happened in the past few years, such as the Windscale fire accident (United Kingdom, 1957), Three Mile Island accident (USA, 1968), Chernobyl disaster (Ukrainian SSR, 1986) and Fukushima Daiichi nuclear disaster (Japan, 2011) attracted the attention of many researchers to find an effective solution. All these disasters are due to the malfunctioning of active cooling systems, which compelled the researcher to hunt for a new reliable and passive cooling technique to keep the system safe. The absence of moving components drastically reduces the probability of a failure in the removal of heat from the source and becomes a desirable option to minimize the such damages. This is the main reason for preferring natural convection over forced convection in power plants, in which safety is a primary concern. This study is carried out on natural circulation loop to understand the transient flow behavior and heat transfer capability.

### 1.1 Natural circulation loop

Convective heat transfer is the study of heat transport phenomena affected by the flow of fluids. In general, convection heat transfer deals with thermal interaction between a surface and an adjacent moving fluid. Convection also includes the study of thermal interaction between fluids. The convection heat transfer is classified into two major categories (i) forced convection and (ii) natural convection. When convection takes place inside a close circuit/loop, then it is called circulation. In a forced circulation, fluid motion is generated mechanically through a fan, blower, nozzle, pump/compressor etc. It has better effectiveness but requires additional cost for heat transfer. While in natural circulation, heat is transferred from lower altitude to higher altitude by the circulation of fluid due to the buoyancy effect caused by temper-

ature gradient. A natural circulation loop (NCL) is a simple and veracious heat transfer device that does not require any moving components like pumps and compressors. To enhance circulation rate and establish a thermal gradient in the NCL system, a heat source is kept below, and the heat sink is located at a higher elevation. The fluid absorbs heat from the source, becomes lighter and rises to the sink where it gets cooled, becomes heavier and moves downward, thus establishing a circulation in the loop. Due to the absence of moving/rotating parts to generate the motive force for flow, i.e., its passive nature makes it less prone to failures, reducing the maintenance and operating costs. In NCLs, flow can continue indefinitely if the loop's integrity is maintained and as long as the heat source and heat sink are maintained at distinct temperatures. Due to its simplicity, passiveness and intrinsic safety, it is employed in many applications like solar heater (Yamaguchi et al. 2010), geothermal process (Kreitlow et al. 1978), turbine blades cooling (Greif 1988), electronic components cooling (Chauhan and Kandlikar 2019; Samba et al. 2013), and nuclear reactor cooling systems (Chatoorgoon et al. 2005).

## 1.2 Mechanism of NCL

To exemplify the basic mechanism of NCL, Fig. 1.1 shows a schematic of rectangular NCL consisting of a heater as a source, two adiabatic vertical legs and a cold heat exchanger (CHX) as a sink. The fluid inside the closed-loop is heated at the heater with constant heat input and is cooled sensibly by rejecting heat to the external fluid (water) in the CHX. In NCL, due to continuous heating of the fluid at the heater, the fluid becomes lighter and moves into one of the vertical leg. Accelerated fluid enters the sink and rejects heat, becomes heavier and fall downwards due to gravity. Due to continuous heating/cooling at the heater and cooler surface, the whole cycle repeats. Continuation of this entire process leads to the transfer of thermal energy in the loop. Under steady conditions, let us consider flow is in a clockwise direction. The hot fluid vertical riser leg density with the upward flow is  $\rho_h$  and  $\rho_c$  to the cold fluid in the other

vertical downcomer leg with the downward flow. Now, equations 1.1 and 1.2 can be used to calculate the hydrostatic pressure and at “a” and “b” located near the heater section.

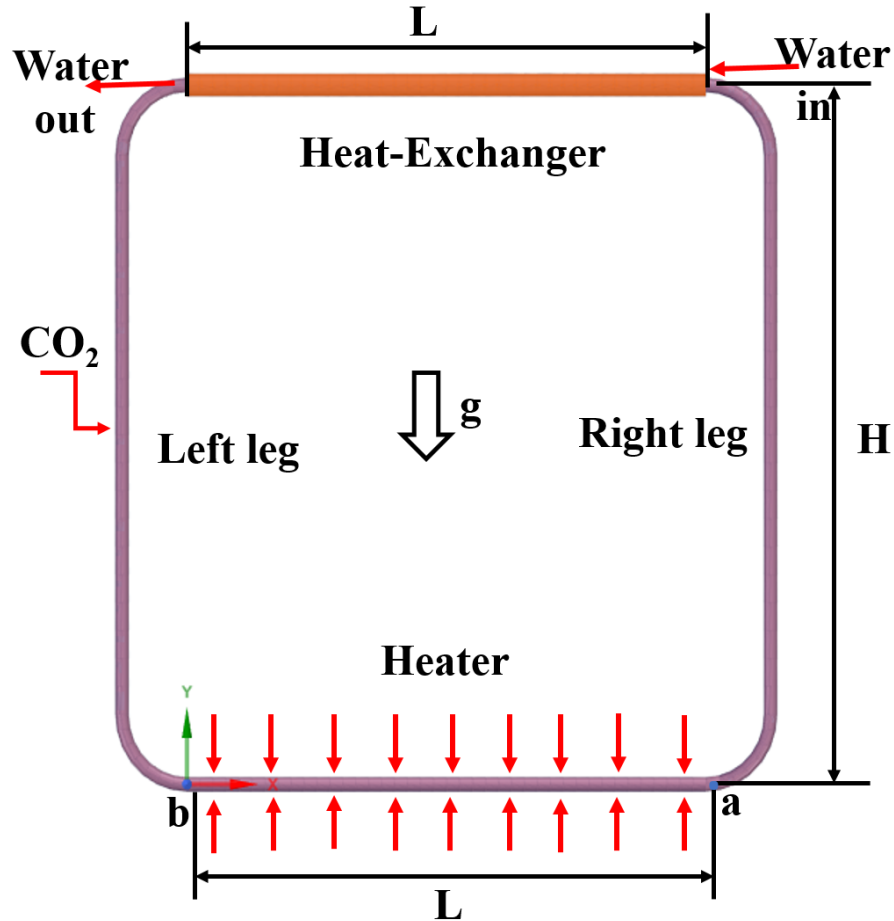


Figure 1.1: Schematic of natural circulation loop.

$$P_a = \rho_c g H \quad (1.1)$$

$$P_b = \rho_h g H \quad (1.2)$$

Where, H is the loop height, and g is the acceleration due to gravity. Since,  $\rho_c > \rho_h$  it lead to a pressure difference between ( $P_a > P_b$ ) which causes loop fluid to flow. At steady-state, the driving pressure difference created by the thermal expansion of working fluid is balanced by the frictional pressure difference, thus providing a basis

for estimating the induced flow.

$$(\rho_c - \rho_h) gH = \frac{Rm^2}{2\rho A^2} \quad (1.3)$$

The hydraulic resistance  $R$  is given by

$$R = \sum_{i=1}^N \frac{f_i L_i}{D_i} + K_i \quad (1.4)$$

Where  $f_i$ ,  $L_i$ ,  $D_i$  and  $K_i$  are respectively the friction coefficient, the length, the diameter and the loss coefficient of the  $i^{th}$  section of the loop. Equation 1.3 can be rearranged as

$$m = \sqrt{\frac{2\rho A^2 (\rho_c - \rho_h) gH}{R}} \quad (1.5)$$

Hence, the above equation 1.5 helps in calculating the induced driving pressure difference. It is noted that the flow rate is enhanced by increasing the loop height and the density difference between the two vertical legs. It also gets improved by increasing the loop flow area, reducing the hydraulic resistance, and decreasing the opposing frictional pressure gradient.

### 1.3 Different configurations of NCLs

A classification of NCLs often helps us to choose the most suitable configuration for the required application. However, it is laborious and tiring work to have an elaborated discussion on the different configurations of each of the NCLs. Hence, in the present section, an effort has been made to mention some of the most significant types of NCLs and their associated configurations. Fig. 1.2 shows the detailed description of various configurations of NCLs based on its working fluid, surrounding interaction, shapes, inventory, number of channels and body force.



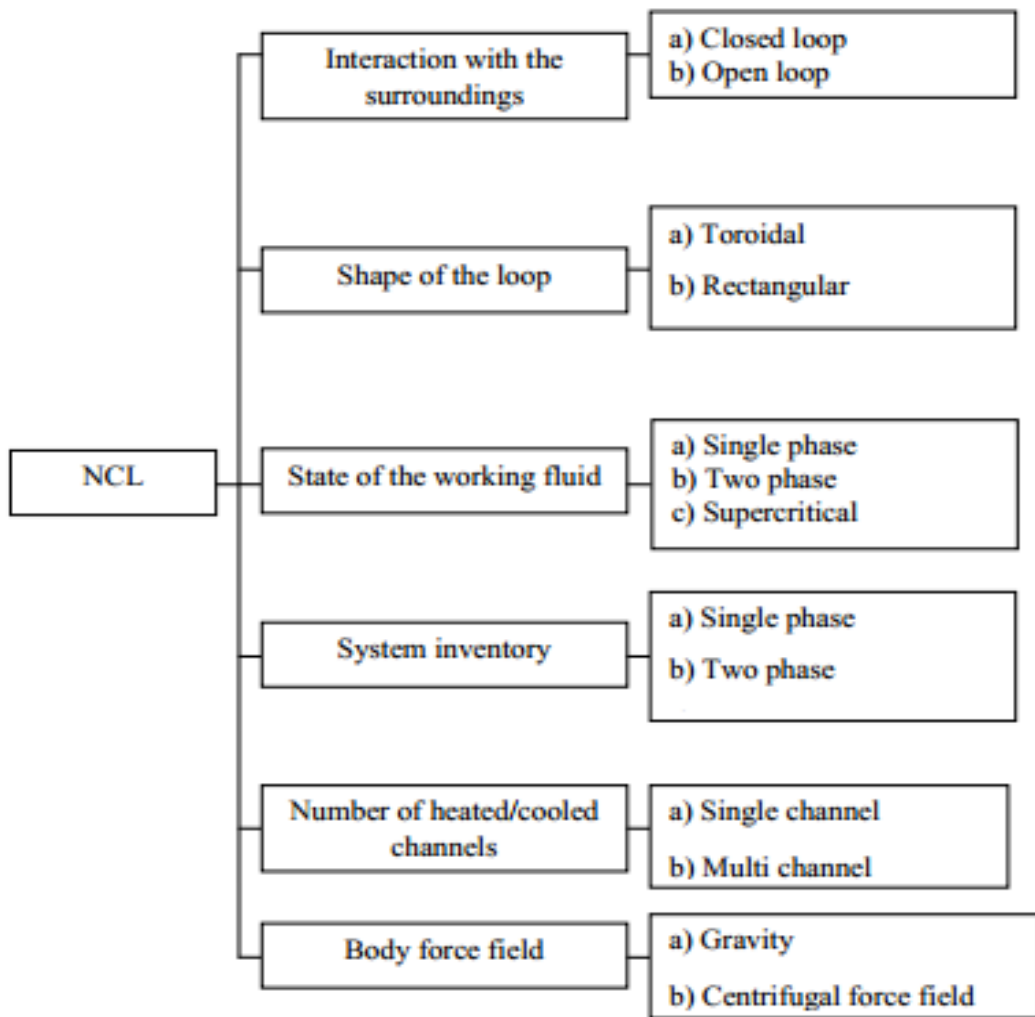
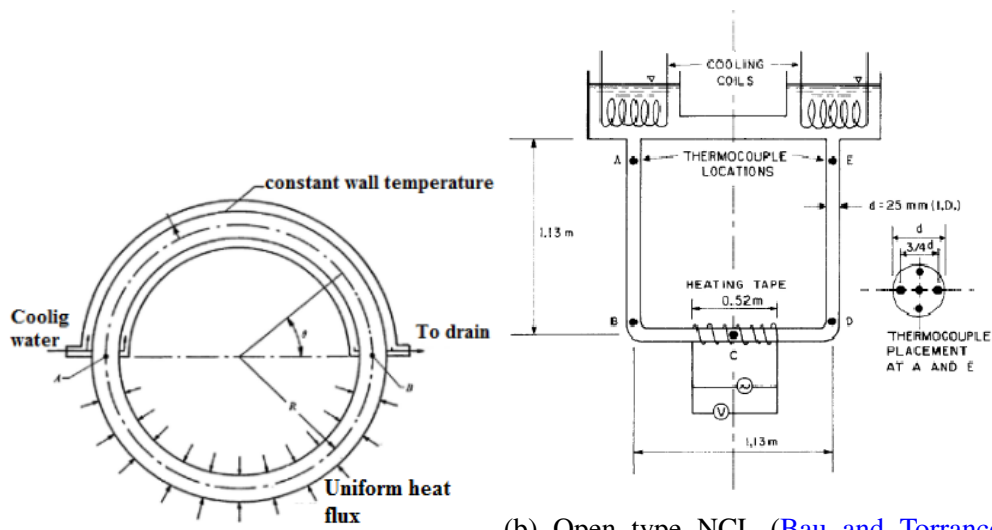


Figure 1.2: Classification of NCL (Vijayan and Nayak 2010).

Depending on the application in various engineering fields, NCL configurations used for theoretical studies or experimental studies are shown in Fig. 1.3. Based on the loop shape, NCLs are classified as toroidal, rectangular, square, U-loop, figure-of-eight, etc. Industrial NCLs are quite complex in geometry and challenging to do theoretical and computational modeling. While simple-shaped loops have contributed significantly to improve our understanding of the natural circulation process. The vertical open U-loop has been studied for instability behaviour (Welander 1967), and the toroidal loop has been extensively studied because of its simplicity. Stability characteristics of simple rectangular loops have been studied extensively theoretically (Keller 1966; Chen

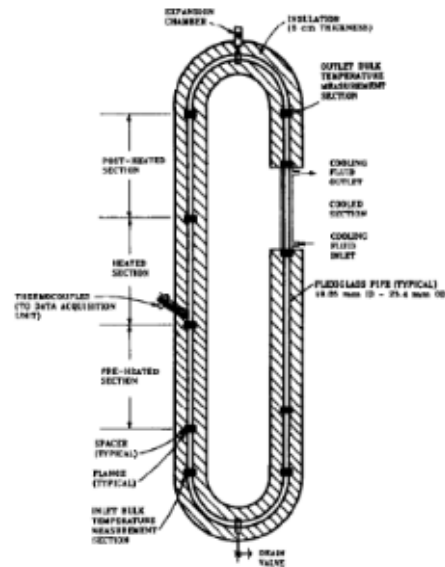
et al. 2013c; Yadav et al. 2014) and experimentally (Vijayan et al. 2007; Misale 2016). Sharma et al. (2013) investigated the NCL fluid flow and instability phenomena in a figure-of-eight loop. However, it is a genuinely arduous job to discuss and elaborate on each classification of NCL with available within the scope of a few pages.



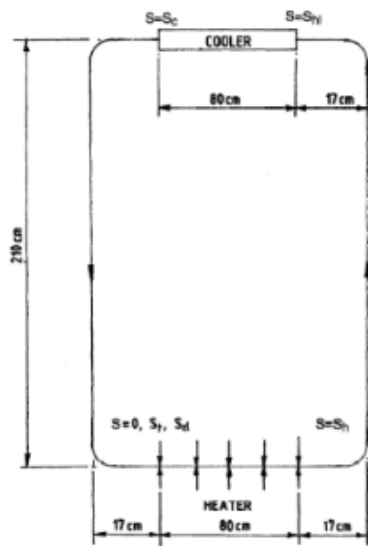
(a) Toroidal NCL (Creveling et al. 1975) (b) Open type NCL (Bau and Torrance 1981)



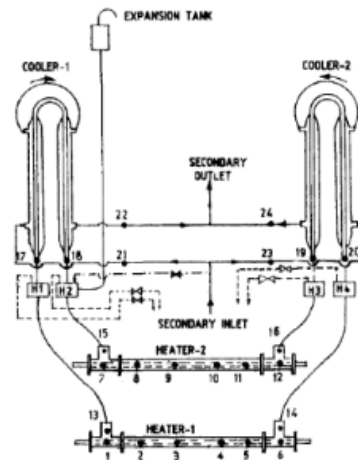
(c) Rectangular NCL (Welander 1967)



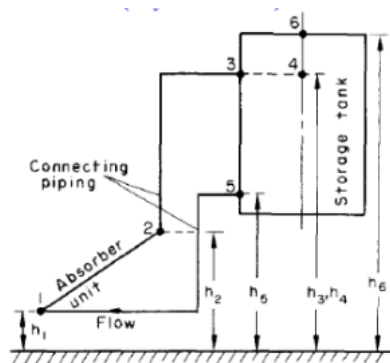
(d) Semi rectangular NCL (Bernier and Baliga 1992)



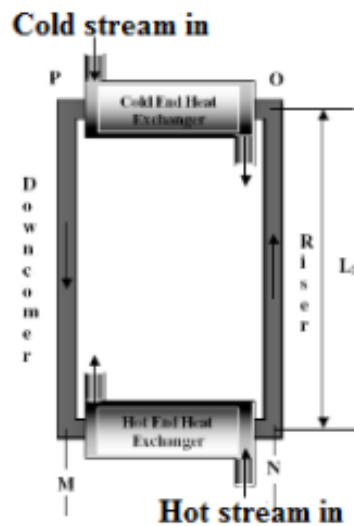
(e) Closed type NCL (Nayak et al. 1995)



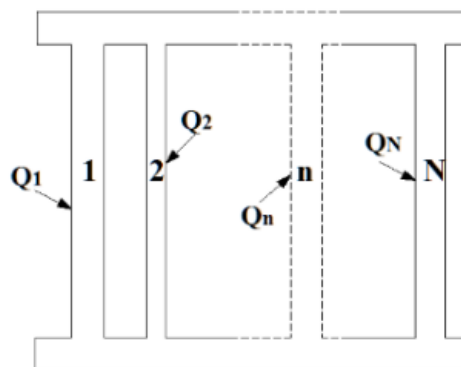
(f) Figure of eight loop (Vijayan and Date 1992)



(g) Typical solar heating NCL (Ong 1974)



(h) Rectangular NCL with end heat-exchanger (Rao et al. 2005)



(i) Multiple path thermosyphon (Chato 1963)

Figure 1.3: Various geometrical configurations of natural circulation loop (Vijayan and Nayak 2010).

#### 1.4 Advantages of NCL

- a. **Elimination of pumps:** The elimination of active power supplies and pumps can significantly simplify the construction, operation and maintenance of the system. In addition, eliminating the primary circulating pumps reduces capital, operating, maintenance costs and ensures safety.
- b. **Better flow distribution:** Another advantage is that the flow distribution in the parallel channel is much more uniform in the natural circulation system. However, the use of pumps causes mal-distribution of pressure in the headers leading to the nonuniform flow in the parallel channels. Operating experience with fossil-fueled natural circulation boilers (NCBs) suggests that the problem is eliminated or an order of magnitude is less than the pump-assisted circulation systems.
- c. **Safety aspects:** NCL is based on a natural physical law like gravity which is not expected to fail. As a result, the reliability of such systems is expected to be enhanced. In contrast, fluid-moving machineries, such as pumps/compressors, are prone to mechanical and external power supply failure.
- d. **Flow features:** In a pump-driven two-phase circulation system, the flow decreases with an increase in power, whereas the flow increases with power in natural circulations.
- e. **Simplicity:** Simplicity is the primary advantage of a natural circulation loop. Elimination of the pump makes it simpler and more reliable. To minimize pressure losses and enhance flow rates, designers of NCLs tend to eliminate all unnecessary pipe bends, elbows, etc. The result is a system with a simple piping layout that can be factory fabricated with reasonable quality assurance.

#### 1.5 Disadvantages of NCL

- a. **Low driving head:** The primary disadvantage of the natural circulation system is that the driving head is low. Therefore, to increase the flow rate at fixed power

would require either an increase in the loop height or a decrease in the loop resistance, either of which might increase plant costs. While for pump assisted flow, the required driving head can be obtained with a higher capacity pump without affecting the rest of the loop.

- b. **Low mass flux:** In general, the mass flux in the a natural circulation loop is low. Since the driving force is very low, the consequent use of larger diameter pipes results in lower mass flux in NCL systems than pumped circulation systems. At low mass flux, the Reynolds number is smaller, which lowers the heat transfer coefficient compared to forced circulation.
- c. **Instability effects:** The non-linear nature and its small driving force of the NCL, intrinsically make the natural circulation systems more unpredictable than the forced circulation systems. NCL shows instability in the form of flow oscillation, chaotic non-linear dynamic behaviour, and a flow reversal. It is undesirable, as it creates potent vibration on mechanical parts and also abates the system performance.
- d. **Low-pressure low-flow regime:** In NCLs, the flow rate is a strong function of heating power and system pressure. Also, the flow is stagnant during the initial startup in NCLs and where validated thermal-hydraulic relationships are not readily available. So, NCL designs might need an assessment of the applicability of the thermal-hydraulic relationships.

## 1.6 Selection of CO<sub>2</sub> as working fluid

Environmental pollution due to energy demand is an appealing aspect for the researcher to expand their investigation to enhance the efficiency of the system and also to find an eco-friendly energy resource. The environmentally benign nature of CO<sub>2</sub> (GWP =1, ODP =0) made it one of the most popular secondary fluid in recent years, and its use in various heating/cooling systems reduces the amount of greenhouse gases in the at-

mosphere. The admirable thermophysical properties of CO<sub>2</sub> as a working fluid offers a compelling alternative so that it can be used in the process of deposition and preparation of materials (Kondoh 2004; Blackburn et al. 2001), nuclear reactor applications (Dostal et al. 2006), chemical extraction (Bondioli et al. 1992), refrigeration (Kumar and Gopal 2009a; Yamaguchi et al. 2008), and for the heat pump systems (Nekså et al. 1998). Compared to other fluids, CO<sub>2</sub> offers very low viscosity and a very high thermal expansion coefficient, as shown in Table 1.1.

Table 1.1: Comparison of properties for different secondary fluids.

<b>Refrigerant</b>	<b>R12</b> (CFC)	<b>R22</b> (HCFC)	<b>R134a</b> (HFC)	<b>R717</b> (Natural)	<b>R744</b> (Natural)
Molecular formula (g/mol)	CCl <sub>2</sub> F <sub>2</sub>	CHClF <sub>2</sub>	CH <sub>2</sub> FCF <sub>3</sub>	NH <sub>3</sub>	CO <sub>2</sub>
ODP	0.82	0.055	0.0	0.0	<b>0.0</b>
GWP	8100	1700	1300	0.0	<b>1</b>
Flammability	No	No	No	Yes	<b>No</b>
Toxicity	No	No	No	Yes	<b>No</b>
Molecular weight	120.9	86.5	102.03	17.03	44.01
Normal Boiling Point (°C)	-29.8	-40.8	-26.2	-33.3	-78.4
Critical pressure (bar)	41.1	49.7	40.7	114.27	<b>73.8</b>
Critical temperature (°C)	112.0	96.0	101.1	133.0	<b>31.2</b>
Sat. pressure at 0 °C (bar)	3.09	4.98	2.93	4.29	34.8
Volumetric refrigeration capacity at 0 °C (kJ/m <sup>3</sup> )	2740	4344	2860	4360	22545
Viscosity at 0°C (mPa.s)	248.7 (L)	218.2 (L)	271.1 (L)	170.1 (L)	99.4 (L)
	10.74 (V)	11.50 (V)	10.73 (V)	9.06 (V)	14.79 (V)
Density at 0 °C, (kg/m <sup>3</sup> )	1396.1 (L)	1281.5 (L)	1294.8 (L)	638.6 (L)	927.4 (L)
	17.87 (V)	21.23 (V)	14.42 (V)	3.45 (V)	97.65 (V)
Thermal conductivity 0°C (mW/mK)	75.9 (L)	94.8 (L)	92.0 (L)	559.2 (L)	110.4 (L)
	8.84 (V)	9.42 (V)	11.51 (V)	23.37 (V)	19.67 (V)

In addition, it is non-toxic and acts as a flame retardant, thus perfectly safe to use. However, unlike other working fluids, the operating pressure is very high in CO<sub>2</sub> systems. A comparative study by Kumar and Gopal (2009b) found that it is possible to design a more compact system with CO<sub>2</sub> as the working fluid compared to water.

There has been considerable interest in utilising fluids at pressures and temperatures above their vapour-liquid critical point in many industrial applications. When gas is heated beyond a specific temperature where no amount of compression will cause it to become liquid, known as the critical temperature. A supercritical fluid contains the properties of both gas and liquid beyond the critical point. Supercritical fluids exhibit significant deviations from ideal thermodynamic behaviour and do not undergo vaporisation or condensation phase transitions. For water or other fluids, where at high temperature, a phase change occurs, and the flow becomes abrupt, in that situation where phase change is to be avoided, supercritical fluid can serve as a feasible alternative. The critical point of CO<sub>2</sub> is  $P_c = 7.38$  MPa and  $T_c = 31.2$  °C (shown in Fig. 1.4), due to its low critical temperature, CO<sub>2</sub> exhibit significant deviations from ideal-gas law behaviour, and their properties can be utilized to increase productivity and efficiency of many technical processes.

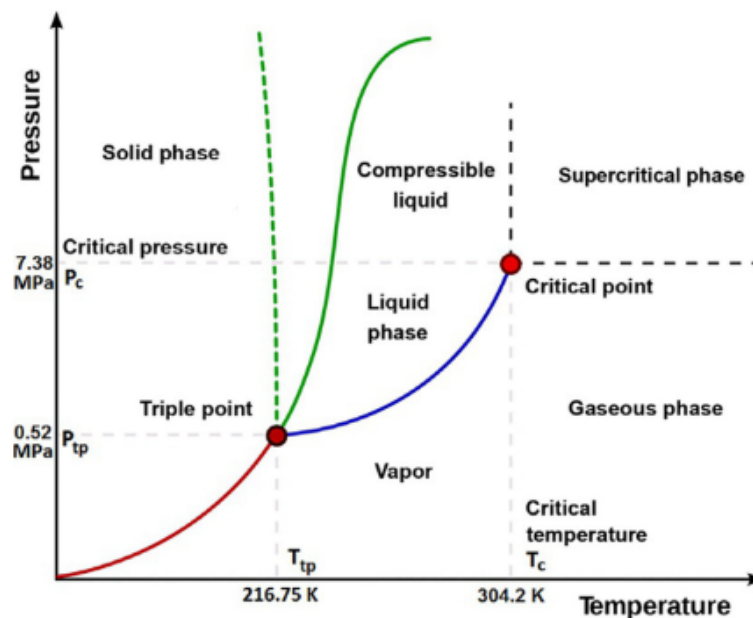


Figure 1.4: Phase diagram (NIST 2013).

CO<sub>2</sub> systems are patented way back in 1867 by T. S. C. Lowe in the USA. In 1939, USA first used CO<sub>2</sub> to air-conditioned cinema halls. In the early 20th century, supercritical CO<sub>2</sub> was used in marine refrigeration, cold storage, comfort cooling etc. In recent times

there is a growing interest in using carbon dioxide in various cooling, heating and power applications.

Research indicates that supercritical CO<sub>2</sub> based NCLs (scCO<sub>2</sub>-NCLs) are very compact and its performance will be better than other working fluids (Yadav et al. 2012a; Liu et al. 2016). Yadav et al. (2012b) carried out a numerical study on supercritical CO<sub>2</sub> and showed that, near the pseudo-critical region, CO<sub>2</sub> yields a very high heat transfer rate, approximately seven times higher than water for the same operating temperature. Single-phase water loop was compared with supercritical CO<sub>2</sub> based NCL (scCO<sub>2</sub>-NCL), and it was reported that the scCO<sub>2</sub>-NCL yields a higher mass flow rate and lower fluid temperature level making it the better option until the flow-induced heat transfer deterioration occurs (Sarkar and Basu 2017). scCO<sub>2</sub>-NCL creates a significantly higher driving head and high Reynolds number even for small differences in temperature between source and sink, which induces a high circulation rate in the system than conventional fluid-like subcritical water (Liu et al. 2016). Experiments were conducted by (Thippeswamy and Yadav 2020) on the heat transfer effectiveness of subcritical and supercritical CO<sub>2</sub> based NCL. The performance of CO<sub>2</sub> is compared with water and brine solution and concluded that the maximum heat transfer rates in the case of subcritical vapour, subcritical liquid, two-phase and supercritical CO<sub>2</sub> based natural circulation loops are 400%, 500%, 900%, and 800% higher than the water/brine-based system respectively. Dostal et al. (2006) showed that the supercritical CO<sub>2</sub> based Brayton cycle could be used for a next-generation nuclear reactor.

### **1.7 Instability in NCL**

Natural circulation loops are prone to several kinds of instabilities. Due to the non-linearity of the natural convection process, any disturbance in the driving force causes the disturbance in the flow and leading to oscillatory behaviour even in cases where an eventual steady-state is expected. To define instability in NCLs, need to determine the decay ratio ( $DR$ ).



Decay ratio is defined as the ratio of the amplitude of the succeeding oscillation ( $A_2$ ) to the amplitude of the preceding oscillation ( $A_1$ ), the two oscillations being consecutive.

Referring to Fig. 1.5.

Decay ratio is defined as,

$$DR = \frac{A_2}{A_1} \quad (1.6)$$

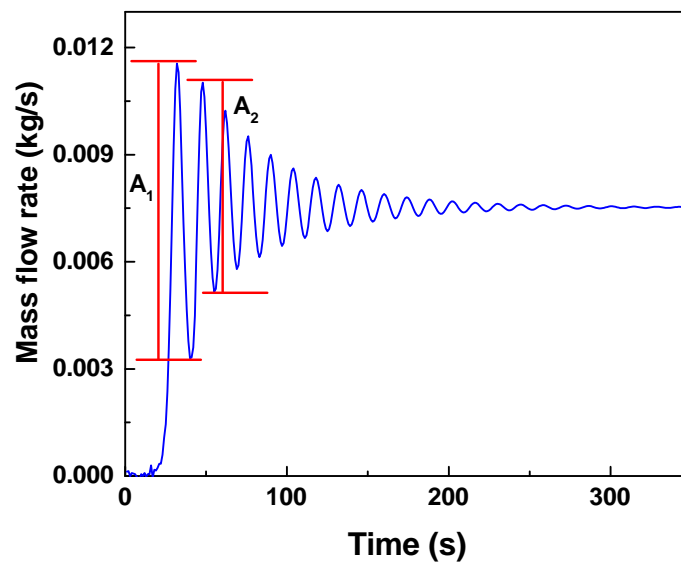


Figure 1.5: A transient flow behaviour in NCL.

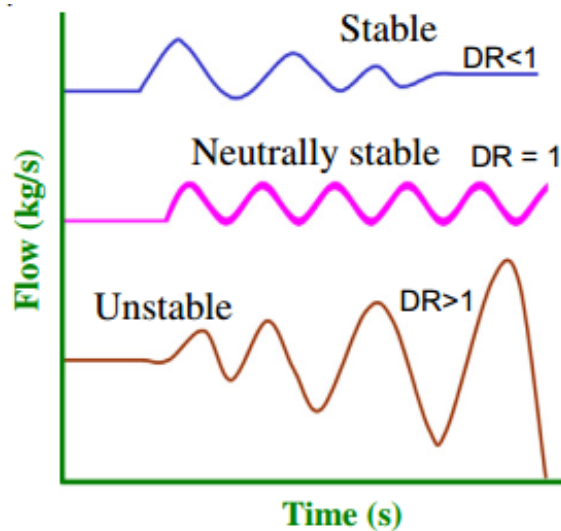


Figure 1.6: Types of instability (Vijayan and Nayak 2005).

In this way, if  $DR < 1$  the system is stable,  $DR = 1$  it indicates that the system is neutrally stable and  $DR > 1$  refers to an unstable system (as shown in Fig. 1.6).

Instability is nothing but a system to sustain itself against small perturbations. This instability in fluid flow creates flow oscillation, chaotic non-linear dynamic behaviour, and a flow reversal. To quantify the instability, oscillations amplitude as a certain percentage of the steady-state value is considered an unstable system. Thus, amplitudes greater than  $\pm 10\%$  of the mean value are often considered an indication of instability. However, some authors recommend the use of  $\pm 30\%$  as the cut-off value (Mochizuki 1994).

Flow instability in NCL is highly unacceptable as it can induct potent mechanical vibration in the system components, and eventually, it may lead to catastrophic incidences due to fatigue development in the components. Further, if oscillations get augmented, it can affect the heat transfer characteristics, which detriments to the system efficiency. Instability can also disrupt control systems and pose operational problems in commercial power plants. Flow instability in NCL is still an investigation aspect of physical and mathematical problems to comprehend. Hence, analysis of instabilities in the natural circulation loop is very important for the loop system's safety.

### **1.8 Classification of instability**

Types of instability in NCLs depends on the methods of excitation. Differences in instabilities also rely on the propagation method, oscillatory mode, the instability threshold's nature, and prediction methods. Also, the loop geometry and secondary phenomena affect the observed instabilities. In the present section, some of the most significant types of instabilities related to NCL are discussed. In general, instabilities can be classified according to the following bases (Vijayan and Nayak 2005):

- Propagation method
- Nature of the oscillations
- Flow direction

### **1.8.1 Propagation method**

The type of instability involves the propagation or transport of disturbances. The disturbance can be transported by two types of waves: (i) pressure (acoustic waves) and (ii) void (or density) waves. In single-phase flow, only density wave instability is observed. While, in two-phase flow, both type of instability is present.

(i) Pressure wave instability is considered to be caused by the resonance of pressure waves. This type of wave oscillation is found in subcooled boiling, bulk boiling, and film boiling. High frequencies of characterize pressure oscillations 10-100 Hz are related to the pressure wave propagation time.

(ii) Density wave instability is the most commonly observed instability in natural circulation loops (NCLs). When fluid absorbs heat at the source, it becomes lighter in density or higher in void fraction and starts moving along one of the vertical risers, it increases the driving force, and hence the flow begins. The increased flow reduces the exit enthalpy and the void fraction, causing a fluid packet of high density (dense or heavy fluid packet) to emerge from the heat source. As the heavy fluid packet ascends along the vertical legs riser, the driving force reduces, causing the flow rate to decrease. This decrease in flow rate again increases the exit enthalpy and void fraction leading to the process's repetition. However, this instability is observed when the light and heavy fluid packets are formed with appropriate spacing (related to time delay) and magnitude, depends on the operating conditions and the loop geometry. This type of instability is also known as thermally induced oscillations or time delay oscillations instability. The fundamental difference between acoustic instability and density instability is characterized by low-frequency oscillations (of the order of 1 Hz ([Vijayan and Nayak 2005](#))).

### **1.8.2 Nature of the oscillations**

All types of instability ultimately lead to some oscillations. Oscillations are characterized as periodic and chaotic based on their periodicity. Based on oscillatory mode, the

oscillations are classified as a fundamental mode or higher harmonic modes. In NCLs, flow direction can also change during oscillations. Based on the flow direction, the oscillations can be characterized as uni-directional, bidirectional, or switch between the two (shown in Figs. 1.7(a-c)).

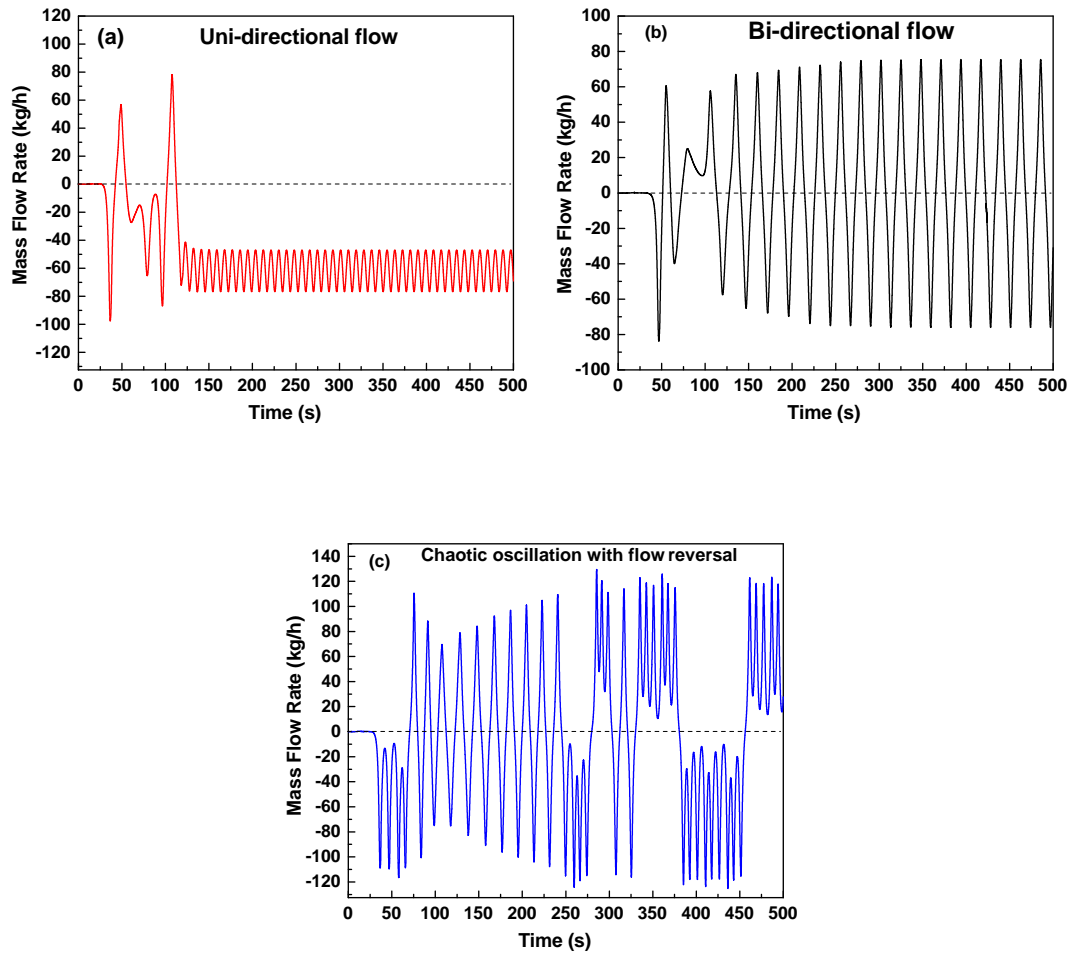


Figure 1.7: Nature of oscillation (a) Uni-direction flow (b) Bi-directional flow (c) Chaotic oscillations with flow reversal.

### 1.8.3 Flow direction

In NCLs, steady-state flow can take place in the clockwise or anticlockwise direction. Uni-directional flow is considered more stable than the other. The directional instability often depends on critical heat input, below that, it shows flow reversal, such transients also depend on flow initiation from rest and power raising.

Controlling instability without deteriorating the performance of the loop is a challeng-

ing task for researchers. Various researchers have done extensive studies on the cause of instabilities and methods to mitigate these instabilities by using multiple tools like introducing orifice, use of nanofluids, varying loop diameter, changing the heater’s positions and cooler, and tilting of the loop. Thus, the possibility of implementing a modified Tesla valve in the loop has been discussed here as it is one of the most promising adaptations due to its high effectiveness and reliability.

### 1.9 Tesla valve

The Tesla valve is a passive type of flow-control valve invented by Nikola (1920) to facilitate directional flow (shown in Fig. 1.8). The interior of the tube consists of amplifiers, recesses, projections, baffles and buckets. It is seen from the Tesla valve Fig. 1.8 that it is a series of 11 flow control segments that regulate the flow. The flow regulators can be increased or decreased by a number of other such segments as desired. The design was such that the reverse direction flow experiences more impedance than the forward direction, effectively creating a fluidic diode. The valve’s efficiency is often expressed in diodicity ( $Di$ ), which is the ratio of pressure drop across reverse to forward direction at a constant flow rate  $Q$ .

$$Di = \left| \left( \frac{\Delta p_r}{\Delta p_f} \right)_Q \right| \quad (1.7)$$

Where,  $\Delta p_r$  is the reverse flow pressure drop, and  $\Delta p_f$  is the forward flow pressure drop. Thus, a diodicity greater than unity implies flow in a forward direction.

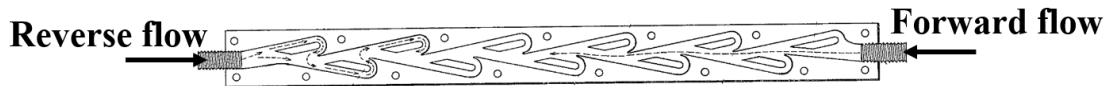


Figure 1.8: Cross-section of Tesla valve (Nikola 1920).

Due to the Tesla valve’s unique design and passive operation, several researchers conducted comprehensive studies to visualize flow patterns and improve the diodicity. Systematic design optimization of the Tesla valve is done by (Truong and Nguyen 2003) to

find its optimum angle and length.

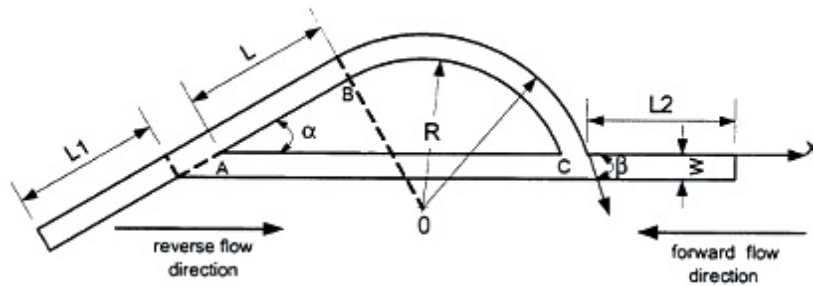


Figure 1.9: Geometry of Tesla valve (Truong and Nguyen 2003).

As shown in Fig. 1.9, a Tesla valve geometry consists of a channel width  $W$ , channel depth  $D$ , entry and exit length  $L1$  and  $L2$ , angle  $\alpha$ , the straight length  $L$ , and the radius  $R$  of the inner curve. Based on all six above mentioned parameters, the optimization of a Tesla valve can be obtained. It is found that the valve diodicity is inversely proportional to the radius  $R$  and the optimum configurations  $(\alpha, L)$  depend on the flow rate.

Later several design modifications on the Tesla valve have been done based on its utilization. Keeping diodicity as a significant factor to rank the efficiency of different modified Tesla valves. Figure 1.10(a) shows some modified Tesla valve designs, with its pressure difference in Fig. 1.10(b).

It is evident from above Fig. 1.10(a) that the D-valve design has a higher diodicity compared to the TMW design. The absolute pressure difference between reverse and forward flow can better compare different designs' effectivity, as shown in Fig. 1.10(b). This proves that the D-valve design is a properly performing Tesla-type valve, having an absolute pressure difference close to the T45C valve, which is very promising, especially concerning the inlets and outlets' alignment of NCL. While the GMF valve results show better potential, but it isn't easy to incorporate in NCL.

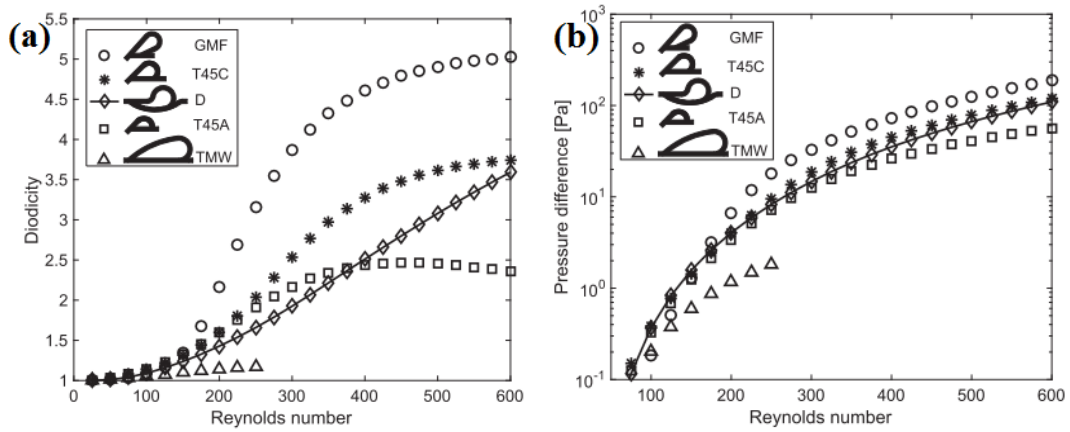


Figure 1.10: Plot of the single-phase (a) diodicity and (b) Pressure difference against the Reynolds number (Vries et al. 2017).

### 1.10 Structure of the thesis

**Chapter 1** presents a brief introduction to NCL and its types, the selection of  $\text{CO}_2$  as working fluid, Instability in NCL and the description of Tesla valve design.

**Chapter 2** presents an extensive review of the relevant literature. It contains the study on different heat transfer loops of NCLs, instability in NCLs with different loop fluids including supercritical  $\text{CO}_2$ , mitigation of instability, a summary of the literature, research gap, and objective of the present study.

**Chapter 3** deals with the transient analysis of 3-D supercritical  $\text{CO}_2$  based NCL with a heater as a heat source and heat exchanger as a heat sink. Parameters that affect flow behaviour, the existence of threshold heat input and a possible mechanism of instability with different pressure and heat inputs are investigated.

**Chapter 4** presents a CFD simulation of flow instability and heat transfer phenomenon for a regular natural circulation loop and a new modified single Tesla supercritical  $\text{CO}_2$  based NCL. In addition, the feasibility of implementing a modified Tesla valve in the loop has been discussed here.

**Chapter 5** emphasizes the development of NCL integrated with twin Tesla type valves to mitigate instability in supercritical  $\text{CO}_2$  based NCL. The heat transfer capability of twin Tesla NCL is compared with regular NCL and single Tesla NCL.

**Chapter 6** deals with the design and fabrication of the experimental setup. Experimental investigations have been carried out to understand the transient behaviour of the NCL employing supercritical CO<sub>2</sub> as a working fluid.

**Chapter 7** concludes the dissertation with important findings based on the present study, significant conclusions, and future work recommendations.



## CHAPTER 2

### Literature Review

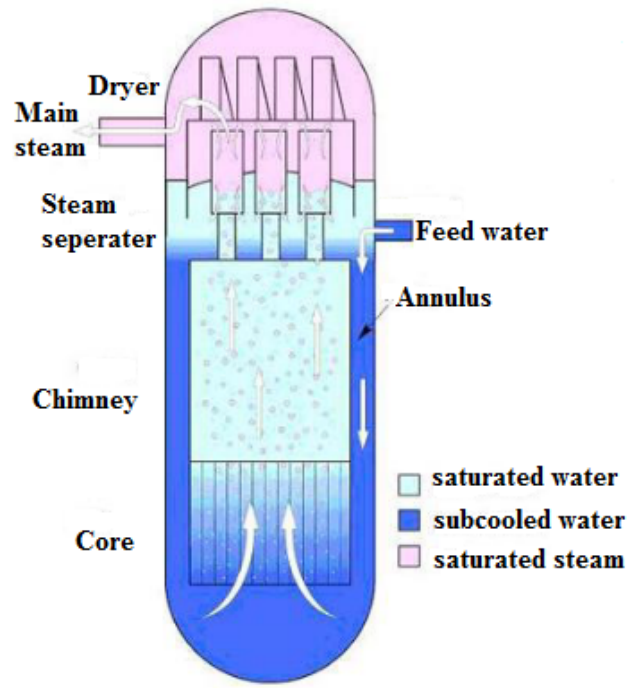
This chapter presents a detailed literature review on experimental and theoretical studies related to the instability in the natural circulation loop. The review also emphasizes different methods to mitigating the instability. Finally, this chapter ends with the research gap and objectives of the present study.

#### 2.1 Natural circulation loop

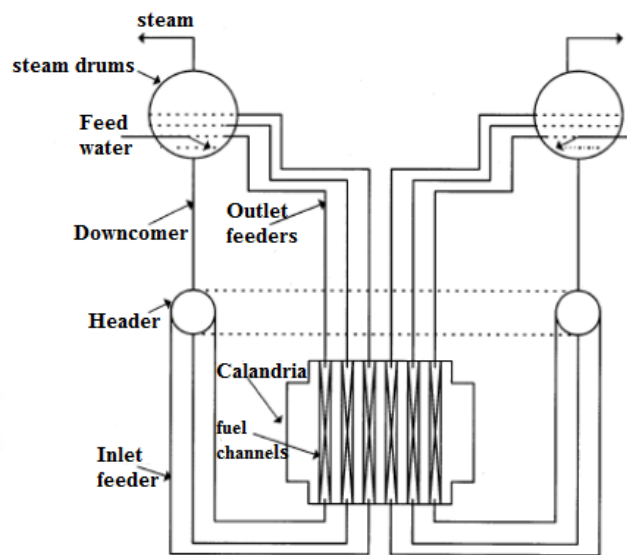
The phenomenon of natural circulation offers a very efficient option of fluid transport within a closed system without employing any mechanical drives. Such system is commonly known as Natural Circulation Loop (NCL), a term coined by (Japikse 1973). So, NCLs are loop-type designs with energy conversion and fluid transfer systems from a distinctive location of the source to sink.

NCLs have many industrial and domestic applications like solar heaters, thermosyphon reboilers, electronic chip cooling, turbine blade cooling, chemical process industries, geothermal energy extraction processes, closed-loop pulsating heat pipe, nuclear power generation and plenty more. Some interesting applications of NCLs also include the models of thermal springs of Virginia (Torrance 1979), heat dissipation investigation (Madejski and Mikielewicz 1971), chaos determination (Wang et al. 1992a) and its application in refrigeration (Kumar and Gopal 2009a). Nuclear scientists have shifted their focus towards the natural circulation mode, mainly to enhance the reactor's passive safety. Probably one of the most recent and vital applications of NCL is in nuclear industries. This is used to cool the reactor core due to its passive nature of cooling. The emergency core cooling mechanism of Dodewaard nuclear reactor of Netherlands (Hagen and Stekelenburg 1997), Economic Simplified Boiling Water Reactor (ESBWR) (Gamble et al. 2006) designed by General Electric and Advanced Heavy Water Reactor

(AHWR) (Sinha and Kakodkar 2006) (in Fig. 2.1) of India are fine examples of NCL in nuclear power applications.



(a) ESBWR



(b) AHWR

Figure 2.1: Natural circulation loop in nuclear power plants.

From the theoretical aspect, a natural circulation can be achieved by any type of body

force such as electromagnetic, centrifugal or gravitational forces. However, practical applications concern only the use of buoyancy created by gravity forces. Buoyancy is nothing but a density difference in the adjacent part of the fluid in the system, which can be achieved either by thermal effects or by introducing a lighter phase in the flow domain. The term NCL is typically attached with a loop with distinct heating and cooling zones, and circulation occurs solely due to density differences created by thermal energy. The fluid motion concept due to bottom heating and top cooling evoked from Lord [Rayleigh \(1916\)](#) work. Heat addition to the loop fluid can be done using an electric heater ([Vijayan 2002](#); [Vijayan et al. 2008](#)) by convective heat transfer with a hot fluid in a heat exchanger ([Thippeswamy and Yadav 2020](#)) or a combination of radiation and convection. For CFD simulations, heat addition has many options, such as an isothermal heater ([Yadav et al. 2016](#)), sudden increase or decrease in power ([Chen et al. 2013c](#)), internal heat generation and many more.

## **2.2 Instability in various NCLs**

NCLs always offers assured reliable heat transport mechanism and safety with respect to thermal failure. The elimination of active power supplies and pumps makes it a suitable option in many typical applications. For example, without bothering about cavitation and pump malfunctioning, a two-phase NCL can work well. Mechanical drives also introduce noise and vibration into the system, whereas NCL comes across as a serene relief. However, due to the strong coupling between momentum and thermal fields, it is not possible to envisage desirable outcomes in the natural circulation system. The dynamics of the NCL significantly depend on the operating conditions and geometry. Hence, any change in these parameters leads NCL to flow oscillations, possible flow reversals, flow bifurcation and chaotic behaviour, also known as instability. Instability is undesirable, as it creates potent vibration on mechanical parts and even abates the system performance. Therefore, NCLs require precise design assessment that focuses on the interaction of all the transient responses of buoyancy and friction forces, ensur-

ing a stable zone of operation.

When NCL subjects to disturbance due to thermal imbalance and the forces or equivalent acceleration field acted on the fluid senses the destabilization, the irregularities grow exponentially with time and amplitude. The inability of NCL to sustain themselves against these irregularities created due to small perturbations is known as “instability”. Mathematically, instability is the existence of multiple solutions so that NCL is unable to settle down to any one of them permanently instead, it swings from one solution to the other.

[Keller \(1966\)](#) was the first to analytically study the instability in an NCL. He found that NCL shows a periodic motion when fluid is heated at the mid-point of the lower arm and cooled at the mid-point of the upper arm, and it behaves like a self-excited oscillator when subjected to certain operating conditions. He also predicted that the flow oscillations are merely an interaction between frictional and buoyancy forces, but inertia was found to have a negligible effect on such oscillations. Later, [Welander \(1967\)](#) provided a plausible explanation for the mechanism of instability in NCL. According to him, the unstable motions are associated with thermal anomalies in the fluid that are advected materially around the loop, and the anomalies amplify through the correlated variations in flow rate. His well-celebrated theory is known as ‘warm and cold pockets of fluid’. He investigated that the fluid behaves like a pendulum with its centre of mass towards the cold pocket. Keller and Welander both analytically showed that flow instabilities strongly depend on the nature of temperature distribution. [Creveling et al. \(1975\)](#) were the first to observe the instability in a water-based toroidal loop with a distributed heating and cooling of loop experimentally. They observed two different stable operation regimes, with the region of instability matching the transition from laminar to turbulent flow. At lower or higher heat input, fluid flow was stable, while at intermediate, the flow was highly oscillatory. They also developed a theoretical model for stability prediction and turbulent region and found a good agreement with the test data. [Mertol et al. \(1982\)](#) carried out a two-dimensional analysis for a toroidal loop by considering both radial

and axial directions variation employing the finite-difference technique. They defined a non-monotonic function of Graetz number ( $Gz$ ), which is the function of the Reynolds number ( $Re$ ) and Prandtl number ( $Pr$ ). Graetz number is defined as

$$Gz = \frac{D_H}{L} Re \cdot Pr \quad (2.1)$$

Initially, the average velocity increases with the increase in  $Gz$  until it reaches its maximum value and then decreases because at the higher velocity, the friction increases, and the temperature difference decreases. As a further improvement, [Lavine and Humphrey \(1987\)](#) investigation for the 3-D steady-state analysis of toroidal NCL showed that 1-D and 2-D analyses over-predicted the total buoyancy and average axial velocity. They also found some real-time phenomena like stream-wise flow reversal, secondary motion and non-axisymmetric temperature profiles. To suppress chaos in a toroidal NCL, [Bošković and Krstić \(2001\)](#) suggested an active feedback control mechanism to conquer the convection loop's chaotic instability. Later, [Jiang and Shoji \(2003\)](#) proposed a non-linear dynamical model to formulate the wall effects in a convection loop. They suggested that flow is more stable with high thermal conducting materials. [Hitt et al. \(2011\)](#) did a three-dimensional unsteady numerical simulation on the toroidal loop by fixing the Prandtl number at 5.83 and varying the Rayleigh number from  $10^3$  to  $2.6 \times 10^7$ . Simulation reveals a complex three-dimensional flow behaviour inside the loop characterized by localized recirculation zones and helical motion of the bulk circulation. A comparative numerical assessment of the steady and dynamic performance of rectangular and toroidal loops with identical dimensions was carried out by [Basu et al. \(2012\)](#). Rectangular loop exhibits higher flow rates with more instability than toroidal loop which can be attributed to strong buoyancy force. Hence for real-life application, the toroidal geometry of natural circulation loops does not have much significance. Therefore, the emphasis has moved towards more practical geometrical structures, i.e., rectangular NCL, which can be applied in reality. Hence, the hunt begins with the de-

velopment of knowledge related to the underlying physics of rectangular NCL.

### **2.3 Instability in rectangular NCL**

Rectangular NCLs encompass a broad range of applications and phenomena. Basic experimental and theoretical studies and overall performance and systems testing/analyses in this vital area are being vigorously conducted throughout the world, and many representative works and programs are discussed. [Holman and Boggs \(1960\)](#) first investigated the heat transfer to R-12 near the critical point in a rectangular NCL. The loop consisted of two vertical branches, two horizontal sections at the bottom and top and four curved connectors at the corners. The cooling heat exchanger was mounted around the upper part of the right vertical arm, whereas the lower portion of the left vertical arm was a heat source. Pressure fluctuation was observed in order 136 to 204 kPa, close to a critical point. Fluctuations intensified with a decrease in coolant flow or increase in supplied heat flux and subside with the increase in coolant flow rate. Later, [Keller \(1966\)](#) and [Welander \(1967\)](#) both did theoretical analysis of rectangular NCL with a point source of heating and cooling. According to them, the amplitude of these perturbed hot/cold pockets is progressively amplified or damped according to the system's specific geometrical and physical characteristics. However, their analysis failed to predict any type of instability, concluded that the instability is due to thermal anomalies. [Zvirin and Greif \(1979\)](#) did transient theoretical analysis for a similar configuration to [Welander \(1967\)](#). Integral forms of the momentum and energy equations are derived and solved to get the flow rate and temperatures as functions of the time. They concluded that the stability characteristics strongly depend on the shape of temperature distribution. Experimental observation of de-ionized water-based rectangular NCL was conducted by [Hallinan and Viskanta \(1986\)](#) and found that the friction parameter is a straight-line function of Re and suggested a correlation for the average heat transfer coefficient. [Zvirin \(1982\)](#) did theoretical and experimental survey work on water-based rectangular natural circulation loops. He defined three types of instabilities based on

his experiments with thermosyphons: (i) instability at the beginning of motion in the entire loop or legs; (ii) small oscillation amplitude development that can induce flow reversals; and (iii) the existence of multiple steady-state solutions for the system. [Ramos et al. \(1985\)](#) used a one-dimensional model to investigate the stability in rectangular NCLs with the variable area. Their Poiseuille flow assumption showed that flow was possible only when the heat source is at a lower elevation than the heat sink. This type of NCLs always has multiple steady-state solutions. Later, [Acosta et al. \(1987\)](#) experimental study on a water-based tilted square loop with a circular cross-section confirmed the existence of multiple steady-states. They also showed that it is possible to have two distinct stable states for certain heat supplies and tilt angles. The stability of rectangular natural convection flows for a range of loop aspect ratios and radii was analytically and numerically investigated by [Chen \(1985a\)](#). He defined a single dimensionless parameter; when this dimensionless parameter is less than a critical value, flow is stable; above a critical value, oscillatory instability exists. The calculated neutral stability conditions show that the flow is least stable when the aspect ratio of the loop approaches unity. [Chen \(1985b\)](#) another theoretical study, shows the influence of loop configuration on natural convection loops with isothermal heater and cooler. He combined the aspect ratio and cross-sectional area of the loop into a single dimensionless parameter, used as criteria for maximum heat transfer. Later, to know the diametral effect on the stability, [Vijayan et al. \(2008\)](#) carried out detailed experimentation on three different diameter loops, namely 6 mm, 11 mm and 23.2 mm. The test was conducted over a wide range of heater power and cooling water flow rate and found with less diameter are more stable. [Vijayan \(2002\)](#) conducted an extensive experimental study on water-based NCL instability behaviour and obtained a relation for steady-state Reynolds number as a function of modified Grashof number and geometric ratio. Experiments performed by [Cammarata et al. \(2004\)](#) on a loop by varying the gravity field over a range between  $10^{-2}g$  and  $1.8g$ , with  $g = 9.81 \text{ m/s}^2$ , show the reduction of the gravitational field plays a stabilizing role in the dynamics of NCLs but enhances the thermal stresses.

One-dimensional transient stability behaviour of NCL with end heat exchangers was investigated by [Rao et al. \(2005\)](#). Based on two non-dimensional parameters, namely heat capacity rate and Grashof number; stable, neutrally stable, and unstable states are demonstrated. They also analyzed the dynamic performance of an NCL under the step, ramp, exponential and sinusoidal excitations. It was observed that NCL experiences initial transients before reaching the steady state. The time required to achieve a steady state depends on the type of excitation method used. [Misale et al. \(2011\)](#) carried out experimental study by varying the sink temperature from  $-20\text{ }^{\circ}\text{C}$  to  $+30\text{ }^{\circ}\text{C}$  and heat flux from 0.1 kW to 2.5 kW. They reported that with increase in the heat sink temperature the circulation frequency increases smoothly. This might cause discontinuity when the system abruptly crossed the stability threshold in laminar flow. Later, [Devia and Misale \(2012\)](#) combined experiment and CFD to visualize the thermo-hydraulic behaviour of the loop. Comparative study shows that CFD properly estimates the temperature oscillation amplitude, frequency and the pressure difference oscillations, while fails to do correct calculation for the number of times that the mass flow rate oscillates between two consecutive flow reversals.

With the advancement in computational techniques and higher-order analytical models, predicting the stability behaviour and dynamic response becomes more precise. To construct a neutral stability map in NCL, both linear and non-linear methods have been implemented. In linear analysis, algebraic governing equations are perturbed to find the root of the equation. The roots of the equation suggest the nature of NCL i.e., the system whether it is stable, unstable or neutrally stable. For non-linear analysis, a numerical method is implemented to observe the transient nature of NCL after being perturbed from a steady-state. The amplitude of growth or decay in the oscillation decides the nature of the system. Linear stability analysis is a less time consuming and effective method to predict neutrally stable points, unlike non-linear methods. However, non-linear methods are needed to ascertain the nature of the instability, development of oscillations and envisage the evolution of transients during the startup period.



Several codes have been developed for both linear and non-linear methods. For linear stability analysis, NUFREQ (Peng et al. 1986) and DENSITY-PARA (Xiao et al., 1993) are examples of codes developed. Chatoorgoon (1986) has developed a simple code SPORTS for two-phase flow. RAMONA (Rohatgi et al. 1993) code is designed to predict the large amplitudes oscillations. The above two codes are of a non-linear type. Vijayan and Date (1992) include linear stability analysis and non-linear finite difference analysis to investigate natural circulation stability in a figure-of-eight loop. The unconditionally stable, conditionally stable, and unconditionally unstable regimes have been determined by non-linear finite difference analysis with different initial conditions. On the other hand, the linear stability analysis shows only instant flow reversal instability. Later, Nayak et al. (1995) did mathematical modelling to find the loop's stability behaviour using the linear theory. By examining the amplitude of flow and temperature oscillations with time for a given set of operating conditions, stable, unstable and neutrally stable points were identified. Mousavian et al. (2004) did one-dimensional linear and non-linear stability analysis using the perturbation method for single-phase NCL to obtain the stability map by employing the Nyquist criteria. Luzzi et al. (2017) used two different numerical models: an Object-Oriented (O-O) one-dimensional model and a three-dimensional CFD model to analyze NCL. The object-Oriented model acts as a fast tool for the assessment of velocity and the temperature fields in the loop along the axial coordinate. While the CFD model is characterized by a high computational burden but highlights the interesting 3-D spatial effects.

Various authors attempted to apply commercial software, e.g., RELAP5, CATHARE2, ATHLET, FLUENT, etc. Misale et al. (1999) did simulations with CATHARE and RELAP codes to know the performance of rectangular NCL. At low power, the CATHARE code shows an excellent capability to predict the steady-state quantities after the initial transient. The RELAP code can show oscillating quantities but not at the same power levels as in the experiments. Vijayan et al. (1995) used the computer code ATHLET to predict the unstable oscillatory behaviour of NCL with repetitive flow reversals. ATH-

LET code needs fine nodalization to predict the instability. While the coarse grid failed to envisage instability when the experiment exhibits unstable oscillations.

Instabilities are always associated with the thermodynamic irreversibility of the system. An irreversibility process reduces the performance of a thermodynamic system which is intended to produce cooling or heating. The entropy produced by the system has a primary influence on the system's thermodynamic irreversibility. So, entropy generation analysis is an excellent method to improve the thermodynamic performance of a system. [Sekulicá \(1986\)](#) performed calculations for entropy generation to know the optimized size of a counter-flow heat exchanger and observed that the entropy generation rate decreases with an increase in heat-exchanger size. Later, [Goudarzi and Talebi \(2015\)](#) have performed an analysis to know the effect of various parameters such as loop dimensions and heater power on the single-phase natural circulation stability and entropy generation in the loop that is how stability and entropy generation are related. They observed that increase in length to diameter ratio, entropy generation rate and instability increases, which concludes that the entropy generation rate in the loop is directly proportional to the loop's instability. [Inampudi et al. \(2018\)](#) did 3-D computational steady-state simulations for entropy generation analysis in water-based NCL with isothermal source and sink conditions. They observed that with the increase in loop height, the entropy generation rate increases due to increased heat transfer and fluid friction. A 3D CFD simulation has been carried out with different loop configurations by [Kudariyawar et al. \(2016\)](#) in water-based NCL. Horizontal heater and horizontal cooler loop observed uni-directional/bi-directional pulsation depending on heater power. Energy and exergy analysis by [Sahu and Sarkar \(2019\)](#) on NCL with different water-based hybrid nanofluids reveals that effectiveness and entropy generation decrease with increased loop diameter and height.

## 2.4 Instability in supercritical CO<sub>2</sub> based NCL

Several previous studies have been recorded on subcritical water-based systems for NCL; however, it remains difficult to comprehend how supercritical fluids cause instabilities in NCL. For supercritical CO<sub>2</sub> (scCO<sub>2</sub>), the underlying physics for instability is complex and not well characterized. There is a pseudocritical point for each isobar in the supercritical region, characterized by substantial changes in thermo-physical properties, which is mainly due to maximum value of specific heat is obtained at a particular pressure. This pseudocritical region is advantageous for the operation of an NCL. On the other hand, density variations are also dominant, making NCL susceptible to dynamic instability. These possible density variations lead to dramatic changes in the driving force, i.e., buoyancy force hindering the loop's smooth operation. The supercritical fluid's viscosity is also relatively low, and fluid flows are significantly influenced whenever the operating forces are marginally altered. Flow instability at a supercritical state is highly unacceptable (due to the high Reynolds number) as it can induct potent mechanical vibration in the system components, and eventually, it may lead to catastrophic incidences due to fatigue development in the components. Further, if oscillations get augmented, it can affect the heat transfer characteristics, which detriments to the system efficiency. Hence, it is essential to comprehend the characteristics of supercritical CO<sub>2</sub> based NCL (scCO<sub>2</sub>-NCL) stability before integrating it into any practical applications.

Several numerical studies were performed by [Chatoorgoon et al. \(2005\)](#) to assess the non-dimensional parameters crucial for the flow stability in supercritical CO<sub>2</sub>. Assessments suggested that the inlet temperatures, heated lengths and vertical loop heights significantly affect stability. Later, linear stability for supercritical CO<sub>2</sub> loops was performed by [Jain and Corradini \(2006\)](#), and critical mass-flux pulsations of CO<sub>2</sub> were discovered, which were caused by the dramatic property changes in the near-pseudocritical region. [Jain et al. \(2008\)](#) used FORTRAN90 to simulate and understand flow instabilities in scCO<sub>2</sub> -NCL. Simulations predicted that the stability threshold of a scCO<sub>2</sub>-NCL

is not confined to the near-peak region of the (steady-state) flow-power curve. [Chen et al. \(2010\)](#) observed that near critical and pseudocritical regions, scCO<sub>2</sub> based NCLs experience strong pulsations in the mass flow rate, leading to instability due to dramatic changes in the thermophysical properties. To understand behaviour when fluid crosses the critical point, [Zhang et al. \(2010\)](#) kept the simulation temperature range from 298.15 K to 323.15 K. Results show periodic reversal flow phenomena and high mass flow rate for the small temperature difference between sink and source. Later, [Cao and Zhang \(2012\)](#) studied parametric influences of the sink temperature and the temperature difference on scCO<sub>2</sub>-NCL instability. Change in the heat sink temperature shows a significant effect on heat transfer and flow behaviour. Both the flow rate and heat transfer performance are initially found to increase with the temperature difference, reach a peak, and then decreases gradually. [Chen et al. \(2013c\)](#) carried out an experimental study with transcritical/supercritical CO<sub>2</sub> to know the effects of operating parameters like charging mass, heating power and coolant temperature on stability. At high-pressure, transcritical CO<sub>2</sub> shows three different types of instabilities. Experiments conducted by [Sharma et al. \(2013\)](#) observed instability near the pseudocritical temperature range of operation. [Chen et al. \(2013b\)](#) did experiments over a wide range of pressures from around 6.0 to 15.0 MPa in the near-critical region. It is found that NCL flow changes from unstable sub-critical two-phase flow to stable liquid flow and then become stable supercritical circulation with the increase of initial system pressure. Based on the experimental observation of the thermal and hydrodynamic characteristics of scCO<sub>2</sub>-NCL, the CO<sub>2</sub> loop stability map is drawn by [Chen et al. \(2013a\)](#). [Yadav et al. \(2014\)](#) did transient numerical simulation studies for subcritical/supercritical CO<sub>2</sub> based NCL with operating pressure in the range of 50–100 bar and operating temperature in the range of 323 K to 363 K. Simulation shows that the time to reach steady-state decrease as operating pressure increases for stable flow. [Archana et al. \(2015a\)](#) developed a one-dimensional transient code to analyze the flow transients, initiation, power step-up and power step effect on scCO<sub>2</sub>-NCL, but instability is not observed in vertical

heater vertical cooler configuration. [Yadav et al. \(2017\)](#) did experimental work with scCO<sub>2</sub> based on both sides heat-exchanger loop and showed that within the range of 50 to 90 bar and 323 to 353 K, the NCL is found to be stable. [Sadhu et al. \(2018\)](#) experimented with an air-cooled scCO<sub>2</sub>-NCL to analyze the thermal anomalies with different heater power levels. It is found that due to the low critical temperature of scCO<sub>2</sub>, NCL shows interesting transient behaviour, i.e., moving from single phase to two-phase and vice versa. [Deng et al. \(2019\)](#) carried out a numerical and experimental study on the flow transition characteristics of supercritical CO<sub>2</sub> based NCL, and it is noticed that the flow in supercritical NCL is susceptible to heat flux changes.

## **2.5 Mitigation techniques for instability**

Several researchers have tried to curb instability in NCL by using various techniques. Several theoretical and experimental investigations have been reported to suppress unstable oscillations in a rectangular loop. [Zvirin et al. \(1981\)](#) suggested the introduction of an orifice at the inlet of the heater section to stabilize the flow. However, this technique leads to a significant reduction in the mass flow rate and affecting the heat transfer rate. [Wang et al. \(1992b\)](#) showed a simple control strategy to suppress the chaotic motion or induce chaos in a toroidal thermal convection loop. The control method consists of sensing the variation of fluid temperatures from desired values at different locations of the loop and then altering the wall heating to counteract or enhance such deviations. [Misale and Frogheri \(2001\)](#) performed a series of experimental tests to stabilize unstable flow using orifices of different diameters located in the vertical legs. [Muscato and Xibilia \(2003\)](#) used a non-linear lumped parameter model, derived using a truncated Fourier series expansion to model and control instability in NCL by a feedback controller system. All types of feedback controllers were found capable of stabilizing the system. Derivative action reduced the settling time slightly but did not exhibit any significant impact. Control based on temperature difference was found to be superior due to higher bandwidth and lower noise of temperature sensor compared to flow sen-

sor. Later, [Fichera and Pagano \(2003\)](#) also used the same Fourier series expansion for suppressing unstable dynamics in NCL. The flow velocity and temperature difference across the heating section were used as the feedback variable, but a slight mismatch between experimental and simulated results was found. One-dimensional computational fluid-dynamic models developed by [Pilkhwil et al. \(2007\)](#) for the arbitrary configurations of heat sources and sinks to analyze the unstable behaviour of NCL reveal that the vertical heater with vertical cooler (VHVC) configuration is always stable. [Bodkha et al. \(2010\)](#) did experiments by using different spool pieces in the loop to suppress the instability and found very encouraging results. [Nayak et al. \(2011\)](#) did an experimental investigation to stabilize the flow behaviour of loop fluid using  $\text{Al}_2\text{O}_3$  nanofluid. With nanofluid, flow stability was observed with the penalty on the heat transfer capability of NCL due to the high viscosity of nanofluid. Later, a similar type of experiment was performed by [Misale et al. \(2012\)](#) to know the thermo-hydraulic performance of a mini NCL using distilled water and nanofluid (distilled water with nanoparticles of  $\text{Al}_2\text{O}_3$  of different concentrations (0.5% and 3.0% by volume)). It was found that for both fluids, the mini-loop was always stable. The effect of loop diameter on stability was investigated by [Chen and Zhang \(2011\)](#) and found a higher degree of stability in a larger diameter, due to the developed flow field and the higher heat transfer rate in supercritical  $\text{CO}_2$ . Later, [Chen et al. \(2013d\)](#) did two-dimensional analysis with  $\text{scCO}_2$ -NCL, it was found that when the inclination angle is greater than  $60^\circ$ , the effect of inclination on the state of flow is not significant which occurred due to the different distribution of gravity components along the NCL plane. [Chen et al. \(2014\)](#) performed an analysis focused on the influence of the orientation of the heater and cooler on  $\text{scCO}_2$ -NCL. Instability, flow rate and heat transfer rate found to be maximum for the horizontal heater and cooler orientation among all the other configurations. However, when both, heater and cooler were kept vertical, VHVC system was highly stable but with the least flow rate. [Ruiz et al. \(2015\)](#) used a semi-analytical linear method and a non-linear numerical method to investigate the dynamic stability behaviour of different loop configurations with in-

ternal heat generation. The result illustrates that the VHVC configuration shows better stability behaviour. Later, the study of the heat exchange effect on single-phase natural circulation's dynamic behaviour with internal heat generation was studied by [Pini et al. \(2016\)](#). It was found that the internal heat generation combined with the heat exchange effect can induce a stabilization or a destabilization of the system dynamics depending on its action on the loop symmetry. 3-D computational simulations were carried out by [Krishnani and Basu \(2017\)](#) to know the influence of inclination angle on the stability behaviour of NCL. With an increase in inclination, unstable oscillations decreased drastically due to a reduction in gravitational acceleration in the tilted flow direction. This method leads to a reduction in the heat transfer rate, which is undesirable. [Yadav et al. \(2014, 2016, 2017\)](#) did numerical and experimental studies on the transient behaviour of carbon dioxide-based natural circulation loops operating in subcritical/supercritical conditions. They also proposed a solution to instability through tilting the loop, but it leads to a reduction in the heat transfer rate. [Liu et al. \(2017\)](#) investigated that for scCO<sub>2</sub>-NCL, system instability increases with an increase in system pressure and the local resistance coefficient in the cold section, and a decrease in the local resistance coefficient in the hot section could enhance the system stability. [Goudarzi and Talebi \(2018\)](#) found that in the horizontal heater and horizontal cooler (HHHC) orientation loop, shortening the cooler extends the unstable region and decreasing the heater length constricts the unstable area. [Zhu et al. \(2019\)](#) carried out CFD simulations studied the methodology to reduce the flow oscillation of natural circulation in non-inertial systems. Simulations showed that the flow oscillation increased with angular acceleration and the area enclosed by the loop but decreased with the angle between the loop normal vector and the angular acceleration. [Pegallapati et al. \(2020\)](#) developed a mathematical model for scCO<sub>2</sub>-NCL which shows that wall thermal capacitance suppresses oscillations during loop transients and increases the time required to reach a steady state.

## 2.6 Tesla valve applications

As discussed above, various researchers have done extensive studies on the cause of instabilities and methods to mitigate these instabilities by using multiple tools like introducing orifice, using nanofluids, varying loop diameter, changing the positions of the heater and cooler, and tilting of the loop. However, each of these methods has inherent limitations and hence, controlling instability without reducing the performance of the loop is still a challenging task. Thus, the possibility of implementing a modified Tesla valve in the loop has been discussed here as it is one of the most promising adaptations due to its high effectiveness and reliability.

As discussed above in section 1.9, the Tesla valve was invented by [Nikola \(1920\)](#). Due to the Tesla valve's unique design and passive operation, several researchers conducted comprehensive studies to visualize flow patterns and improve the diodicity. To explore the steady-state flow pattern for different Tesla valves, [Truong and Nguyen \(2003\)](#) have used a numerical approach and derived formulae for optimum geometric parameters. Later, a two-dimensional CFD optimization study with six independent, non-dimensional geometric design variables was carried out, and results showed a 25% higher diodicity for Reynolds number in the range  $0 < Re \leq 2000$  compared to commonly used Tesla valve ([Gamboa et al. 2005](#)). [Forster et al. \(1995\)](#) carried out both CFD and experimental studies to prove the Tesla valve's effectiveness in a micro-pump. [Zhang et al. \(2007\)](#) concluded that a Tesla valve with a higher aspect ratio gave a better diodicity for constant hydraulic diameter. A study done by [Nobakht et al. \(2013\)](#) revealed that in the Tesla valve, major pressure losses happen at the inlet irrespective of the flow direction. Hence, to increase the diodicity, the flow losses in the forward direction have to be reduced. Computational analysis on three-dimensional multi-staged Tesla valves of [Thompson et al. \(2014\)](#) reveals that the multi-staged Tesla valve has higher diodicity than a single Tesla valve. [Vries et al. \(2017\)](#) performed a computational and experimental study on water-based pulsating heat pipe (PHP) with a Tesla valve to increase diodicity and promote unidirectional flow.



However, till date, no literature reflects on the use of a Tesla valve in scCO<sub>2</sub>-NCL. Therefore, it is essential to understand supercritical CO<sub>2</sub> flow stability and methods to curb instability.

## **2.7 Research gap**

A thorough survey of the available literature presents a broad overview of research related to NCLs, instabilities and the use of CO<sub>2</sub> as a loop fluid. With the intensive literature review, the following observations are made:

- i. The absence of any rotating machinery in NCL often supersedes the drawbacks of low driving head and stability-related apprehensions. However, controlling instability without deteriorating the performance of the loop is a challenging task for researchers. It is observed that the work carried out to control the instability of NCL is scarce.
- ii. The benign environmental nature and admirable thermophysical properties of CO<sub>2</sub> offer a compelling alternative secondary working fluid in NCLs. However, a dedicated analysis for supercritical CO<sub>2</sub> based NCL and its instability analysis appears missing from the reported studies.
- iii. Effect of operating conditions (like pressure, heat flux, geometrical modifications etc.) on supercritical CO<sub>2</sub> based NCL needs more physical explanation.
- iv. Understanding the flow behaviour by creating an asymmetrical flow resistance in NCL has not received due attention from a geometrical complexity perspective.
- v. Till date, no literature reflects on the use of a Tesla valve in supercritical CO<sub>2</sub> based NCL. Therefore, it is essential to understand supercritical CO<sub>2</sub> flow behaviour in Tesla-based NCLs.

## 2.8 Thesis objectives

After going through the intensive literature survey with a careful analytic mind, some research gaps are found. These research gaps need more practical applications, simulations for visualization and a comprehensive physical explanation. Hence, the present work focuses on analyzing natural circulation systems with an emphasis on physical variables and design aspects. Many vital areas have been marked from the survey of available literature, then the following objectives for the thesis are summarized:

1. Three-dimensional CFD transient simulation of supercritical CO<sub>2</sub> based NCLs with a heater as a source and heat exchanger as a sink to know the parameters that affect the flow behaviour, threshold heat input to decides the nature of flow and a possible instability mechanism for NCL.
2. CFD simulation of a modified Tesla valve integrated with NCL at different operating conditions (heat inputs and pressures) of supercritical CO<sub>2</sub> to mitigate instability.
3. CFD simulation of twin Tesla type valve integrated with NCL to further decrease the instability, and to compare the results with single Tesla NCL for supercritical CO<sub>2</sub>.
4. Design and development of experimental facility with and without Tesla valve NCLs to carry out experiments and validate numerical results.

## CHAPTER 3

### Supercritical CO<sub>2</sub> Flow Instability in Natural Circulation Loop

A three-dimensional computational fluid dynamics (CFD) simulation on a supercritical CO<sub>2</sub> based natural circulation loop (scCO<sub>2</sub>-NCL) is carried out to explore the effects of various parameters (i.e., pressure and heat inputs) on instability, and to find out the possible cause of its occurrence. A geometrically square loop with a heater as heat source, and a heat exchanger as a heat sink is considered for the study. Horizontal heater and horizontal cooler configuration are chosen to analyze the most efficient and unstable loop. Obtained results from the study are found to be helpful in identifying the critical design and operating parameters that strongly affect the performance of supercritical CO<sub>2</sub> based NCL in terms of instability.

#### 3.1 Physical Model of NCL

In this investigation, a supercritical CO<sub>2</sub> based NCL (as shown in Fig. 3.1) is explored to understand the impact of heat input and operating pressures on the flow instability. All the geometrical and material specifications of the model are given in Table 3.1. The dimensions of the loop are chosen in such a way that the aspect ratio of the loop becomes unity and  $L_t/D < 300$  to make the system highly unstable (Chen 1985a; Vijayan et al. 2008). These design choices enable us to capture a wide range of instability in NCL. Figure 3.1 shows a rectangular NCL schematic consisting of a heater, a left leg, a cold heat exchanger (CHX), and a right leg. The loop fluid is heated from bottom at heater with constant heat input, and is cooled sensibly at top by rejecting heat to the external fluid (water) in the cold heat-exchanger (CHX). At the heat-exchanger, water is used as a coolant at a fixed rate of 0.038 kg/s to ensure the turbulent flow.

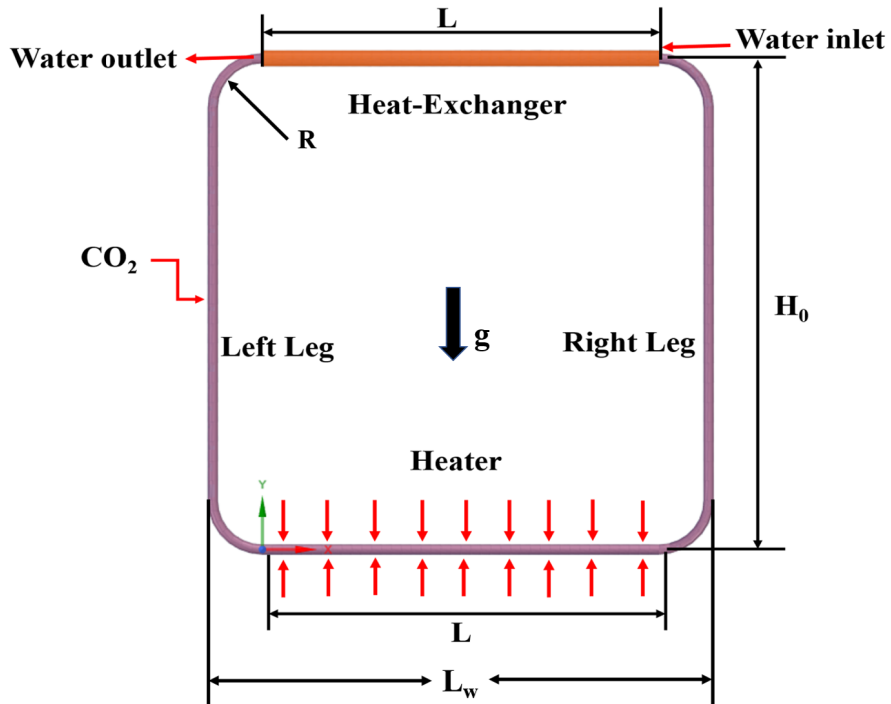


Figure 3.1: Schematic of NCL analyzed in the present study.

Table 3.1: Geometrical specification of loop used in present study.

Parameters	Values
CHX	
Inner tube diameter	16 mm
outer tube diameter	22 mm
Length of heat-exchanger ( $L$ )	400 mm
Height of loop ( $H_0$ )	500 mm
Length of heater ( $L$ )	400 mm
Width of the loop ( $L_w$ )	500 mm
Diameter of loop ( $d$ )	10 mm
Curvature radius of the bend ( $R$ )	50 mm
Total length of loop ( $L_t$ )	1914 mm
Material of loop	Stainless steel

### **Grid independence study**

The geometry modelled for CFD simulation involves primary side fluid (scCO<sub>2</sub>) region, pipe thickness and secondary side cold heat-exchanger fluid (water) region. For a grid independence study, a sensitivity analysis has been carried out to reach the solution's independence from the adopted grid. Mesh was started with a coarse mesh and gradually refined until an independent mesh result was obtained. The meshing of a three-dimensional geometry is done using the design modeler of the ANSYS 19.0 software. Figure 3.2 shows the meshing of a cross-section at CHX for both water and the CO<sub>2</sub> side. For the CO<sub>2</sub> side, a minimum grid size of 0.25 mm is taken in a radial direction near the wall, increasing to a maximum grid size of 1 mm away from the wall. A uniform grid size of 1 mm is considered for water side due to its marginal property variation. Coarse meshing is adopted in the axial direction (1 mm grid size in horizontal pipes including bends and 2 mm for vertical pipes). Mesh generation yielded a total of 400,704 nodes.  $Y^+$  and  $Y^*$  values have been checked to ensure the optimal choice of fineness of the grid. Their values are checked for the heat input of 1500 W and found to be 38.39 and 38.1 for  $Y^+$  and  $Y^*$  respectively, which ensure that the grid is suitable for assuming a standard wall function near the wall. To deal with the turbulence models near-wall region is to use the wall functions. Wall functions are equations empirically derived and used to satisfy the physics in the near-wall region. The first cell center needs to be placed in the log-law region to ensure the accuracy of the results. Wall functions are used to bridge the inner region between the wall and the turbulence fully developed region. When using the wall functions approach, there is no need to resolve the boundary layer causing a significant reduction of the mesh size and the computational domain. First grid cell needs to be  $30 < y^+ < 300$  (if this is too low, the model is invalid, if this is too high, the wall is not properly resolved, [Sarkar and Basu \(2017\)](#)). To ensure the optimal choice of fineness of the grid, a minimum value of 38.39 for  $Y^+$

value has been used with standard wall function near the wall.

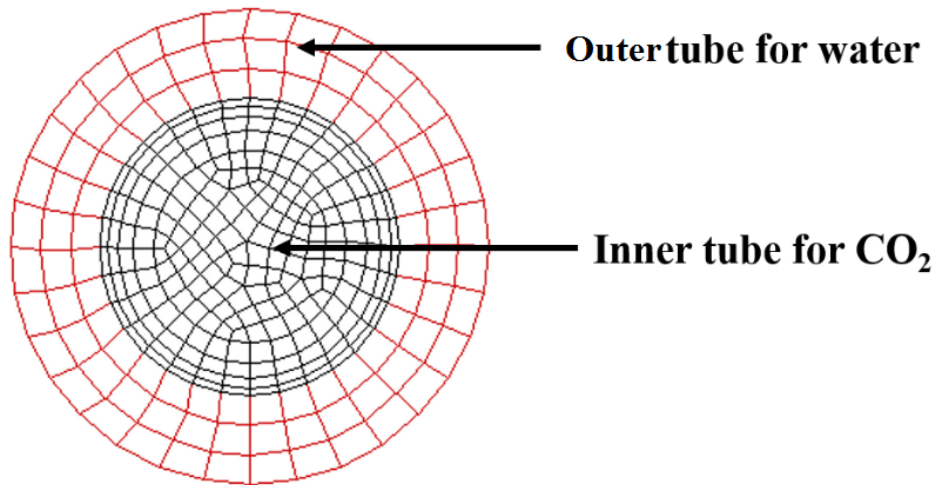


Figure 3.2: Mesh generated at cross section of a heat exchanger.

Grid independence test (as shown in Fig. 3.3) is carried out to ensure the reliability of obtained results.

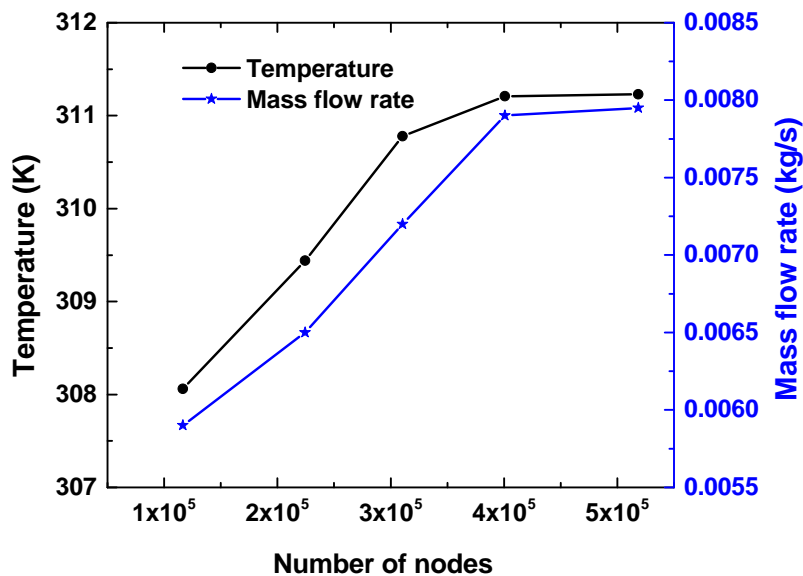


Figure 3.3: Grid independence study at 90 bar and heat exchanger inlet temperature of 305 K for 1500 W heat input.

The grid-independent study results are performed using the grid convergence index

(GCI) method proposed by (Roache 1986). This method is based on the application of Richardson's extrapolation, in which as the grid is refined (grid cells become smaller and the number of cells in the flow domain increase), the spatial and temporal (in unsteady numerical simulations) discretization errors approach to zero asymptotically. The error estimated of NCL with GCI method (Roache 1986, 1994) is 1.6 % with the mesh generated using 400,704 nodes.

With the mesh consisting of 400,704 nodes, time step independence study was then performed. The flow initiation transient in the model configuration was computed with time steps of 0.5 s, 1 s and 2 s at an operating pressure of 100 bar and a heat input of 1000 W. The result is shown in Fig. 3.4.

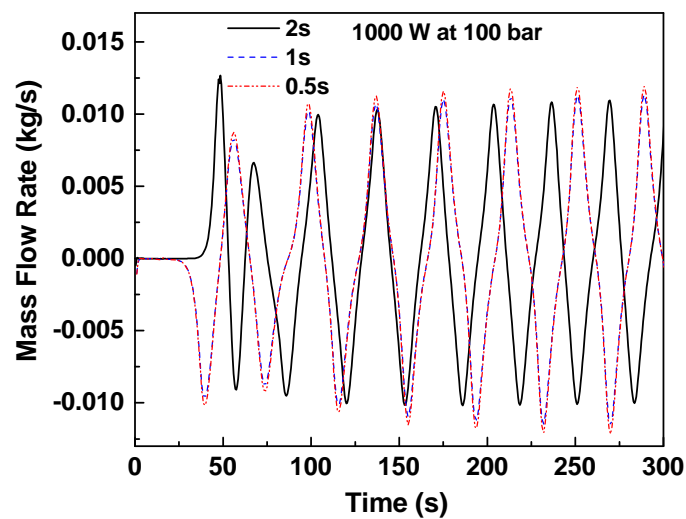


Figure 3.4: Time independent study.

It can be seen that there is barely any difference between 0.5 s and 1 s result. For computational purposes, the time step of 1 s is finally chosen.

### 3.2 Mathematical formulations

The fundamental conservation equations (mass, momentum and energy) solved for the simulation are given below. The commercial software ANSYS (FLUENT) V-19.0 is

employed to solve these equations with the associated boundary specifications. The mass conservation equation can be given as:

$$\frac{\partial \rho}{\partial t} + \nabla \cdot (\rho \mathbf{V}) = 0 \quad (3.1)$$

Momentum Conservation:

$$\frac{\partial (\rho \mathbf{V})}{\partial t} + \nabla \cdot (\rho \mathbf{V} \mathbf{V}) = -\nabla p + \nabla \cdot (\bar{\bar{\tau}}) + \rho g \quad (3.2)$$

Where the stress tensor ( $\bar{\bar{\tau}}$ ) can be defined as

$$\bar{\bar{\tau}} = \mu \left[ (\nabla \mathbf{V} + \nabla \mathbf{V}^T) - \frac{2}{3} \nabla \cdot \mathbf{V} \mathbf{I} \right] \quad (3.3)$$

Second term in stress tensor is the effect of volume dilation, and  $\mathbf{I}$  is the unit tensor.

Energy ( $E$ ) equation is given as

$$\frac{\partial (\rho E)}{\partial t} + \nabla \cdot [\mathbf{V} (\rho E + p)] = \nabla \cdot (\lambda_{eff} \nabla T + \bar{\bar{\tau}} \cdot \mathbf{V}) \quad (3.4)$$

Where  $E$  can be written as

$$E = \int_{T_{eff}}^T C_p dT + \frac{V^2}{2} \quad (3.5)$$

### **Turbulence Model**

Turbulence models for supercritical fluids are in a developing stage. In previous studies ([Chen et al. \(2010\)](#); [Yadav et al. \(2012a\)](#); [Chen et al. \(2014\)](#)) have used the Renormalization Group (*RNG*)  $k$ - $\varepsilon$  model for scCO<sub>2</sub>-NCL and achieved accurate results.

Governing equations for the RNG  $k$ - $\varepsilon$  model include two equations.



Turbulent kinetic energy equation

$$\frac{\partial}{\partial t} \rho k + \frac{\partial}{\partial x} \left( \rho u k - \frac{\mu_T}{\sigma_\kappa} \frac{\partial k}{\partial x} \right) + \frac{\partial}{\partial y} \left( \rho v k - \frac{\mu_T}{\sigma_\kappa} \frac{\partial k}{\partial y} \right) + \frac{\partial}{\partial z} \left( \rho w k - \frac{\mu_T}{\sigma_\kappa} \frac{\partial k}{\partial z} \right) = G - \rho \varepsilon \quad (3.6)$$

Where

$$G = \mu_T \left( 2 \left[ \left( \frac{\partial u}{\partial x} \right)^2 + \left( \frac{\partial v}{\partial y} \right)^2 + \left( \frac{\partial w}{\partial z} \right)^2 \right] + \left( \frac{\partial u}{\partial y} + \frac{\partial v}{\partial x} \right)^2 + \left( \frac{\partial u}{\partial z} + \frac{\partial w}{\partial x} \right)^2 + \left( \frac{\partial v}{\partial z} + \frac{\partial w}{\partial y} \right)^2 \right) \quad (3.7)$$

Turbulent kinetic energy dissipation equation

$$\frac{\partial}{\partial t} \rho \varepsilon + \frac{\partial}{\partial x} \left( \rho u \varepsilon - \frac{\mu_T}{\sigma_\varepsilon} \frac{\partial \varepsilon}{\partial x} \right) + \frac{\partial}{\partial y} \left( \rho v \varepsilon - \frac{\mu_T}{\sigma_\varepsilon} \frac{\partial \varepsilon}{\partial y} \right) + \frac{\partial}{\partial z} \left( \rho w \varepsilon - \frac{\mu_T}{\sigma_\varepsilon} \frac{\partial \varepsilon}{\partial z} \right) = c_{1\frac{\varepsilon}{\kappa}} G - c_2 \rho \frac{\varepsilon^2}{\kappa} - R \quad (3.8)$$

where

$$R = \frac{c_\mu \eta^3 \rho \left( 1 - \eta / \eta_0 \right) \varepsilon^2}{\kappa (1 + \beta \eta^3)} \quad (3.9)$$

$$\eta = \frac{S \kappa}{\varepsilon} \quad \text{and} \quad S = \frac{1}{\sqrt{2}} \left( \frac{\partial u}{\partial y} + \frac{\partial u}{\partial z} + \frac{\partial v}{\partial x} + \frac{\partial v}{\partial z} + \frac{\partial w}{\partial x} + \frac{\partial w}{\partial y} \right) \quad (3.10)$$

where the values of constants are as follows :

$$\eta_0 = 4.8, \beta = 0.012, c_\mu = 0.0845, \sigma_\varepsilon = \sigma_\kappa = 0.7178, c_1 = 1.42 \text{ and } c_2 = 1.68 \quad (3.11)$$

$$\mu_T = c_\mu \rho \frac{\kappa^2}{\varepsilon} \quad (3.12)$$

The following terms are defined to describe the fluid flow and heat transfer phenomena.

Mass flow rate at any cross section is defined as,

$$\dot{m} = \int_0^A \rho_r \bar{V}_r \cdot dA' \quad (3.13)$$

The local flow velocity can be given as:

$$u_x = \frac{\int_0^A u_r |\rho_r \bar{V} \cdot dA|}{\int_0^A |\rho_r \bar{V} \cdot dA|} \quad (3.14)$$

The local temperature is given as:

$$T_x = \frac{\int_0^A T_r |\rho_r \bar{V} \cdot dA|}{\int_0^A |\rho_r \bar{V} \cdot dA|} \quad (3.15)$$

Modified Grashof number (Vijayan et al. 1995) are defines as follows:

$$Gr_m = \frac{g\beta d^3 \rho^2 Q H_0}{A\mu^3 C_p} \quad (3.16)$$

Reynolds number is calculated using below expression:

$$Re = \frac{\rho VD}{\mu} \quad (3.17)$$

The dimensionless quantity, modified Grashof number ( $Gr_m$ ) introduced in equation 3.16, serves as an indication of driving buoyancy force, whereas Reynolds number ( $Re$ ) in equation 3.17 is representative of flow inertia, which in turn, is proportional to loop friction. Hence, these two parameters are expected to suitably depict the phenomenon and hence characterize the system performance. Both being direct functions of important geometric parameters such as loop diameter and height, variation in system geometry will always get reflected in their values and hence, corresponding system response can satisfactorily be represented by them.

When there is no change in the system diameter and height,  $Gr_m = Gr_m(\beta)$ . Now  $\beta$  is a function of average loop fluid temperature, which in turn depends on loop flow rate and hence on  $Re$ . Higher value of  $Re$  implies a higher mass flow rate leading to lower temperature level of fluid, lower value of  $\beta$  and thus smaller  $Gr_m$ . So, for systems where

$Gr_m$  solely depends on  $\beta$ , profile of  $Gr_m$  and  $Re$  exhibits opposite trends.

Nusselt number is defined as:

$$Nu = \frac{\bar{h}d}{\lambda} \quad (3.18)$$

The effective thermal conductivity is calculated using  $\lambda = \alpha C_p \mu$  expression.

$\bar{h}$  is the area weighted average wall function heat transfer coefficient. It is given as

$$\bar{h} = \frac{\int_0^A h_L dA}{\int_0^A dA} \quad (3.19)$$

All the properties are calculated at the bulk mean temperature ( $T_m$ ) of loop fluid, defined as:

$$T_m = \frac{\sum_{i=1}^n T_i}{n} \quad (3.20)$$

Where  $n$  is the number of cross-sections considered in the loop.

### 3.3 Simulation detail

In the present study, a supercritical CO<sub>2</sub> based NCL with heater (at the bottom) and heat exchanger as a sink (at the top), as shown in Fig. 3.1 is investigated to comprehend heat input influence and operating pressure on the flow field. At the sink (heat exchanger), the water inlet temperature is kept at 305 K while heat input is varied from 250 W–2500 W at heater. These heat input values are typically used in a parabolic/dish type solar collectors and even in a nuclear reactor, etc. (Swapnalee et al. 2012; Sharma et al. 2013; Archana et al. 2015a). Geometry has been prepared, and transient simulations have been performed using ANSYS Fluent version 19.0.

To resolve the coupling between velocity and pressure, the pressure- implicit with the splitting of operators (*PISO*) algorithm is used (Yadav et al. 2012a). The momentum and energy parameters are iterated by a second-order upwind scheme, which calculates the value for a control volume by means of upstream values and gradients. Turbulence parameters ( $k$ ,  $\varepsilon$ , etc.) are iterated with the second-order upwind scheme. To discretize

the pressure term, *PRESTO* (Pressure staggering option) is used (Chen et al. 2010). A general Renormalization Group *RNG*  $k - \varepsilon$  model is selected to account for turbulence. The axial conduction and viscous dissipation of the flow are considered. Convergence is obtained when residuals of the all-governing equations were less than  $10^{-3}$  except energy equation which was less than  $10^{-6}$ . All the standard properties of  $\text{CO}_2$  are obtained from the NIST REFPROP software (NIST 2013). All thermophysical properties of fluid for every 2 K temperature difference are entered into the FLUENT database, and piecewise-linear interpolation is considered to obtain property at any given temperature using following equation (3.20) and the R-square of the fit for each property generally exceeds 0.999.

Any property at temperature  $T (T_2 \geq T \geq T_1)$  is given by

$$m(T) = \frac{m(T_2) - m(T_1)}{T_2 - T_1}(T - T_1) + m(T_1) \quad (3.21)$$

Where,  $m(T_1)$  and  $m(T_2)$  are the known properties at two given temperatures  $T_1$  and  $T_2$  respectively. Loop fluid, i.e.,  $\text{CO}_2$ , is kept in the supercritical region with different operating pressure 80, 90 and 100 bar. To obtain the simulation results, following assumptions/boundary conditions are considered in the analysis:

- i. Loop fluid is supercritical  $\text{CO}_2$  (pressure varies from 80 bar to 100 bar).
- ii. No-slip condition near the walls.
- iii. Left leg and right leg wall are assumed to be adiabatic.
- iv. The wall thickness is kept 3 mm.
- v. CHX inlet water temperature is supplied at 305 K.
- vi. Heat inputs at heater are varied from 250 W to 2500 W.
- vii. Coolant used in the heat-exchanger is water

### 3.4 Validation

For the validation of the obtained CFD results, two methods have been used (i)  $Re-Gr_m$  numerical correlation given by [Chen and Zhang \(2011\)](#) and experimental correlation of [Swapnalee et al. \(2012\)](#) (shown in Fig. 3.5(a)) and (ii) [Yadav et al. \(2012b\)](#) and [Filonenko \(1954\)](#) correlations for friction factor (shown in Fig. 3.5(b)). High Reynolds number is not rare for supercritical flow conditions ([Zhang et al. 2010](#)). A good agreement was found between the generated results and existing correlations, as shown in Fig. 3.5. The maximum discrepancies are found to be less than 13% with experimental correlation and 2% with numerical correlation.

Correlation suggested by [Chen and Zhang \(2011\)](#),

$$Re = 1.129(Gr_m d/L_t)^{0.3924} \quad (3.22)$$

Correlation suggested by [Swapnalee et al. \(2012\)](#),

$$Re = 1.907(Gr_m d/L_t)^{0.364} \quad (3.23)$$

Correlation for friction factor by [Yadav et al. \(2012b\)](#),

$$f = (0.7907 \ln Re - 1.868)^{-2} \quad (2700 \leq Re \leq 180000) \quad (3.24)$$

Correlation for friction factor by [Filonenko \(1954\)](#),

$$f = (0.7907 \ln Re - 1.64)^{-2} \quad (3.25)$$

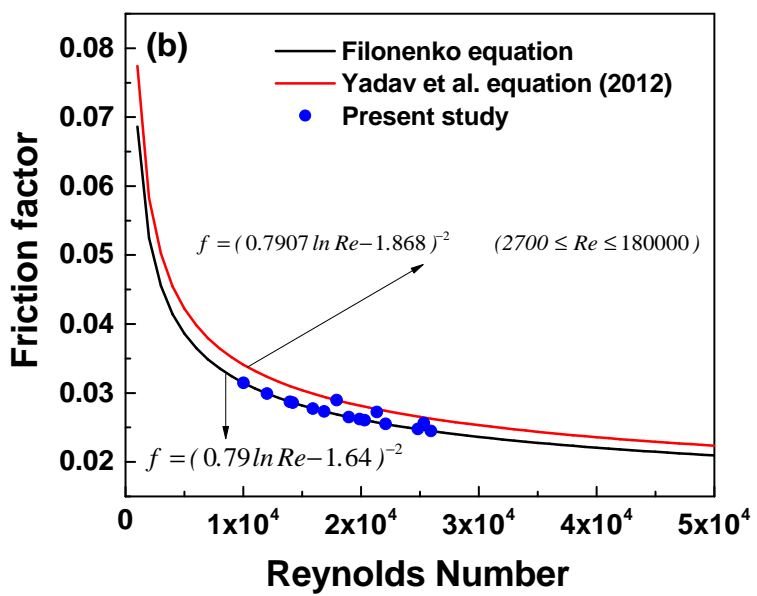
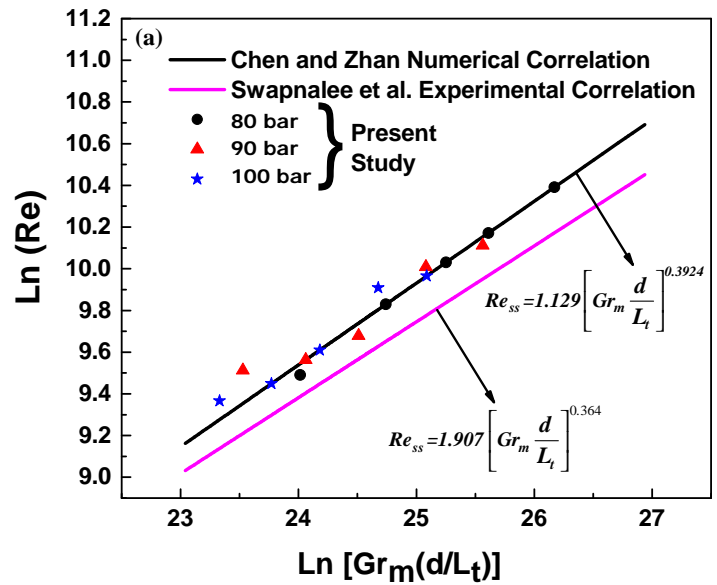


Figure 3.5: Validation of the obtained result with correlations (a)  $\ln Re$  and  $\ln(Gr_m d/L_t)$  (b) friction factor with Reynolds number.

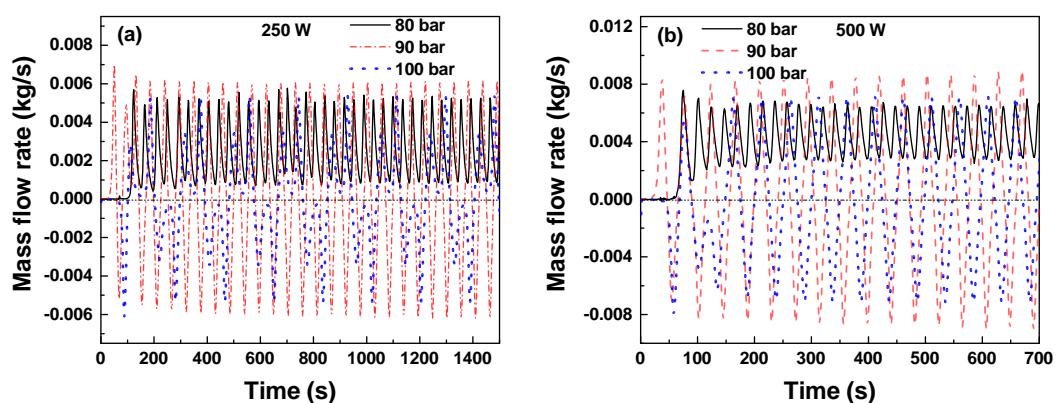
### 3.5 Results and discussion

Results are obtained at the middle of the right leg by considering the area-weighted average across the loop's cross-section. Initially, the entire loop is kept at a uniform

temperature of 305 K to ensure no flow condition to study its transient behaviour. Operating pressure of the loop is kept constant for each set of simulation carried out for the heat inputs varied from 250 W–2500 W. The transient flow behaviour of scCO<sub>2</sub> in NCL is recorded from an initial time  $t = 0$  s until repetitive unstable behaviour or steady-state is achieved. Results are also obtained for different operating pressure of 80, 90 and 100 bar in the supercritical region.

### 3.5.1 Effect of heat input

The effect of heat input on the operation of NCL can be observed in Fig. 3.6 by fixing the operating pressure value. Increase in power enhances the density differential across the heater, yielding substantial buoyancy force and hence a continuous increase in mass flow rate. For operating pressure of 80 bar, it can be observed that at lower heat inputs of 250 W and 500 W, uni-directional oscillations exist whereas, for heat inputs higher than 500 W, the loop achieves a stable steady-state. Similarly, at 90 bar and 100 bar, for lower heat inputs of 250 W, 500 W and 1000 W, the loop experiences bi-directional oscillations where flow continuously changes direction from clockwise to anti-clockwise and vice-versa.



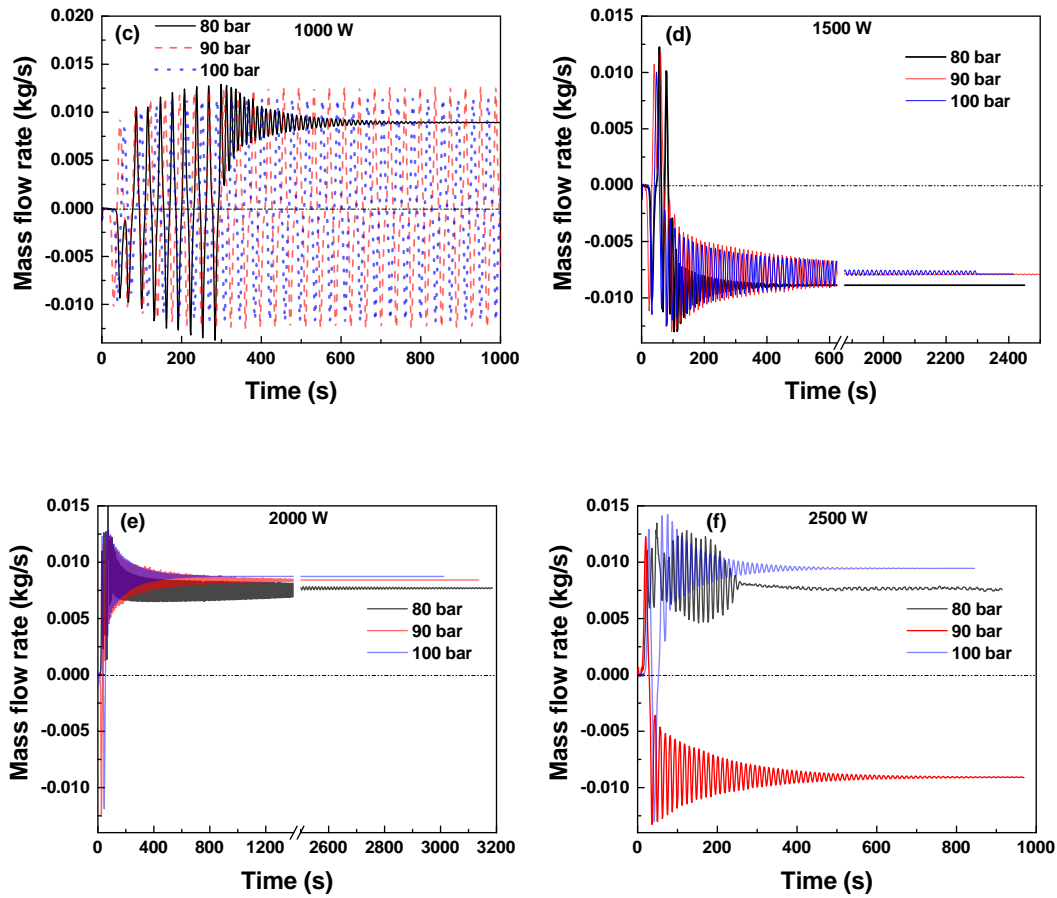


Figure 3.6: Variations of mass flow rate for different operating pressures of 80, 90 and 100 bar for supercritical CO<sub>2</sub> based natural circulation loop for different heat inputs (a) 250 W (b) 500 W (c) 1000 W (d) 1500 W (e) 2000 W and (f) 2500 W.

However, for higher heat inputs i.e., 1500 W, 2000 W and 2500 W, the flow pattern changes from oscillation to stable single-direction flow. CO<sub>2</sub> in the loop flows in one direction barring the initial transients and gradually reaches a stable state. Overall, higher heat input to NCL is required to stabilize flow at higher operating pressures considered in the study (80 to 100 bar). It can be noted that the positive value of flow rate implies anti-clockwise circulation in the NCL or upward flow at the right leg. It not easy to predict the flow direction previously in a symmetrical NCL without applying any asymmetrical flow resistance in the path. However, the direction of flow would be influenced by the Grashof or Rayleigh number.

These findings are attributed to the transition theory of supercritical NCL heating



flux effect, which indicates that there subsist transition regions for supercritical NCL configurations (Chen et al. 2010; Chen and Zhang 2011). However, this kind of flow transition or stability threshold conditions of supercritical NCL depends on many parameters such as the geometry (diameter, aspect ratio, and others), heat flux, inclination and operating procedures (Vijayan et al. 1995; Chatoorgoon et al. 2005).

One of the possible reason for this switching of direction is the interplay between buoyancy and friction. Higher power provides a greater temperature differential across the heater for a given sink temperature, resulting in a larger density difference between the vertical arms. As a result of the increased buoyancy, the loop flow rate increases. However, this is followed by an increase in frictional resistances, subsequently deciding the final flow rate is a balance between these two forces. Enhanced buoyancy always introduces, larger disturbances in the flow stream in the form of temperature and velocity, which leads to the system's inclination for unstable fluctuations. It is interesting to found that, even a stable system undergoes a flow reversal, before producing a steady flow in an particular direction. Due to the symmetric nature of the NCL geometry, warmer and lighter fluid is equally likely to reach either of the vertical arms. A substantial temperature difference is then available between the heater and cooler through the energy interaction during the initial no-flow period. That leads to a considerably large flow through the loop, which subsequently causes a rapid reduction in the temperature differential and hence a reversal in the flow direction. However, for the low heat input power frictional resistances are able to suppress the oscillations, eventually leading to steady flow. Earlier studies indicate that, in a water-based NCL, higher heat input leads to more instability (Vijayan et al. 2007). It is interesting to note that for scCO<sub>2</sub> the opposite phenomenon is found.

To get more insight, let us consider two cases at an operating pressure of 90 bar (i) periodical repetitive flow reversal at 500 W heat input and (ii) stable one-direction flow case at 2000 W heat input. Transient variation of mass flow rate versus time and its corresponding density variation at the centre of right and left leg of the loop is studied

over time duration from 600 s to 700 s in Fig. 3.7. This helps in understanding a strong correlation between mass flow rate and density in scCO<sub>2</sub>-NCL.

Comparing flow rate and density variation plots in Fig. 3.7, the maximum difference between the right and left leg density corresponds to the highest flow in the loop. This is because the flow in NCL is due to the pressure gradient caused by the density difference between its arms. This density difference leads to the buoyancy or driving force. In the case of 500 W (Fig. 3.7(c)), a region with higher density continuously switches between the left and right leg. This leads to continuous switching of the buoyancy force direction in the loop, which causes the repetitive flow reversal. However, in the case of 2000 W (Fig. 3.7(d)), it can be observed that the left leg density is always higher than the right leg, leading to flow always being in the counterclockwise direction. It is also interesting to note that in the case of Fig. 3.7(c), the points of equal density between left and right leg do not correspond to zero flow rate. This is because the fluid has built enough momentum in a particular direction and only when this inertial force is overcome by buoyancy force in the opposing direction, then flow direction changes.

The cause of bi-directional flow and density variation shown in Fig. 3.7(a) and 3.7(c) have been studied with the help of temperature contours obtained during the transient simulation. Figure 3.8 shows that the instability is a manifestation of hot pockets continuously circulating the loop. For 500 W (bi-directional flow) case, the temperature contour consists of one anti-clockwise pulse and one clockwise pulse. Due to continuous heating/cooling at the heater and cooler surface, hot plug/cold plug are formed. This hot/cold plug diffuses axially along the heater and cooler, and finally it covers the horizontal leg (refer 621 s). The hot plug enters the right vertical leg, gets accelerated and reaches half of the right vertical leg (refer 624 s). Due to momentum, it enters the top of the right vertical leg and the hot plug head enters horizontal leg (refer 628 s) and reaches a maximum flow in an anti-clockwise direction (as shown in Fig. 3.7(a)). At this time, the cold plug passes through the left leg and reaches the heater (refer 628 s), and then to the right leg (refer 637 s). After this, a small reverse and forward flow occur.

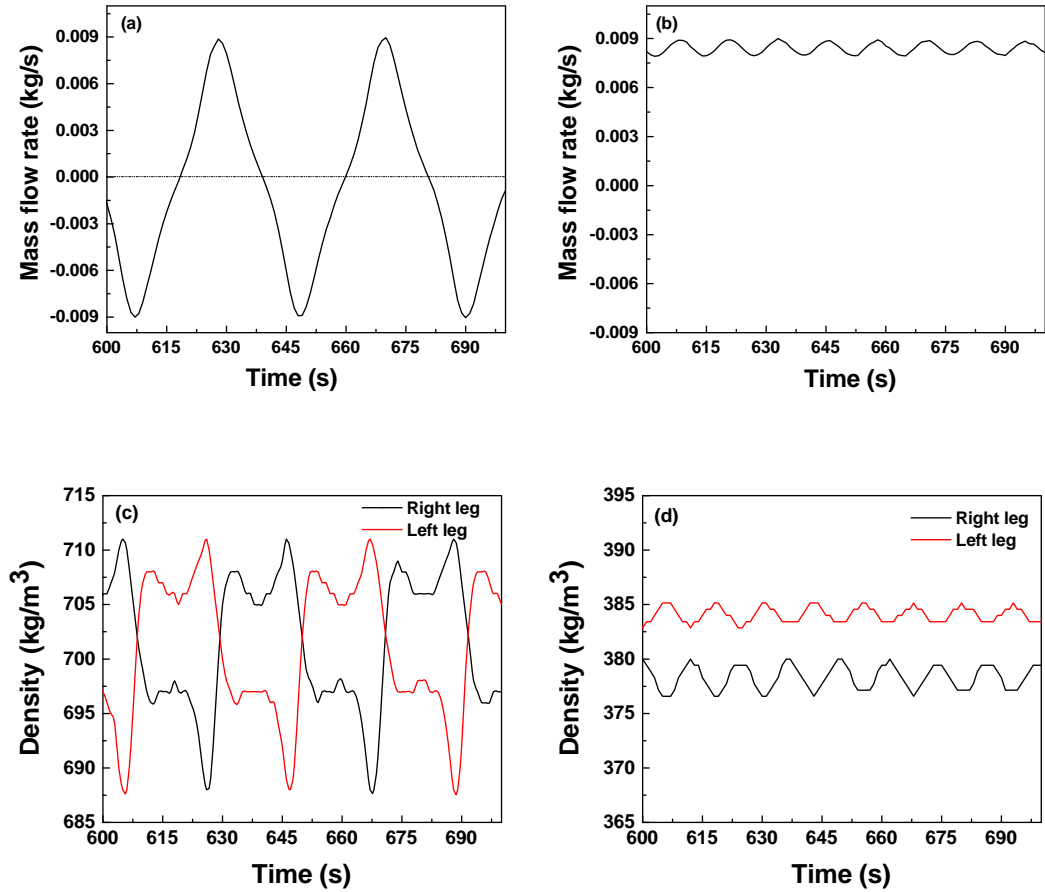


Figure 3.7: Mass flow rate variation at (a) 500 W and (b) 2000 W and density variation at (c) 500 W and (d) 2000 W heat input at 90 bar.

Due to rapid heating of fluid, hot plug gets quickly formed in the heater, and the newly formed hot plug will enter the left vertical leg (refer 646 s). Due to the presence of cold plug at the bottom of the right vertical leg, the newly formed hot plug enters the top of the left vertical leg and reaches a maximum flow in a clockwise direction (refer 649 s). Then the whole cycle is repeated. Continuation of this entire process leads to bi-directional oscillations at this heat input. Hence the creation of hot/cold plugs is the primary cause of instability.

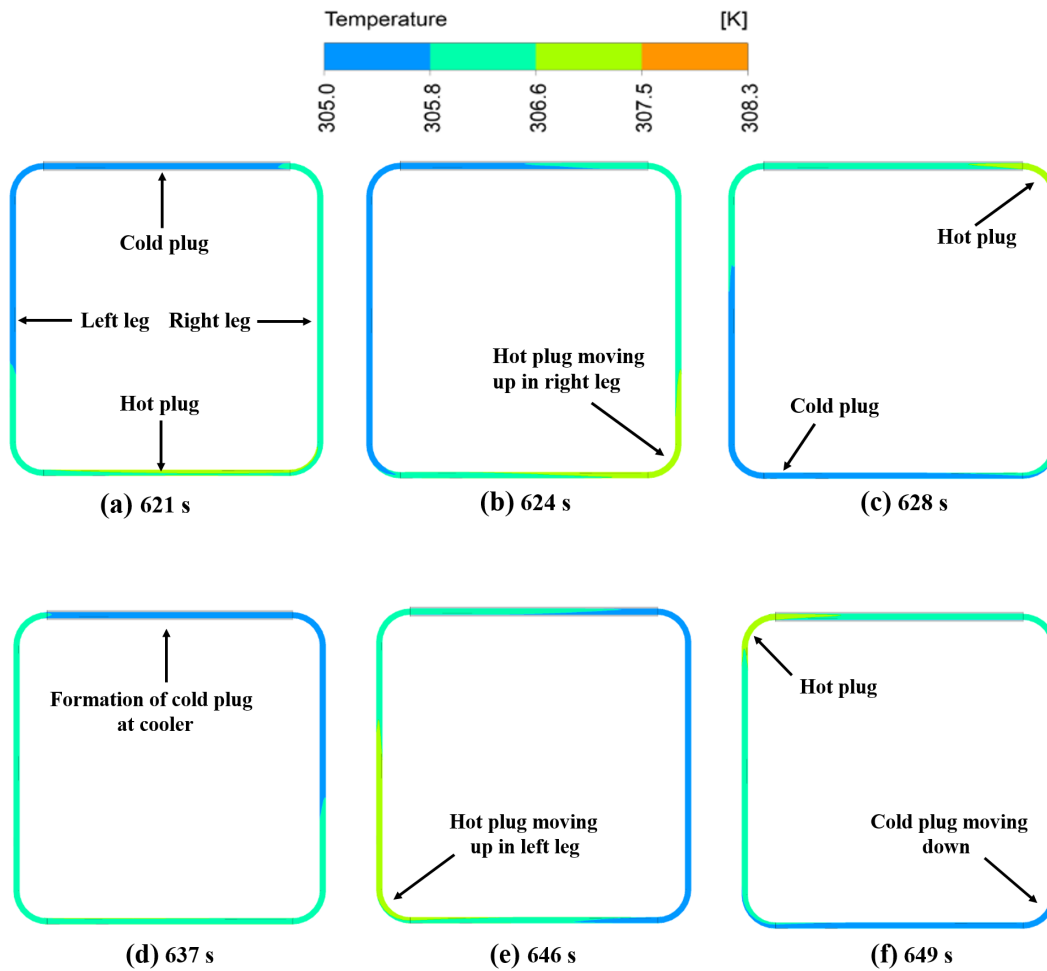


Figure 3.8: Temperature contour in a central vertical plane at different time instances for 500 W at operating pressure of 90 bar.

### 3.5.2 Temperature variation

The variation of the average temperature inside the heater and cooler is plotted in Fig. 3.9 for various heat inputs at 90 bar. Buoyancy forces cause the initial overshoot in temperature due to the longer period of heat-accumulation. This kind of typical overshoot found at the beginning of flow shows the natural convection phenomenon (Yoshikawa et al. 2005; Chen et al. 2010). The flow pattern of temperature also varies in a different mode as the response to heat input changes.

The temperature oscillates vigorously in the initial stage of imposing the heat input at source and later on it continuously fluctuates periodically for 500 W and 1000 W (as shown in Fig. 3.9(a-b)) or slowly converges to a fixed value for 1500 W and 2000 W

(for Fig. 3.7(c-d)). This typical repetitive flow reversal was first studied by (Welander 1967). The periodic fluctuation is caused by the movement of hot/cold plugs in the loop, as shown in Fig. 3.8. It is found that the heater and cooler temperature overlap each other, and temperature fluctuations in heater and cooler show a similar trend. However, overlaps are found only for unstable flow cases, while for stable cases the temperature of the heater and cooler separate from each other. It can be seen that the average heater temperature magnitude is slightly higher than the cooler temperature for unstable cases. The flow rate variation at 1500 W and 2000 W (as shown in Fig. 3.6(d) and Fig. 3.6(e)) indicates that the loop attains uni-directional flow after initial flow reversal. The average temperature of the loop is also observed to be increasing with heat input. Once the temperature inside the heater reaches a certain value, and the fluid moves into one of the vertical legs, the considerable increase in buoyancy force leads to a high flow rate in a particular direction. It has been observed from Fig. 3.8 that hot/cold plugs get formed due to higher residence time inside the heater/cooler. The very low flow rate during flow reversal leads to higher residence time, and this phenomenon is prevented at higher heat inputs due to the unidirectional flow.

For example consider 1500 W (Fig. 3.9(c)), near 100 s observed a very high temperature inside the heater. This hot fluid on entering the left leg causes a significant increase in flow in a clockwise direction (as shown in Fig. 3.6(d)), and the flow eventually stabilizes in this direction. Higher friction can counter the change in buoyancy force's direction when the hotter fluid moves to the right leg. The absence of fluctuations or overlaps show the decay of unsteady heat transfer and oscillations, which contribute to the stabilization of NCL flow. Unidirectional flow leads to better heat transfer in the loop both in heater and cooler, and hence the loop reaches the steady-state faster.

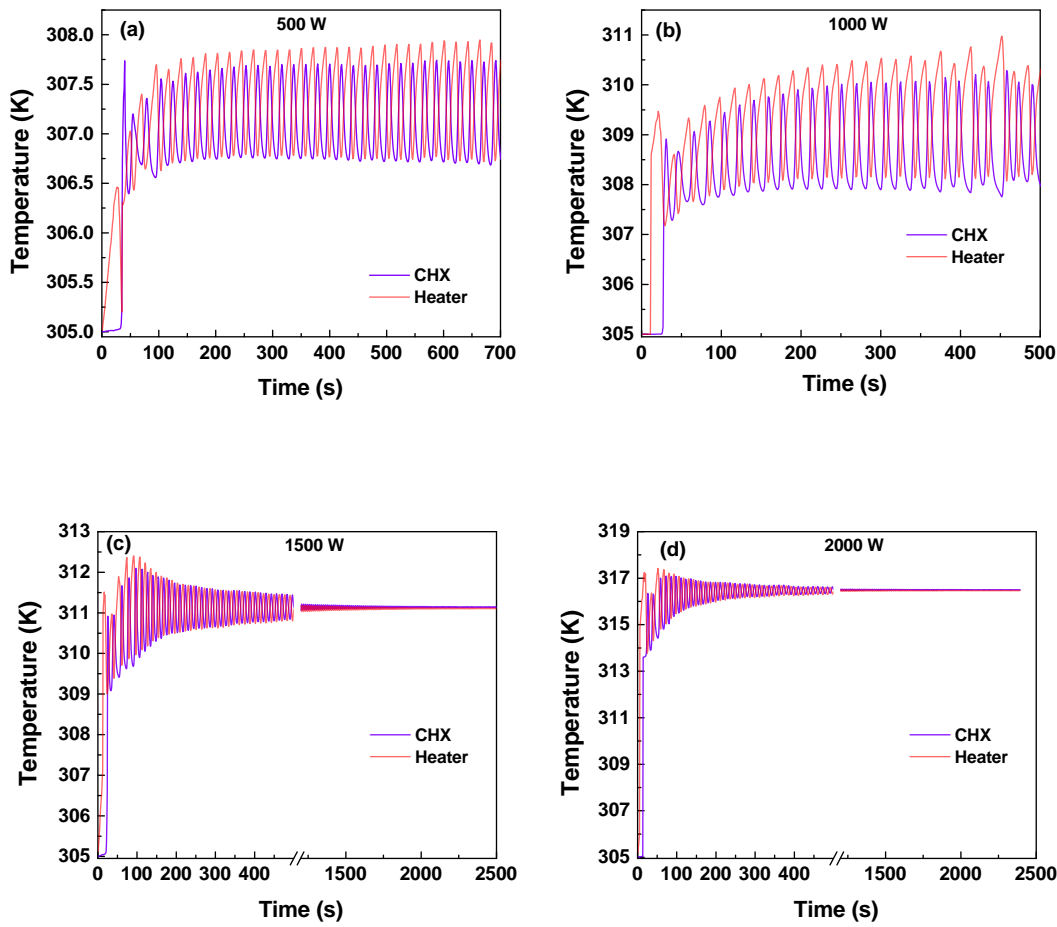


Figure 3.9: **Temperature** variation at (a) 500 W and (b) 2000 W and density variation at (c) 500 W and (d) 2000 W heat input at 90 bar.

### 3.5.3 Effect of operating pressure

The fluid flow dynamics of the NCL significantly depend on the operating pressure. The idea for pressure variation behind this analysis is to produce disruptions in the regular operational condition of NCL that may be attributed to changes in loading conditions in natural circulation systems or occurrence of a perturbation in the system during start-up and shutdown activities. Different operating pressures of 80 bar, 90 bar and 100 bar were studied for all heat input ranging from 250 W to 2500 W as shown in Fig. 3.6. It is found that for heat inputs greater than 1000 W, the loop is stable for all operating pressures considered in the study. Considering lower heat inputs, uni-directional fluctuations are observed at 80 bar, whereas at 90 bar and 100 bar, bidirectional fluctuations

are observed. An explanation for this is attempted using hot plug theory as well as the abrupt change in various thermo-physical properties in the operating temperature range.

Let us consider the case of 500 W and study the influence of operating pressure. Figure 3.10 shows the temperature variation at the centre of the right leg for various operating pressures.

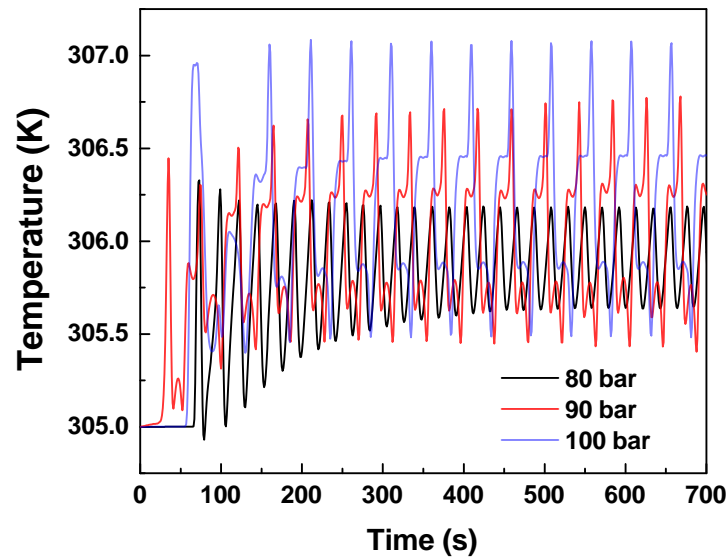


Figure 3.10: Transient Temperature variation for various operating pressures for 500 W.

It can be seen that the variation increases with increase in pressure. The characteristics of a hot plug at various operating pressures provides more insight on stability behavior. To study this, temperature contours have been plotted for time stamps corresponding to a half cycle in periodic mass flow rate variation. Contours are plotted for all three operating pressures and have a uniform temperature range of 305 K to 310 K, as shown in Fig. 3.11. This temperature range is near to the pseudocritical temperature of 80 bar, at which specific heat capacity and volumetric expansion coefficient are very high. It may be inferred that the system operated near critical/pseudocritical region to obtain faster stable condition.

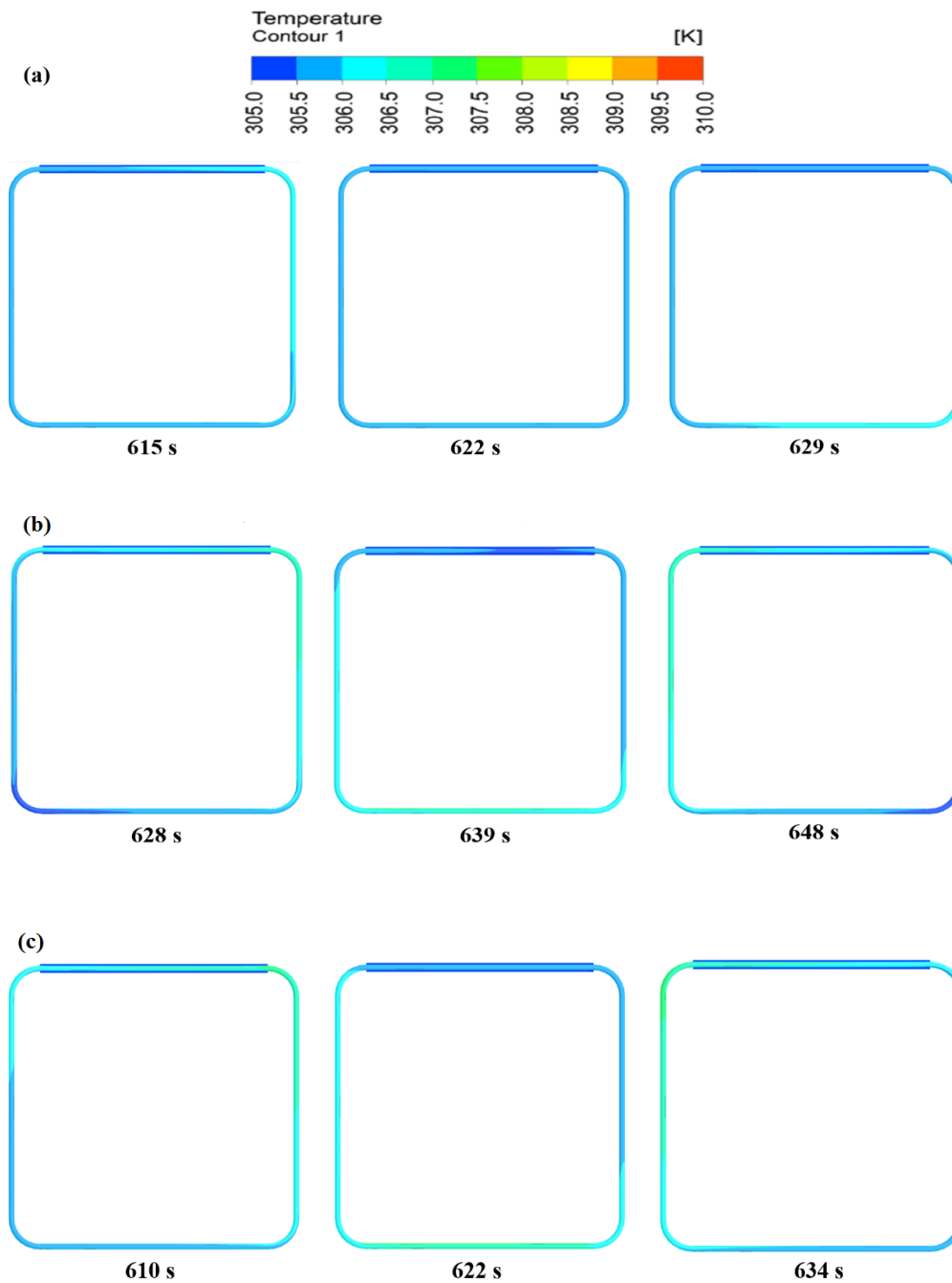


Figure 3.11: Temperature contours at 500 W at various operating pressures of (a) 80 bar, (b) 90 bar and (c) 100 bar at different time intervals.

From contour (Fig. 3.11), it is observed that the hot plug temperature in case of 90 and 100 bar is slightly higher than that of 80 bar. As this hot plug moves from one leg to another, the direction of buoyancy force reverses leading to flow reversal.

The large temperature variation for 90 bar and 100 bar in Fig. 3.10 occurs due to the



combined effect of abrupt change in thermophysical properties and lower  $C_p$  value compared to 80 bar. In the case of 80 bar, due to the higher  $C_p$  (Fig. 3.12), the temperature of a hot plug is lesser, and due to higher volumetric expansion coefficient, the buoyancy force is higher, which play major roles in preventing the flow reversal. Since heat input is the same for all three operating pressures, the magnitude of flow rate or inertial force is almost the same. Flow reversal happens if the hot pocket temperature after passing the cooler is high enough to counter the inertial force.

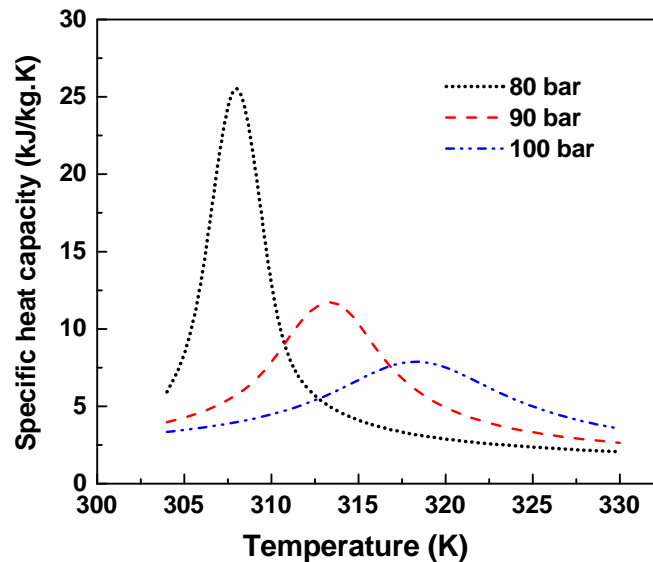


Figure 3.12: Variation of  $C_p$  with temperature for various operating pressures (NIST 2013).

Friction is considered as a stabilizing factor for subcritical fluid (mainly liquid water). In the case of strong buoyancy force in supercritical fluid, the same concept may not be appropriate. With the effect of strong buoyancy force, fluid gains momentum and flow becomes unidirectional (stable) at the early stage of the flow. Such behavior is observed for all the cases of higher heat inputs in the study. For subcritical fluid, it is reversed; for higher heat input, flow becomes more unstable. At higher  $L/d$  ratio, subcritical loops are stable (Vijayan et al. 2008), but in the case of supercritical fluids,

higher diameter loops show more stability than smaller diameter loops (Chen and Zhang 2011) i.e.; Smaller diameter means more friction.

To further confirm the effect of operating pressure on instability, amplitude and frequency analysis of all unstable data obtained during the study is carried out. A parameter 'Measure of Instability' is used to compare the unstable mass flow oscillation for various cases.

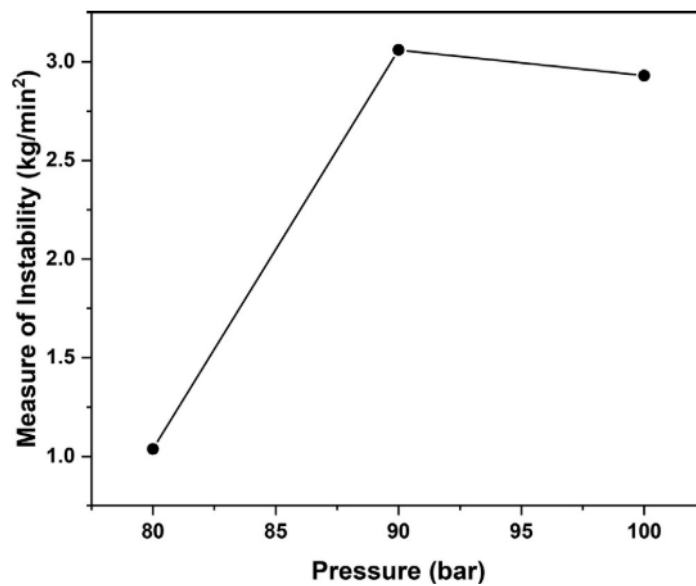


Figure 3.13: Measure of Instability.

It is defined as:

$$\text{Measure of instability} = \frac{\text{Amplitude of mass flow oscillation}}{\text{Time interval between extreme of mass oscillation}}$$

$$= \frac{\dot{m}_1 - \dot{m}_2}{t_1 - t_2}$$

Where  $\dot{m}_1$  and  $\dot{m}_2$  correspond to a maximum and minimum mass flow oscillation after a consistent mass flow pattern is formed at its corresponding time instance value of  $t_1$  and  $t_2$ . It can be observed from the Fig. 3.13 that the measure of instability for 80 bar is much lower compared to 90 bar and 100 bar at 500 W. This study supplements the observation that beyond a threshold operating pressure, bi-directional pulsations are

observed in the system leading to a higher degree of instability. Increase in pressure beyond this point does not lead to significant change in instability behaviour of the loop.

### 3.5.4 Nusselt number

To discuss the present system's heat transfer behaviour, the variation in Nusselt number ( $Nu$ ) at different operating pressure and heat inputs calculated at the cooler section is shown in Fig. 3.14.

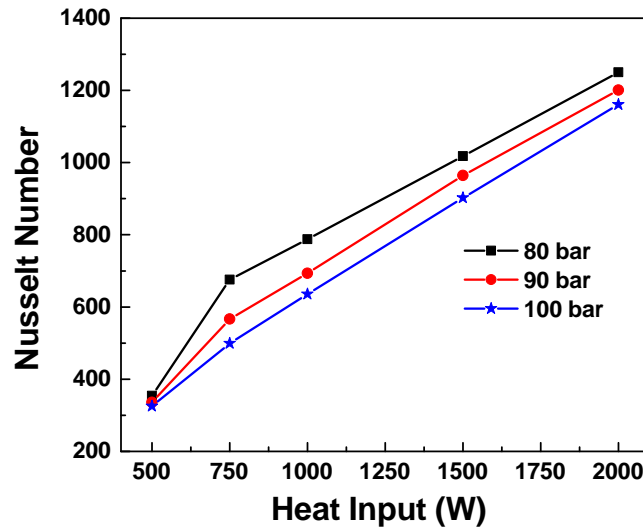


Figure 3.14: Variation of Nusselt number at different heat inputs and operating pressures.

Results show the trend of increase in  $Nu$  with an increase in heat inputs, decreasing with an increase in operating pressure. Higher  $Nu$  indicates a better heat transfer performance and hence a more effective natural convection phenomenon.

### 3.6 Summary

The following conclusions are drawn from the present work:

- i. For  $scCO_2$ -NCL, there exists a threshold heat input value at which the loop switches from unstable bi-directional or uni-directional fluctuations to stable flow.

- ii. In the range of operating pressure (80-100 bar) considered in the study, it is advisable to operate scCO<sub>2</sub>-NCL at a lower supercritical pressure to get minimum instability. The study noticed that operation at lower pressure led to unidirectional pulsations, whereas bidirectional oscillations were observed at higher pressures.
- iii. Hot pockets at higher temperature led to more instability in the loop.
- iv. Nusselt number shows that the loop's heat transfer capability is more at low operating pressure.

## CHAPTER 4

### Stability Enhancement of Supercritical CO<sub>2</sub> based Natural Circulation Loop using a Modified Tesla Valve

This chapter deals with the comparative investigation of instability phenomenon in supercritical CO<sub>2</sub> based regular natural circulation loop (scCO<sub>2</sub>R-NCL) and a new modified Tesla natural circulation loop (scCO<sub>2</sub>T-NCL). Fluid flow behaviour and performance of both the loops are determined over a range of pressures (80 to 100 bar) and heat inputs (500 to 2000 W). The present study focuses on the directional stability of loop fluid (scCO<sub>2</sub>) by creating an asymmetrical flow resistance in a NCL with the help of a modified Tesla valve. The purposes of this investigation are: (i) to check the suitability of the Tesla valve for NCL and to investigate its effect on instability, (ii) to study the scCO<sub>2</sub> flow behaviour at different heat inputs, and (iii) to compare the effect of operating pressure on instability. It is found that in a scCO<sub>2</sub>T-NCL, there exists a pressure drop along with the Tesla valve, which changes the system from having unstable repetitive oscillatory flow into a unidirectional flow at all heat inputs and operating pressures considered in the study.

#### 4.1 Physical model of NCL

Figure 4.1 illustrates two NCLs: (a) Regular natural circulation loop (scCO<sub>2</sub>R-NCL) and (b) Tesla valve natural circulation loop (scCO<sub>2</sub>T-NCL) in which a modified Tesla valve incorporated in the left leg. Both loops are investigated to comprehend the impact of heat input and operating pressure on the flow instability of a scCO<sub>2</sub>-NCL. Regarding the loop topology, all the geometrical parameters for the model presented in Fig. 4.1 are given in Table 4.1. The design and dimensions of the Tesla valve are indicated in Fig. 4.2 and Table 4.2, respectively. The diodicity of the scaled-up design tesla valve used in this study is shown in Fig. 4.3.

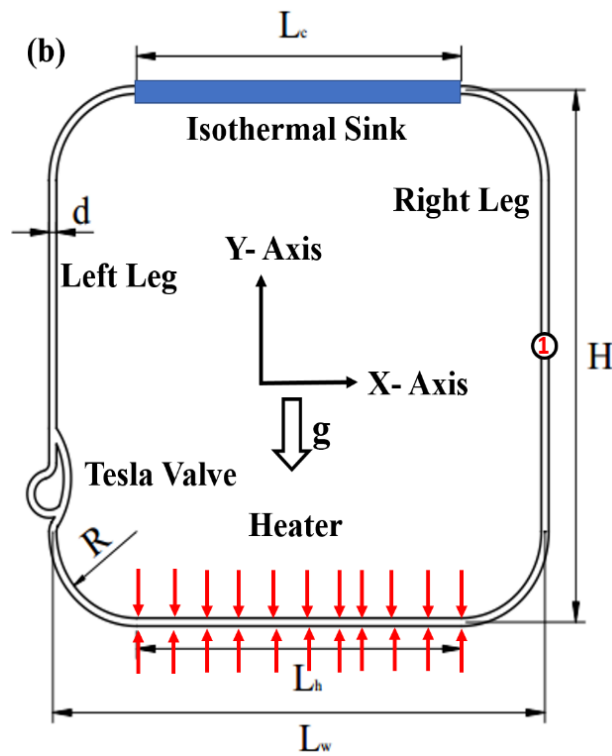
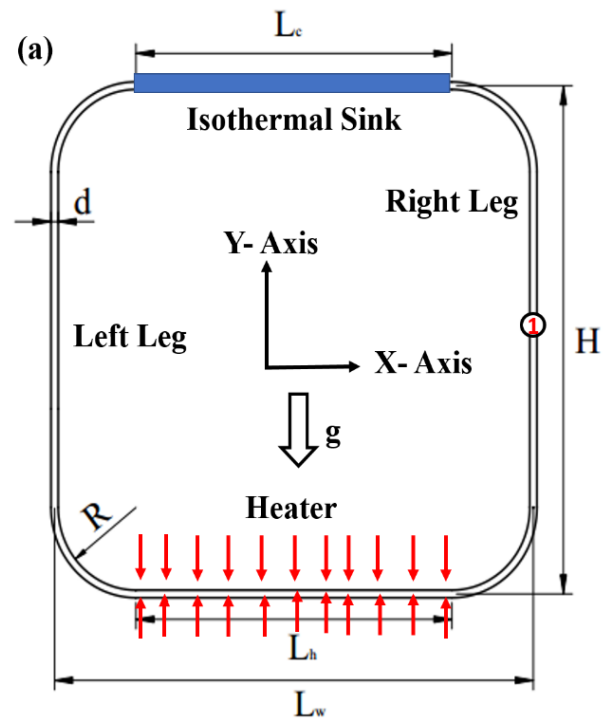


Figure 4.1: Schematic of (a) Regular natural circulation loop (scCO<sub>2</sub>R-NCL) (b) Tesla valve natural circulation loop (scCO<sub>2</sub>T-NCL).

## 4.2 Modified Tesla valve for NCL

While doing the preliminary study on the regular-NCL (R-NCL) for scCO<sub>2</sub>, it was found that the loop is highly turbulent with  $Re$  ranging from 80,000 –160,000, and D-type of Tesla valve was found to be highly effective for these  $Re$ . Thus, this valve has been chosen for the current study, and a scaled-up model is employed in the present study for scCO<sub>2</sub>-NCL. The scaling of the Tesla valve is dependent only on the loop diameter and is independent of loop length.

Table 4.1: Geometrical specification of loop used in present study

Parameters	Values (mm)
Inner diameter of the loop ( $d$ )	15
Length of heater ( $L_h$ )	660
Length of isothermal sink ( $L_c$ )	660
Width of the loop ( $L_w$ )	1000
Height of loop ( $H$ )	1000
Radius ( $R$ )	162.5
Vertical distance from horizon for the ①	500

The left valve channel is known as the side channel, and the primary channel is on the right. The intersections of the channels are allocated as J1 and J2 (shown in black). Principle rules for improving diodicity are the alignment of the side channels with the primary channel in junction J2, so that a substantial quantity of fluid enters the side channel for reverse flow. When fluid moves in the forward direction, the design of the valve forces most of the fluid to move in the right (primary) channel. However, in the reverse direction, fluid splits into both arms, and fluid in the left channel opposes fluid moving in the right channel at junction J1. So, fluid experiences higher resistance (pressure drop) when moving in the reverse direction.

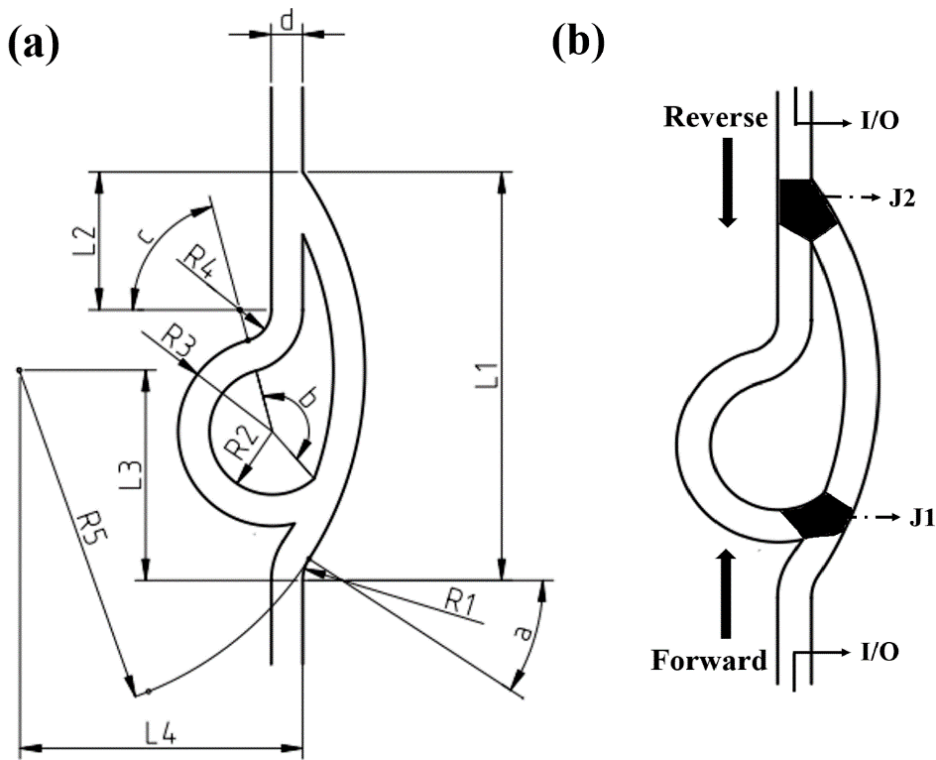


Figure 4.2: (a) Design of scaled model of Tesla valve [Vries et al. \(2017\)](#) used in present study (dimensions are given in Table 4.2). (b) Forward and reverse flow directions are indicated and channel junctions 1 and 2 ( $J1$ ,  $J2$ ) are shown by black region. Inlet and outlet for the valve are indicated with I/O.

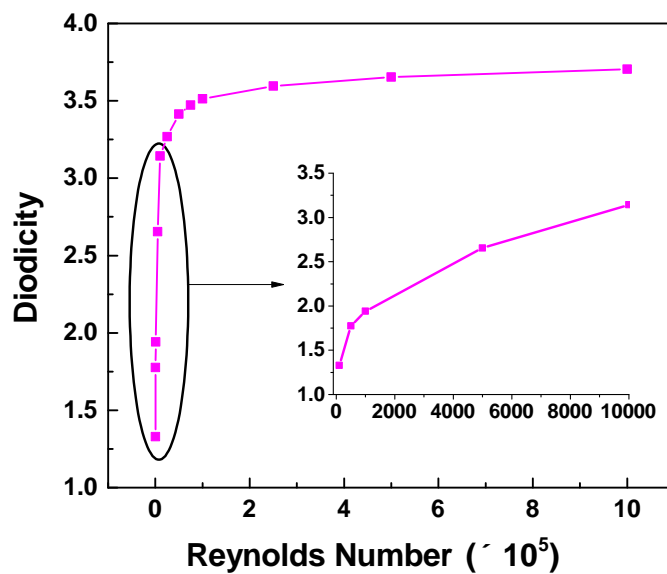


Figure 4.3: Diodicity of Tesla valve design for supercritical  $CO_2$  at 90 bar with different Reynolds numbers.



Table 4.2: Geometrical parameters of Tesla valve used in the study.

Parameter	Dimensions
d	15 mm
L1	199.43 mm
L2	65.64 mm
L3	100.07 mm
L4	135.02 mm
R1	Radius 18.75 mm
R2	Radius 30 mm
R3	Radius 15 mm
R4	Radius 165 mm
a	Angle = 33°
b	Angle = 153°
c	Angle = 75°

To picturize the working of the modified Tesla valve, fluid flow analysis was done on the Tesla geometry at Reynolds number of 100,000 with supercritical fluid CO<sub>2</sub>. Such high Reynolds numbers are common in supercritical CO<sub>2</sub> based NCL (Zhang et al. 2010). The streamlines of forward and reverse flow in the Tesla valve are shown in Fig. 4.4. In forward flow conditions, maximum fluid flow occurs from the primary channel (right side) whereas, in reverse flow, fluid splits into two parts.

Local pressure contours (as shown in Fig. 4.5) indicate that when fluid flows in a forward direction, it moves without much resistance except at the beginning of the curved portion. On the other hand, when fluid moves in a reverse direction, a high-pressure region is set up inside the valve, which acts as resistance to fluid flow.

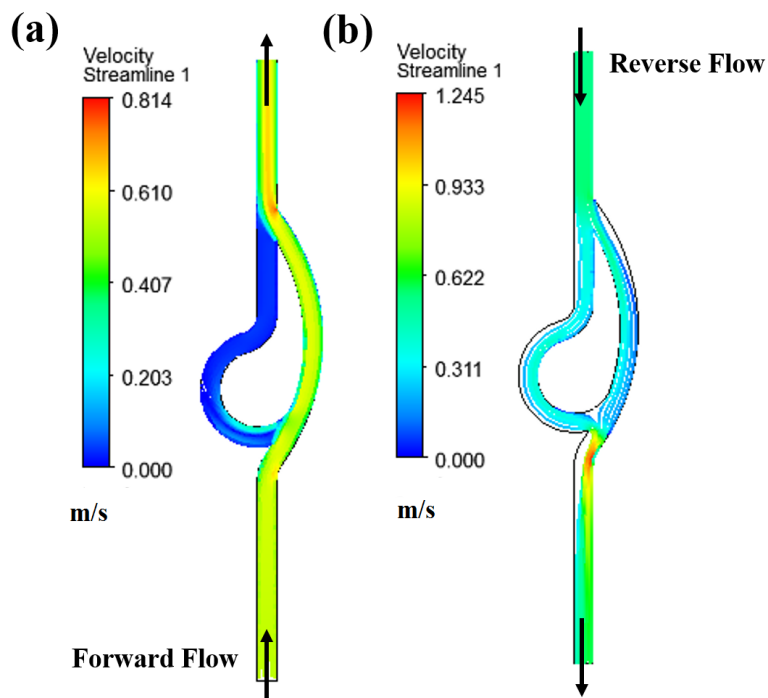


Figure 4.4: Streamlines of the flow field in Tesla valve design for a Reynolds number of 100,000 (a) Forward flow (b) Reverse flow.

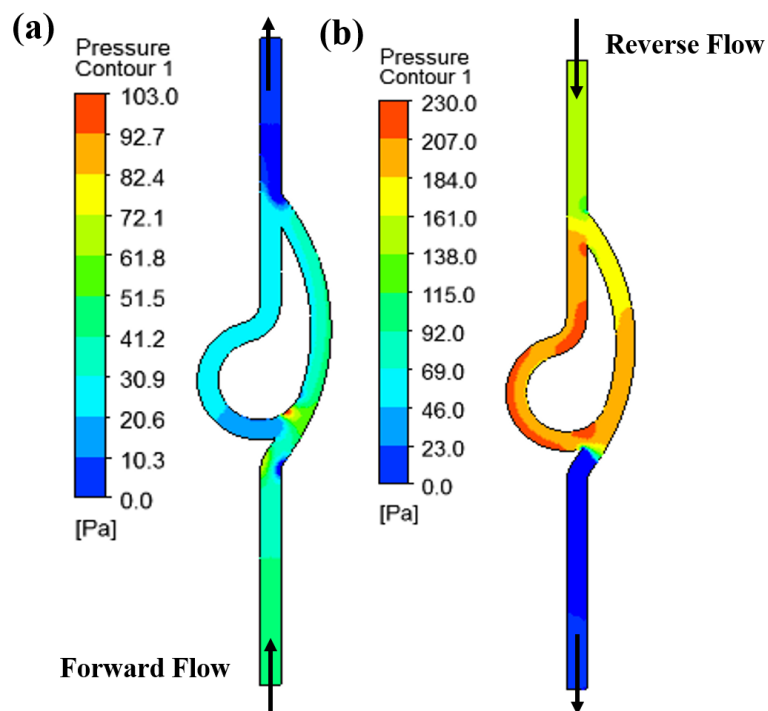


Figure 4.5: Pressure contour in Tesla valve design for a Reynolds number of 100,000 (a) Forward flow (b) Reverse flow.

In a horizontal heater with horizontal cooler (HHHC) NCL, since the system does not predetermine the circulation direction, fluid tends to take any path (clockwise or counterclockwise). Higher resistance in the reverse direction of the Tesla valve would mean that fluid will circulate in a forward direction of the Tesla valve in a HHHC NCL.

### 4.3 Mathematical Formulation

The fundamental conservation equations (mass, momentum and energy) solved for the simulation are given below. The commercial software ANSYS (FLUENT) V-19.0 is employed to solve these equations with the associated boundary specifications for two-dimensional geometry. The mass conservation equation can be given as:

$$\frac{\partial}{\partial t}\rho + \frac{\partial}{\partial x}\rho u + \frac{\partial}{\partial y}\rho v = 0 \quad (4.1)$$

Momentum Conservation:

In X-direction

$$\begin{aligned} \frac{\partial}{\partial t}\rho u + \frac{\partial}{\partial x} \left[ \rho u u - \frac{4}{3}(\mu + \mu_T) \frac{\partial u}{\partial x} \right] + \frac{\partial}{\partial y} \left[ \rho u v - (\mu + \mu_T) \frac{\partial u}{\partial y} \right] = -\frac{\partial p}{\partial x} - \frac{2}{3} \frac{\partial}{\partial x} \left( \mu \frac{\partial v}{\partial y} \right) + \\ \frac{\partial}{\partial y} \left[ (\mu + \mu_T) \frac{\partial v}{\partial x} \right] - \frac{2}{3} \frac{\partial}{\partial x} (\rho \kappa) \quad (4.2) \end{aligned}$$

In Y-direction

$$\begin{aligned} \frac{\partial}{\partial t}\rho v + \frac{\partial}{\partial x} \left[ \rho v u - (\mu + \mu_T) \frac{\partial v}{\partial x} \right] + \frac{\partial}{\partial y} \left[ \rho v v - \frac{4}{3}(\mu + \mu_T) \frac{\partial v}{\partial y} \right] = -\frac{\partial p}{\partial y} - \frac{2}{3} \frac{\partial}{\partial y} \left( \mu \frac{\partial u}{\partial x} \right) + \\ \frac{\partial}{\partial x} \left[ (\mu + \mu_T) \frac{\partial u}{\partial y} \right] - \frac{2}{3} \frac{\partial}{\partial y} (\rho \kappa) \quad (4.3) \end{aligned}$$

Energy equation is given as

$$\frac{\partial}{\partial t} \rho h + \frac{\partial}{\partial x} \left[ \rho h u - \frac{\mu_T}{Pr_T} \frac{\partial h}{\partial x} \right] + \frac{\partial}{\partial y} \left[ \rho h v - \frac{\mu_T}{Pr_T} \frac{\partial h}{\partial y} \right] = \frac{\partial p}{\partial t} + u \frac{\partial p}{\partial x} + v \frac{\partial p}{\partial y} + \frac{\partial}{\partial x} \left( \lambda \frac{\partial T}{\partial x} \right) + \frac{\partial}{\partial y} \left( \lambda \frac{\partial T}{\partial y} \right) \quad (4.4)$$

### Turbulence Model

As found in previous studies for scCO<sub>2</sub> (Chen et al. 2010), the flow Reynolds number can be as high as 10<sup>4</sup> for even a smaller temperature difference (8 K) between source and sink. However, turbulence models for supercritical fluids are less developed and still under intense study (Chen et al. 2014). Therefore, in the present simulation, a general Renormalization group (RNG)  $k$ - $\varepsilon$  model is selected as the first step to introduce the turbulent effect. The RNG  $k$ - $\varepsilon$  turbulent model is used together with standard wall function and no-slip condition near the wall. In previous studies, Chen et al. (2010); Yadav et al. (2012a); Chen et al. (2014) have used the Renormalization group (RNG)  $k$ - $\varepsilon$  for scCO<sub>2</sub>-NCL and achieved accurate results.

Governing equations for the RNG  $k$ - $\varepsilon$  model include two equations.

Turbulent kinetic energy equation

$$\frac{\partial}{\partial t} \rho k + \frac{\partial}{\partial x} \left( \rho u k - \frac{\mu_T}{\sigma_k} \frac{\partial k}{\partial x} \right) + \frac{\partial}{\partial y} \left( \rho v k - \frac{\mu_T}{\sigma_k} \frac{\partial k}{\partial y} \right) = G - \rho \varepsilon \quad (4.5)$$

where

$$G = \mu_T \left( 2 \left[ \left( \frac{\partial u}{\partial x} \right)^2 + \left( \frac{\partial v}{\partial y} \right)^2 \right] + \left( \frac{\partial u}{\partial y} + \frac{\partial v}{\partial x} \right)^2 \right) \quad (4.6)$$

Turbulent kinetic energy dissipation equation

$$\frac{\partial}{\partial t} \rho \varepsilon + \frac{\partial}{\partial x} \left( \rho u \varepsilon - \frac{\mu_T}{\sigma_\varepsilon} \frac{\partial \varepsilon}{\partial x} \right) + \frac{\partial}{\partial y} \left( \rho v \varepsilon - \frac{\mu_T}{\sigma_\varepsilon} \frac{\partial \varepsilon}{\partial y} \right) = c_1 \frac{\varepsilon}{\kappa} G - c_1 \rho \frac{\varepsilon^2}{\kappa} - R \quad (4.7)$$

where

$$R = \frac{c_\mu \eta^3 \rho \left(1 - \frac{\eta}{\eta_0}\right) \varepsilon^2}{\kappa (1 + \beta \eta^3)} \quad (4.8)$$

$$\eta = \frac{S \kappa}{\varepsilon} \quad (4.9)$$

$$S = \frac{1}{\sqrt{2}} \left( \frac{\partial u}{\partial x} + \frac{\partial v}{\partial x} \right) \quad (4.10)$$

where the values of constants are as follows :

$$\eta_0 = 4.8, \beta = 0.012, c_\mu = 0.0845, \sigma_\varepsilon = \sigma_\kappa = 0.7178, c_1 = 1.42, c_2 = 1.68 \quad (4.11)$$

The remaining mathematical equations are already mentioned in section 3.2.

#### 4.4 Simulation detail

In the present study, a supercritical CO<sub>2</sub> based NCL with heater (at the bottom) and isothermal sink (at the top), as shown in Fig. 4.1, is investigated to comprehend the influence of heat inputs and operating pressures on the flow field. Sink wall temperature is kept at 305 K while heat input is varied from 500 W to 2000 W. Initially, I simulated 1200, 1500 and 1800 W, then thought of extending it to the lower side (1000, 750, 500 W) and upper side (2000 W). The wall thickness is kept zero for the simulation simplicity of the model. With low viscosity and high-density fluid flow, the change of the pressure field is a more important determinant factor than the wall friction factor (Zhang et al. 2010). Two-dimensional geometry has been prepared, and transient simulations have been performed by ANSYS version 19.0.

A good number of studies considered 500 W, 1 kW, 1.5 kW, 2 kW heat input in the literature. These heat inputs values are typically used in a thermal power plant (boiler part), parabolic/dish type solar collectors and even nuclear reactor, etc. (Swapnalee et al. 2012; Sharma et al. 2013; Archana et al. 2015a). However, there is no such specific reason for selecting unequal intervals of heat flux. External walls are assumed to be adiabatic. In this simulation, the finite-volume method, based on in-

tegration over the controlled volume, is used to solve the model equations subject to the initial and boundary conditions in this numerical solution (Chen and Zhang 2011). Pressure-Implicit with the Splitting of Operators (*PISO*) algorithm is used for solving the pressure velocity coupling in the Navier-Stokes equation (Zhang et al. 2010). The momentum and energy parameters in the governing equations are iterated with a second-order upwind scheme that calculates the control volume values using upstream values and gradients. Turbulence parameters ( $k, \varepsilon$ ) are iterated with the second-order upwind scheme. To discretize the pressure term, PRESTO (Pressure staggering option) is used. The numerical model has been previously used and validated in many natural heat transfer studies (Zhang et al. 2010; Chen et al. 2010; Chen and Zhang 2011). A general Renormalization Group (RNG)  $k-\varepsilon$  model is selected along with an accurate description of fluid to account turbulence studies (Chen et al. 2010; Yadav et al. 2012a; Chen et al. 2014). The axial conductivity and viscous dissipation of the flow are taken into account. Convergence is obtained when residuals of the all-governing equations were less than  $10^{-3}$  except the energy equation, which was less than  $10^{-6}$ . Choosing appropriate time steps to model the transient processes is difficult. For the computational accuracy, efficiency and convergence, the adaptive time study step method is used. In this adaptive method, the appropriate time step is applied, and then the convergence of residual is monitored. Variable time steps with adaptive refinement are used, and the time step changes within the range from  $10^{-5}$  to 0.01 s according to the convergence condition (Zhang et al. 2010; Chen et al. 2010; Cao and Zhang 2012). Loop fluid, i.e.,  $\text{CO}_2$ , is kept in the supercritical region having operating pressure 80, 90 and 100 bar. The variation in thermo-physical properties of supercritical  $\text{CO}_2$  near the critical point is extremely large, so it is vital to capture the property variation due to temperature changes adequately. Hence, the properties of  $\text{CO}_2$  at any point in the loop are calculated at the fixed operating pressure and local temperature. The required properties of  $\text{CO}_2$ , including density, specific heat, thermal conductivity and viscosity, are obtained from the NIST (2013) version V9.1.

#### 4.5 Grid independence study

The meshing of a 2-D geometry is done in ANSYS 19.0 using design modular. The grid independence test (as shown in Fig. 4.6) is carried out to ensure the reliability of obtained results. Both scCO<sub>2</sub>R-NCL and scCO<sub>2</sub>T-NCL are operated at 90 bar with sink temperature at 305 K. The temperature recorded for the study is an area average temperature of loop fluid at the centre of the right leg. The grid-independent uniform mesh size is found to be 0.85 mm for scCO<sub>2</sub>R-NCL and 0.7 mm for scCO<sub>2</sub>T-NCL. With this grid size, the scCO<sub>2</sub>R-NCL and scCO<sub>2</sub>T-NCL have  $1.1 \times 10^5$  and  $1.6 \times 10^5$  elements, respectively.

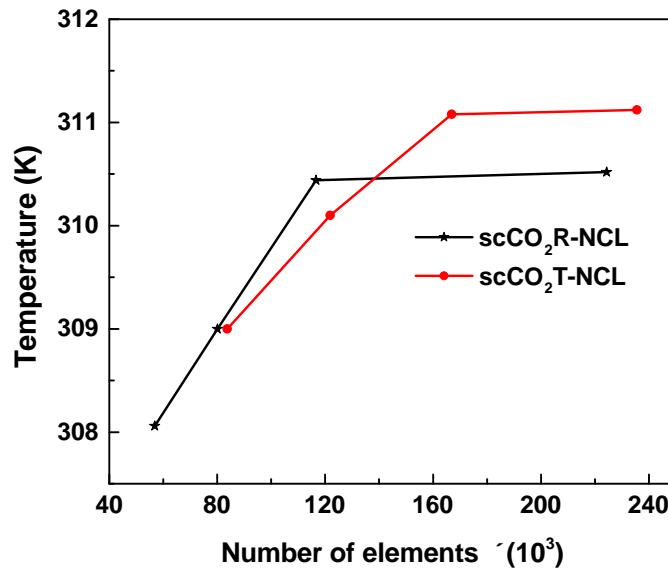


Figure 4.6: Grid independence study with CO<sub>2</sub> at 90 bar and a sink temperature of 305 K for Regular natural circulation loop (scCO<sub>2</sub>R-NCL) and Tesla natural circulation loop (scCO<sub>2</sub>T-NCL)

#### 4.6 Validation

The validation of obtained CFD results with scCO<sub>2</sub>R-NCL and scCO<sub>2</sub>T-NCL are validated with correlation of Reynolds Number and modified Grashof number i.e.,  $Re - Gr_m$  in two different ways:

- i. Experimental correlations validation with  $Re - Gr_m$  developed by [Swapnalee](#)

et al. (2012).

ii. Numerical correlation validation with  $Re-Gr_m$  developed by Yadav et al. (2012b).

The correlations involve non-dimensional parameters like  $Re$ , modified Grashof number ( $Gr_m$ ) calculated at the heater section. Good agreement is found between the generated results and existing correlations, as shown in Fig. 4.7. The maximum differences are 11% and 5%, with experimental correlation and numerical correlation. The deviations are due to the geometric dependence of NCL behaviours and the inability to account for the three-dimensional effects in the current two-dimensional model.

Correlation suggested by Swapnalee et al. (2012),

$$Re = 1.907(Gr_m d/L_t)^{0.364} \quad (4.12)$$

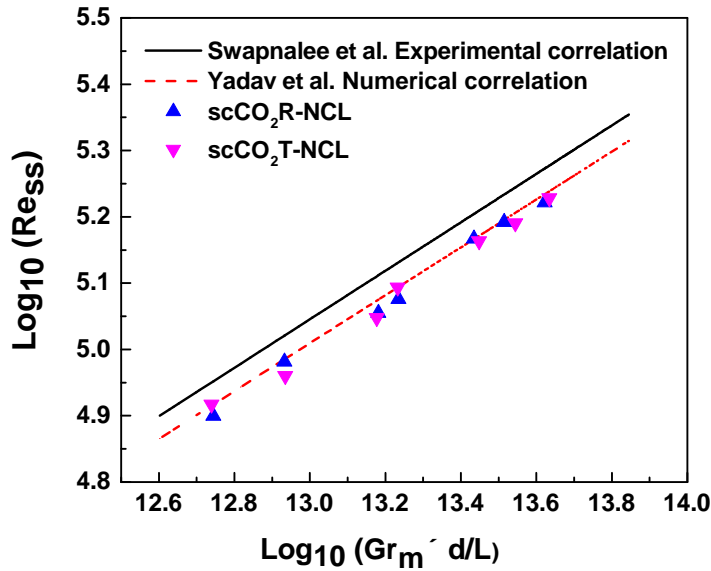


Figure 4.7: Validation plot of obtained results with steady-state Reynolds number  $Re_{ss}$  and modified Grashof number ( $Gr_m d/L_t$ ) correlation for supercritical  $CO_2$  flow.

Correlation suggested by Yadav et al. (2012b),

$$Re = 2.066(Gr_m d/L_t)^{1/2.77} \quad (4.13)$$



## 4.7 Results and discussion

To assess the performance of  $\text{scCO}_2\text{T-NCL}$  and  $\text{scCO}_2\text{R-NCL}$  at various supercritical pressures and heat inputs, two-dimensional CFD simulations are carried out, and the results thus obtained are compared and discussed in the following sections. Results (velocity and temperature) are obtained at the cross-section in the middle of the right leg (marked as ① in Fig. 4.1).

### 4.7.1 Transient variation of loop fluid temperature

Figures 4.8(a-d) show the comparison of temperature variation between  $\text{scCO}_2\text{R-NCL}$  and  $\text{scCO}_2\text{T-NCL}$  at various heat inputs to loop fluid at the source.

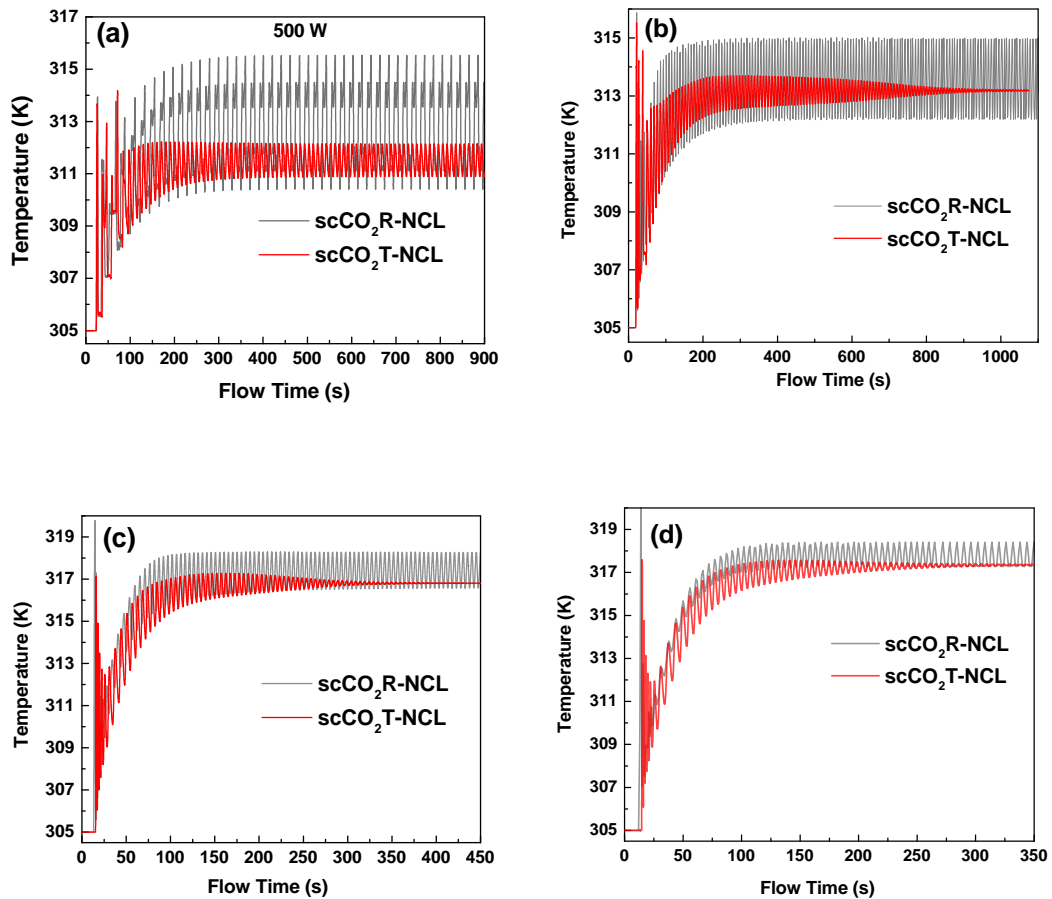


Figure 4.8: Transient variation of temperature at 90 bar of  $\text{CO}_2$  for Regular natural circulation loop ( $\text{scCO}_2\text{R-NCL}$ ) and Tesla natural circulation loop ( $\text{scCO}_2\text{T-NCL}$ ) with different heat inputs (a) 500 W, (b) 750 W, (c) 1800 W and (d) 2000 W.

A Uniform initial temperature of 305 K is specified for the fluid, which is the same as

that of sink wall temperature, so that the complete loop always will be in supercritical condition. Transient temperature variations are studied in the vertical leg because temperature fluctuation in this region depicts the fluctuation of driving buoyancy force in the loop, unlike heater or cooler. Heat inputs over a range of 500 to 2000 W are provided on the heater to trigger stagnant fluid. It is found that up to a specific time, the temperature remains at 305 K, later the flow starts with overshoots. The initial overshoot in temperature is caused by a sudden increase in buoyancy forces due to the heat accumulation at the beginning. This kind of typical overshoot found in the beginning validates the natural convection phenomenon (Yoshikawa et al. 2005; Chen et al. 2010). In both configurations, the temperature oscillates vigorously in the initial stage of imposing the heat input, and later on, it increases with a consistent rate until neutral stability or steady-state establishes in the loop. It is interesting to note that the oscillation trends are fairly analogous for both the loops at all levels of heat input. The magnitude of oscillation in the case of scCO<sub>2</sub>R-NCL persists over time and never converges to a steady-state at all levels of heat input. However, in the case of scCO<sub>2</sub>T-NCL, it converges over some time, predominantly at higher heat inputs. Thus, incorporation of the tesla valve in the NCLs has a twin effect on temperature oscillation, i.e., it reduces the magnitude of temperature oscillation at low heat inputs, and it also establishes a steady-state at higher heat inputs. The temperature of the loop also rises as the heat input increases, causing an increase in flow velocity. Due to the high momentum of fluid at high heat inputs, flow reversal is too difficult. So, the magnitude of temperature oscillation keeps on decreasing in scCO<sub>2</sub>R-NCL and scCO<sub>2</sub>T-NCL with an increase in heat input. The transient variations of temperature do not provide a clear insight into the flow pattern in the loop. Hence, to properly understand instabilities and explain the phenomena observed above, a transient variation of flow is discussed in the next section.

#### 4.7.2 Transient variation of fluid flow

Figures 4.9(a) and Fig. 4.9(b) show the oscillation of loop fluid flow direction and its magnitude in the scCO<sub>2</sub>R-NCL and scCO<sub>2</sub>T-NCL at 500 W (low) and 1800 W (high) heat inputs, respectively, for 90 bar operating pressure.

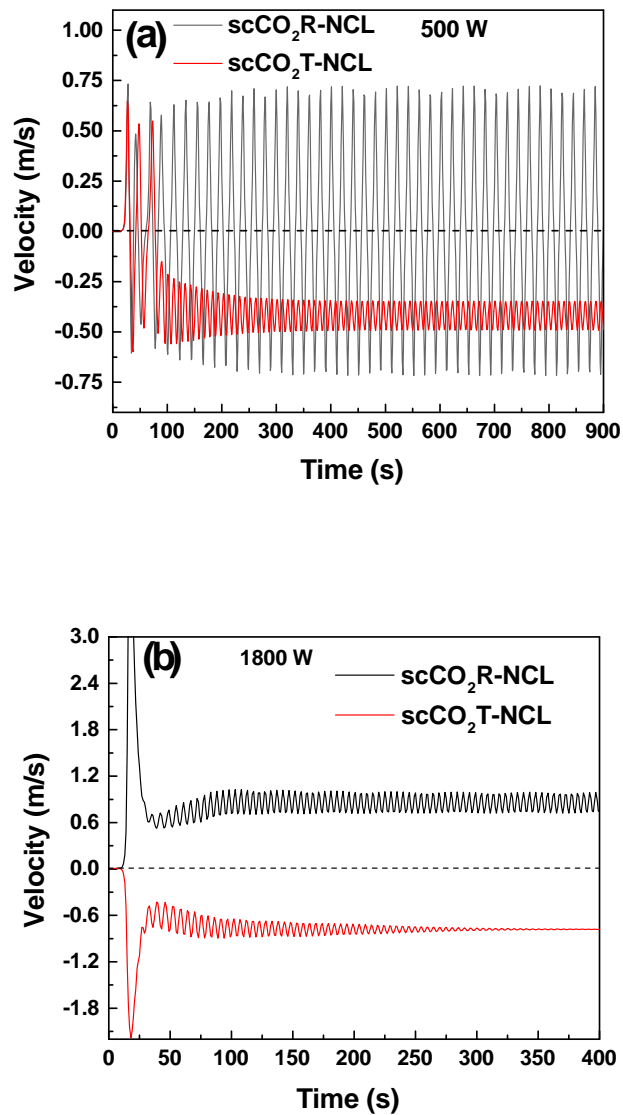


Figure 4.9: Velocity variation at 90 bar of CO<sub>2</sub> for Regular natural circulation loop (scCO<sub>2</sub>R-NCL) and Tesla natural circulation loop (scCO<sub>2</sub>T-NCL) with different heat inputs (a) 500 W and (b) 1800 W.

It is found that the velocity remains stagnant up to a specific time, and later the heater triggers the stagnant fluid with overshoots. The velocity value for this heat input is more

than 0.5 m/s, which is more than the water-based NCL (Yoshikawa et al. 2005). This high value of velocity can be attributed to the significant volumetric expansion coefficient and viscosity difference between water and CO<sub>2</sub> (Cammarata et al. 2004). The negative velocity value in the graph indicates the clockwise direction, and the positive shows anticlockwise, respectively.

At a lower intensity of heat input in the scCO<sub>2</sub>R-NCL case, Fig. 4.9(a) shows that the flow of scCO<sub>2</sub> in the loop begins to fluctuate and attains a flow reversal condition. This type of periodic flow reversal variation is common with previous NCL studies (Chatoorgoon 2001; Chen et al. 2010; Archana et al. 2015a), especially for supercritical CO<sub>2</sub> having smaller friction effect and more density differences. On the other hand, in the case of scCO<sub>2</sub>T-NCL, bidirectional flow can be noticed only for a shorter period, and in due course, unidirectional flow establishes in the loop. It can be observed that the magnitude of velocity oscillation is very high in both NCLs during the initial stages, but it gets mitigated at a faster rate in the case of scCO<sub>2</sub>T-NCL.

An explanation for the above-mentioned results is attempted using the hot pocket theory (Welander 1967; Nayak et al. 2008). When heat is applied to a loop in the stagnant initial condition, a hot pocket emerges from the heater. This hot pocket grows in length and eventually starts moving along one of the vertical legs. The length of the hot pocket can extend much larger than the length of the heater. Due to its relatively higher temperature induces a more significant flow rate due to the increase in buoyancy force. This explains the initial surge in velocity, which is observed in most cases in Fig. 4.9. These high temperature regions are unable to heat or cool properly due to less residence time inside heater or cooler and flow direction changes easily because of high density changes in systems. Figure 4.10 shows existence of hot pockets in scCO<sub>2</sub>R-NCL with 500 W operated at 90 bar. Due to geometrical symmetry in scCO<sub>2</sub>R-NCL, there is continuous switching in the direction of flow inside the loop as observed at 204 s in temperature contours.

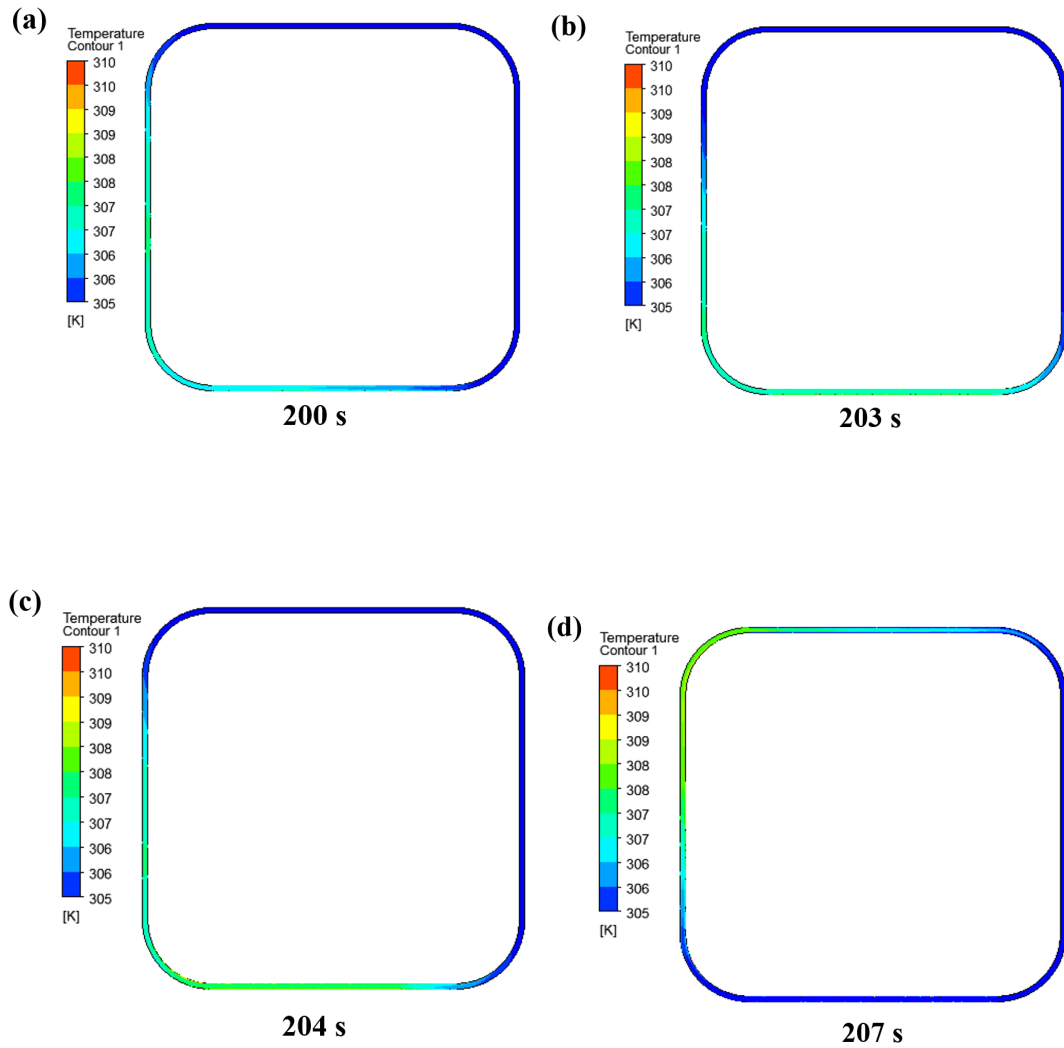


Figure 4.10: Temperature distribution for supercritical CO<sub>2</sub> based regular natural circulation loop for different time steps at 90 bar and 500 W (a) 200 s, (b) 203 s, (c) 204 s and (d) 207 s.

Similar temperature contours are also plotted for T-NCL at suitable time-step to depict circulation with the same operating conditions, as shown in Fig. 4.11. It can be seen that hot pockets created in T-NCL are at a relatively lower temperature when compared to R-NCL. This is because of continuous bidirectional oscillations in R-NCL, which leads to flow being stagnant at certain time-steps, and this allows the creation of high-temperature hot pockets. Whereas, in T-NCL, the flow in a reverse direction with respect to the Tesla valve experiences more resistance than the forward direction due to adverse-pressure gradient. Thus Tesla valve acts as a fluidic diode, and due to its

diodicity, flow reversal phenomena is difficult to occur. In other words, the Tesla valve introduces differing flow impedance to circulation direction and causes unidirectional (clockwise) oscillations in the loop. So, fluid is continuously in motion in this case leading to less time spent inside the heater and lowers the temperature for hot pockets. A hot pocket at a higher temperature will lead to a drastic increase in buoyancy force on the fluid and causes greater instability in the loop. This also explains the high amplitude temperature fluctuations in  $\text{scCO}_2\text{R-NCL}$  compared to  $\text{scCO}_2\text{T-NCL}$ , as observed in Fig. 4.8.

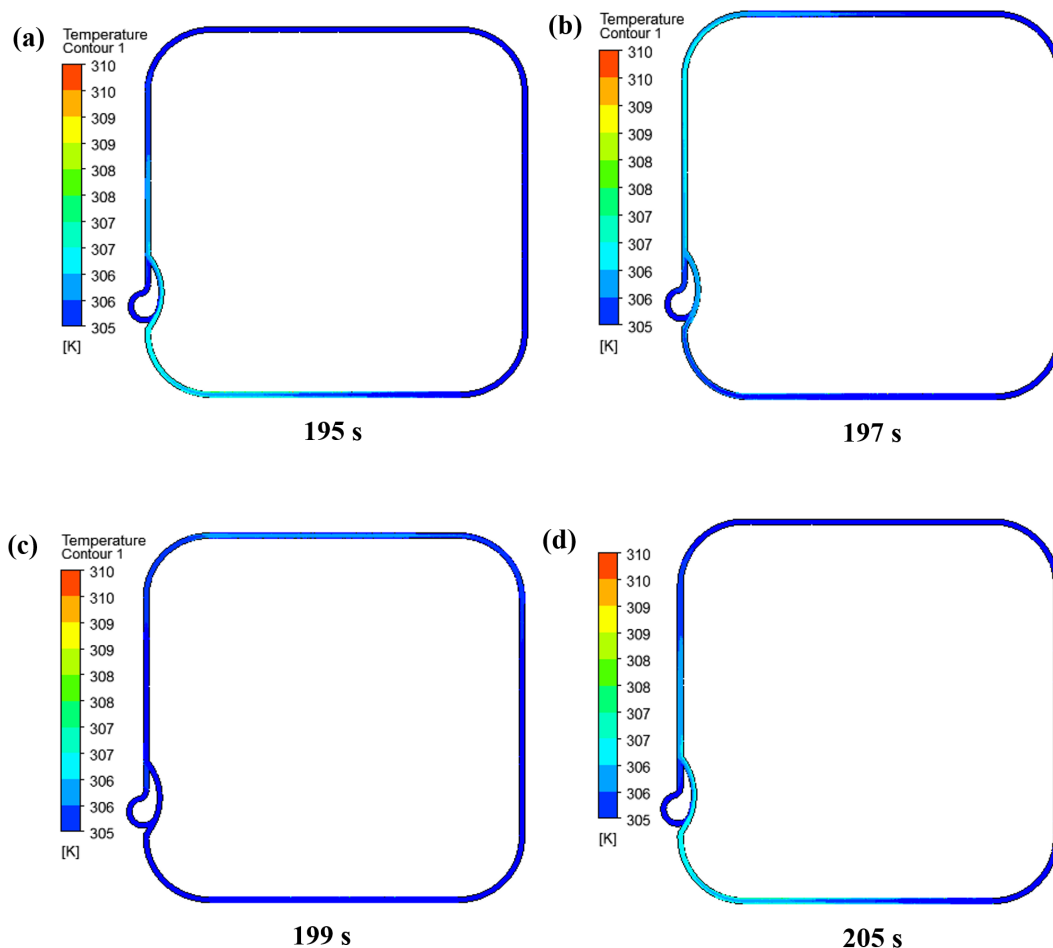


Figure 4.11: Temperature distribution in the 500 W at 90 bar of  $\text{CO}_2$  for Tesla natural circulation loop ( $\text{scCO}_2\text{T-NCL}$ ) at different time steps from 195 s to 205 s.

At higher heat input in both configurations, fluid flow finds its unidirectional path in the loop (as shown in Fig. 4.9(b)). Oscillation in the case of  $\text{scCO}_2\text{T-NCL}$  gets con-

verged to a steady-state after some time. Whereas in R-NCL, these oscillations stabilise to a certain amplitude and never converge to a steady state. This implies that the Tesla valve is able to reduce the hot pockets in the system completely. The absence of hot pockets results in the stable temperature profile observed in Fig. 4.8(a-d) for scCO<sub>2</sub>T-NCL.

Hence, in a loop operating at lower heat input, introducing a Tesla valve reduces the temperature of the hot pocket, and at higher heat input, the effect of hot pockets are negligible as it gets eliminated. Hence, employing a tesla valve in the loop minimises the magnitude of oscillation at low heat input and eliminates the fluctuation at high heat input.

#### **4.7.3 Parametric study on heat input and loop operating pressure**

Figure 4.12 shows the effect of loop fluid pressures (80, 90 and 100 bar) and different heat inputs (500, 750, 1200, 1500, 1800 and 2000 W) on the velocity pattern in R-NCL and scCO<sub>2</sub>T-NCL. The dynamics of the NCL significantly depend on the operating conditions (Saha et al. 2018). For this reason, proper analysis of the fluid flow dynamics in the NCL with operating pressure is very important. The concept behind this study is a replication of disturbances in the normal operating condition of NCL, which could be due to change in the loading conditions of natural circulation systems or the occurrence of a disturbance in the system during start-up and shutdown activities. With this context, the following conclusions are inferred from the results obtained from the CFD simulation.

Figures 4.12(a,c) for scCO<sub>2</sub> R-NCL show that the loop fluid is in the stage of flow reversal when the heat inputs are at 500 W (for all pressure) and 750 W (for 100 bar). For the low heat inputs, i.e., 500 W and 750 W, fluid has less momentum and easily succumbs to change in the direction of buoyancy force (left or right side), leading to bidirectional oscillation (also called flow reversal phenomenon). If the fluid has gained enough momentum in the loop, the change in the direction of buoyancy force in the loop

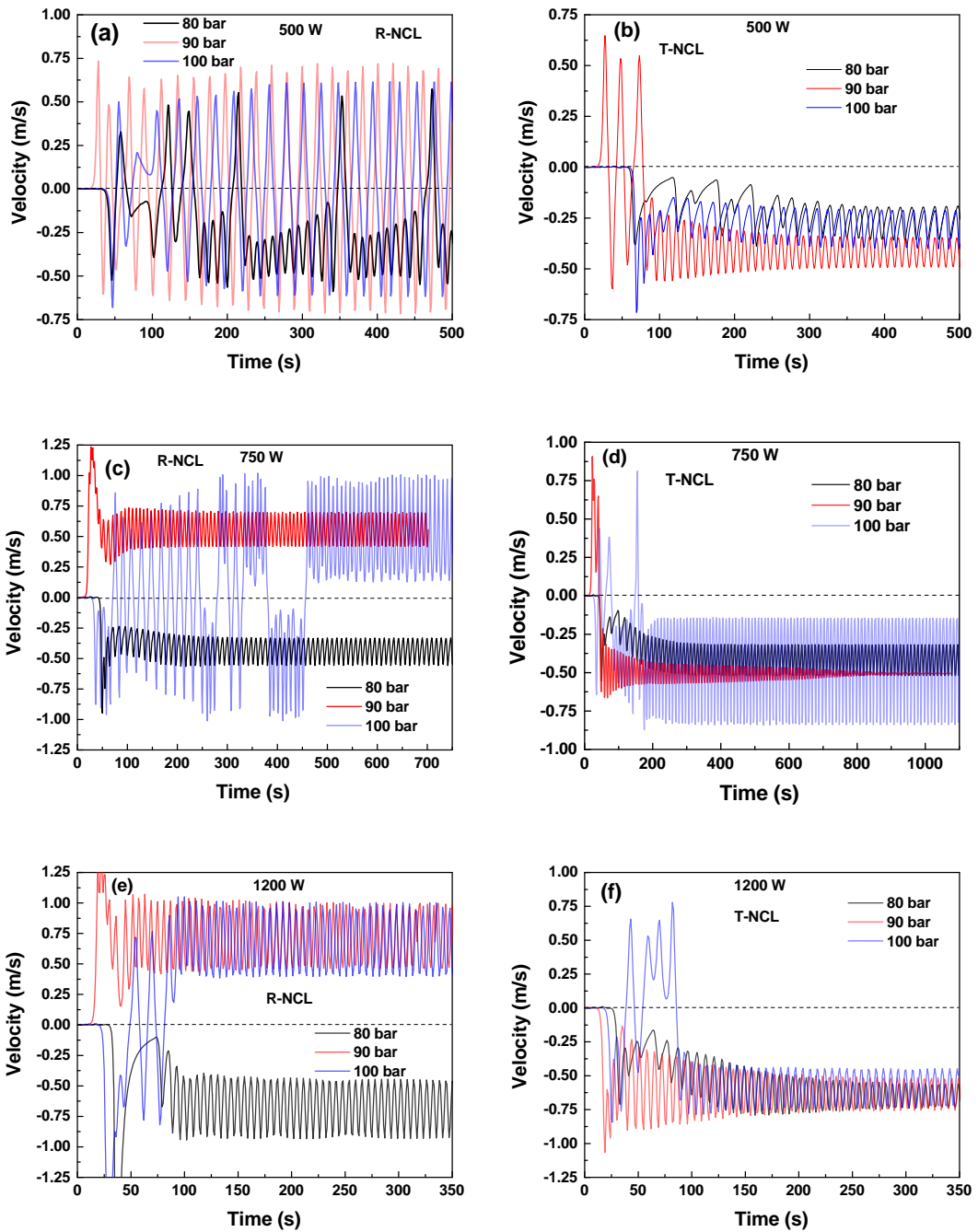
may only lead to unidirectional oscillation rather than complete flow reversal. Mathematically, the cause of instability is the existence of multiple solutions for the system, and the system can not permanently settle for any of them. Geometrical symmetry in scCO<sub>2</sub>R-NCL gives the loop numerous alternative solutions, so the system swings from one solution to another, resulting in unstable conditions. That is why in scCO<sub>2</sub>R-NCL, even in a small fluctuation of temperature, it leads to the formation of hot (light) and cold (heavy) fluid pockets and making it liable to periodic flows. Such fluctuations are like density wave oscillation (Chatoorgoon et al. 2005) and similar to two-phase NCLs (Kreitlow et al. 1978; Nayak et al. 2000; Shitzer et al. 1979).

However, when the heat input is  $> 750$  W for scCO<sub>2</sub>R-NCL, the flow pattern changes from flow reversal to single-direction flow. Such transition flow behaviour (i.e., from flow reversal to uni-direction) has been reported in many literatures (Vijayan et al. 1995; Cammarata et al. 2004; Chen et al. 2014). However, it is also known that the stability of the scCO<sub>2</sub>-NCL depends on the geometrical parameters (diameter, aspect ratio etc.), heat flux, loop inclination, operation procedures and their existing several transition parameters or stability threshold (Vijayan et al. 1995; Muscato and Xibilia 2003; Duffey and Piro 2005). Results show that the prediction of flow direction in scCO<sub>2</sub>R-NCL is difficult at all operating pressure considered in the study. Hence, the designing of the loop for a particular application would be challenging.

Whereas in scCO<sub>2</sub>T-NCL, the flow direction can be decided by putting the Tesla valve in a particular direction. The diodicity developed on the loop establishes clockwise flow (in the present study), and it sustains the convection by continuous heating. Results obtained for scCO<sub>2</sub>T-NCL (as shown in Fig. 4.12) show the clockwise flow (unidirectional) in the loop for all heat inputs and pressures considered in the study. The magnitude of fluctuations is found to be less in the scCO<sub>2</sub>T-NCL case compared to the scCO<sub>2</sub>R-NCL case. For lower heat inputs, the mass flow rate depicts oscillatory behaviour where the amplitude and frequency of the oscillation remain constant over time. The persistent oscillatory behaviour of the loop shows neutral stability. At higher



heat input of 1800 W and 2000 W, in the case of  $\text{scCO}_2$ T-NCL, the flow sustains a definite direction and eventually establishes a steady flow. It is to be noted that at a higher heat input, in the case of  $\text{scCO}_2$ T-NCL, the flow direction never changes even during the initial stage of the flow.



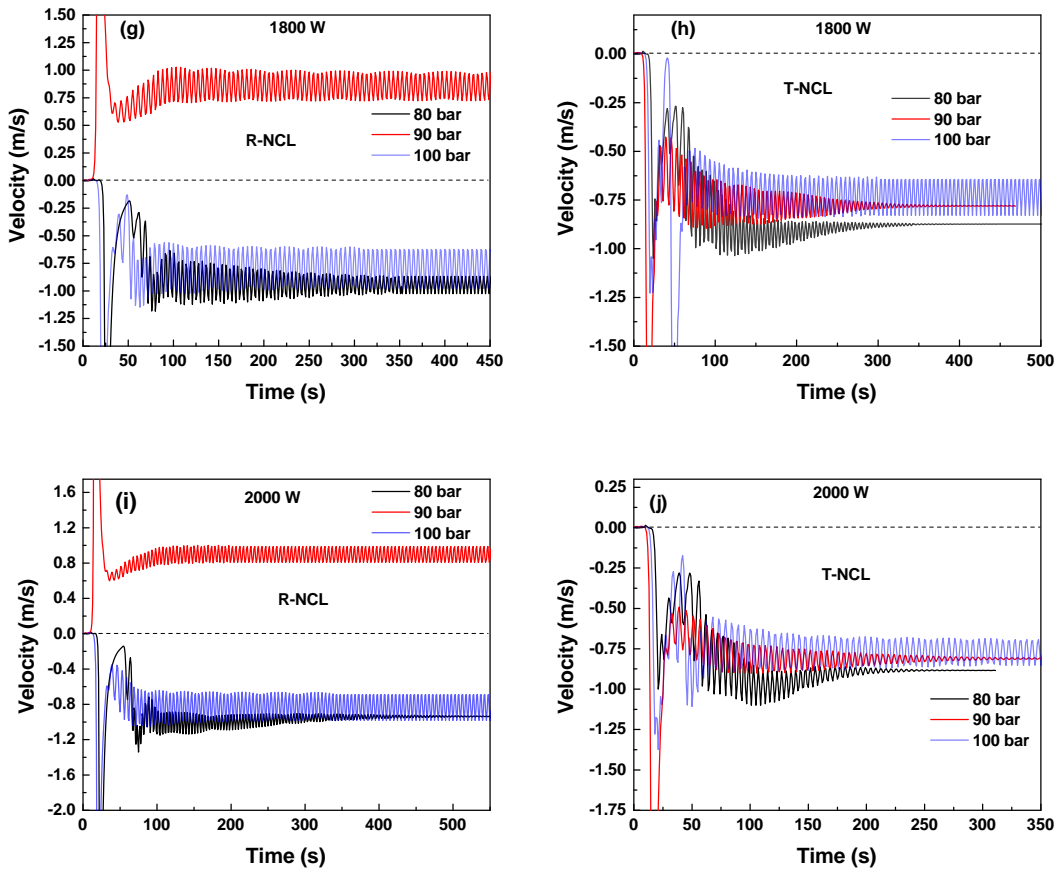


Figure 4.12: Transient variation of velocity with a different operating pressure of CO<sub>2</sub> for regular natural circulation loop (scCO<sub>2</sub> R-NCL) and Tesla natural circulation (scCO<sub>2</sub> T-NCL) loop at different heat inputs (a) 500 W scCO<sub>2</sub> R-NCL, (b) 500 W scCO<sub>2</sub> T-NCL, (c) 750 W scCO<sub>2</sub> R-NCL, (d) 750 W scCO<sub>2</sub> T-NCL, (e) 1200 W scCO<sub>2</sub> R-NCL, (f) 1200 W scCO<sub>2</sub> T-NCL, (g) 1800 W scCO<sub>2</sub> R-NCL, (h) 1800 W scCO<sub>2</sub> T-NCL (i) 2000 W scCO<sub>2</sub> R-NCL and (j) 2000 W scCO<sub>2</sub>T-NCL.

Also, the magnitude of the velocity oscillation keeps on reducing as the heat input increases. Remarkably, the magnitude of flow rate does not deteriorate by incorporating the Tesla valve in the NCLs. So, it is recommended to use a Tesla valve with high heat inputs.

The parametric study of operating pressure in scCO<sub>2</sub>R-NCL and scCO<sub>2</sub>T-NCL show that, in general, higher operating pressures (in the present range of study) led to more instability in the loop compared to lower operating pressure for the same heat input. The possible reasons for this might be as follows: Higher pressure generates

greater temperature differential across the heater and so a bigger density difference is available between the vertical arms. It results in increase in the buoyancy forces, enhanced buoyancy is always responsible for introducing larger disturbances into the flow stream in the form of velocity and temperature fluctuations, leading the system towards unstable fluctuations, as is evident from Fig.4.12.

#### 4.7.4 Nusselt number variation

Figure 4.13 shows the Nusselt number ( $Nu$ ) variation at 90 bar for different heat inputs considered in the study. Nusselt number is calculated at the sink section by taking average thermal conductivity value.

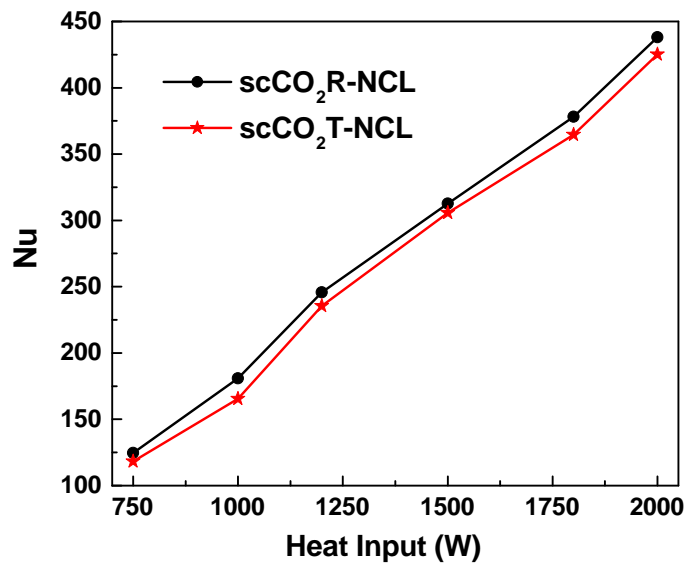


Figure 4.13: Variation of Nusselt number ( $Nu$ ) with different heat inputs at 90 bar for Regular natural circulation loop (scCO<sub>2</sub>R-NCL) and Tesla natural circulation loop (scCO<sub>2</sub>T-NCL).

For the range of operating conditions chosen in the study, regular NCL is unstable in most transient simulation cases. Thus, the heat transfer capacity (in terms of  $Nu$ ) of the loops was compared by considering the maximum absolute value of the parameters (such as heat transfer rate, mass flow rate, etc.) achieved in unidirectional constant fluctuation conditions. Bidirectional fluctuation (like 500 W case) is referred to as a

completely unstable case, and hence these cases are not considered for the comparison. While for Tesla NCL, unidirectional constant fluctuation conditions and steady-state cases are considered. The Nusselt number for scCO<sub>2</sub>R-NCL and scCO<sub>2</sub>T-NCL is approximately the same. The length of T-NCL being marginally larger than the R-NCL, friction loss is more which in turn reduces the Reynolds number due to reduction in velocity. As heat transfer coefficient is the function of velocity, there is overall reduction in the Nusselt number. The maximum drop in Nusselt number in the case of scCO<sub>2</sub>T-NCL is found to be  $\leq 8\%$  compared to scCO<sub>2</sub>R-NCL for all heat inputs considered in the study. Hence, the heat transfer capabilities of the loop are not affected much by using a Tesla valve.

#### **4.8 Summary**

By incorporating the tesla type valve in the natural circulation loops, the following conclusions are drawn based on the obtained CFD simulation:

- i. Directional instability of natural circulation loops can be eliminated by incorporating a Tesla type valve in the loop.
- ii. The incorporation of a Tesla type valve in NCLs mitigates the magnitude of velocity oscillation to a greater extent and eventually establishes a steady-state in the loop.
- iii. In the NCL, the Tesla valve meticulously reduces the temperature oscillation, and in due course, it sets in the steady-state and thereby reduces the thermal shocks in the loops.
- iv. Tesla valve can reduce flow reversal in low heat input conditions (or lower down the reversal limit) and prescribe flow direction, ensuring a steady-state at relatively higher heat input conditions.
- v This modified design of the Tesla type valve is found to be highly effective for supercritical CO<sub>2</sub> based NCL.

## CHAPTER 5

### **Instability Mitigation by Integrating Twin Tesla Type Valves in Supercritical Carbon dioxide-based Natural Circulation Loop**

In the previous chapter, it was observed that the use of a single modified Tesla type valve in NCL is not capable of mitigating the instability in the case of low heat inputs and high pressure. Hence, twin Tesla type of valves is chosen for the study. This chapter emphasizes the development of NCL integrated with two modified Tesla type valves to promote the uni-directional circulatory movement of loop fluid and decrease the magnitude of instability. In this study, numerical simulations have been carried out for a range of supercritical pressures (80 bar to 100 bar) and heat inputs (500 W to 2000 W) to do the comparative investigation of instability phenomenon in supercritical CO<sub>2</sub> based regular natural circulation loop, single Tesla valve NCL and a new modified twin Tesla NCL. The objectives of the study are (i) to investigate the effect of twin Tesla valve on the instability and heat transfer capability, (ii) to know the flow behaviour of supercritical CO<sub>2</sub> based NCL at different heat inputs, and (iii) to compare the effect of operating pressure on instability.

#### **5.1 Twin Tesla model design for NCL**

In this research, a supercritical CO<sub>2</sub> based NCL with and without a Tesla valve (as shown in Fig. 5.1) is explored to understand the impact of heat inputs and operating pressures on flow instability. NCL without a Tesla valve is called a regular natural circulation loop (R-NCL), and NCL with a modified twin Tesla valve is designated as a Tesla natural circulation loop (Twin Tesla-NCL). All the geometrical and material specifications for the model are given in section All the geometrical and material specifications for the model are given in the previous sections of 4.1 and 4.2.

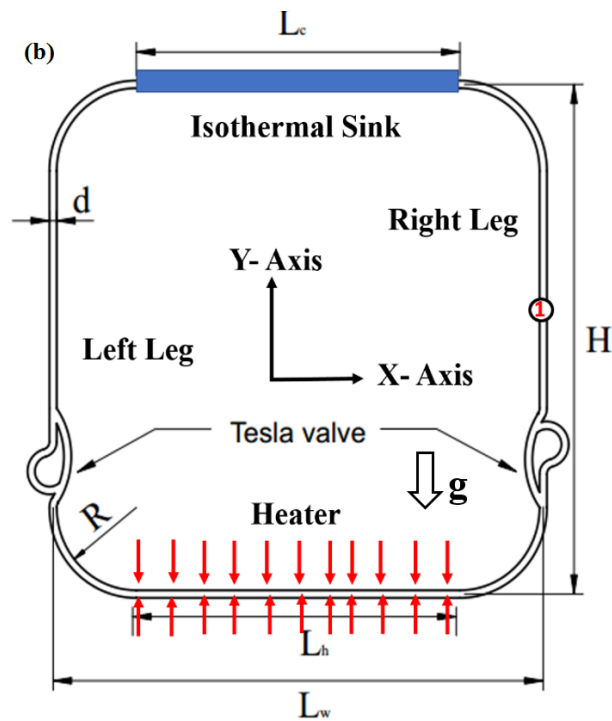
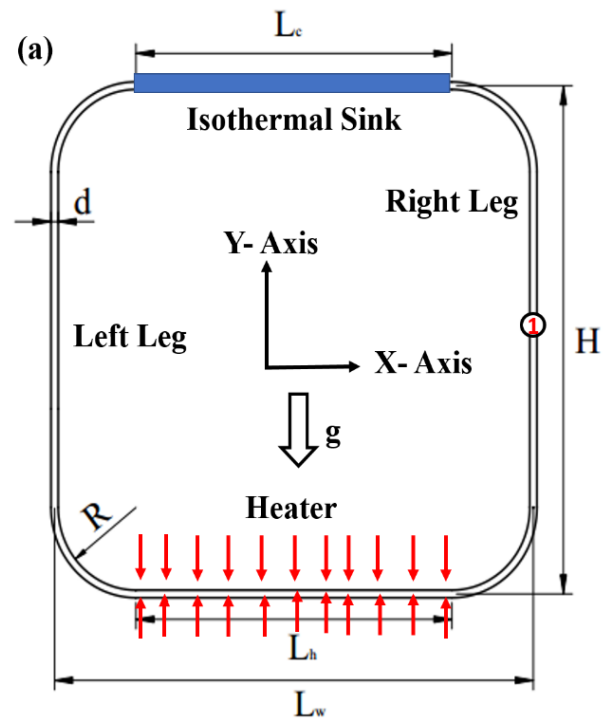


Figure 5.1: Schematic of (a) Regular natural circulation loop (R-NCL) (b) Twin Tesla valve natural circulation loop (Twin Tesla-NCL).

## 5.2 Simulation details and mathematical formulation

In the present study, a supercritical CO<sub>2</sub> based NCL with heater (at the bottom) and isothermal sink (at the top), as shown in Fig. 5.1, is investigated to comprehend the influence of heat inputs and operating pressures on the flow field. Sink wall temperature is kept at 305 K while heat input is varied from 500 W to 2000 W. Two-dimensional geometry has been prepared, and transient simulations have been performed employing ANSYS version 19.0. In this simulation, the finite-volume method, based on integration over the controlled volume, is used to solve the model equations subject to the initial and boundary conditions in this numerical solution (Chen and Zhang 2011). Convergence is obtained when residuals of the all-governing equations were less than  $10^{-3}$  except the energy equation, which was less than  $10^{-6}$ . Choosing appropriate time steps to model the transient processes is difficult. For the computational accuracy, efficiency and convergence, the adaptive time study step method is used. In this adaptive method, the appropriate time step is applied, and then the convergence of residual is monitored. Variable time steps with adaptive refinement are used, and the time step changes within the range from  $10^{-5}$  to 0.01 s according to the convergence condition (Zhang et al. 2010; Chen et al. 2010; Cao and Zhang 2012). Mathematical formulation for the model is given in the previous section 4.3 and boundary condition is given below.

- i. Sink wall temperature is kept at 305 K.
- ii. Heat inputs at heater are varied from 500 W to 2000 W.
- iii. Loop fluid Pressure varies from 80 bar to 100 bar
- iv. External walls are assumed to be adiabatic.
- v. No-slip condition near wall.
- vi. Wall thickness is kept zero.

## 5.3 Grid independence study

The grid independence test (shown in Fig. 5.2) is performed to read minute variations in the properties and ensure that the results are reliable. The meshing of a two-dimensional

geometry is done using the ANSYS (V.19) software. A structured non-uniform grid system is used to mesh the whole area. Quadrilateral (in maximum places) and triangular, and combination of both are used in the meshing. Figure 5.3 shows the mesh at the heater section of the loop. For a grid independence study, a sensitivity analysis has been carried out to reach the independence of the solution from the adopted grid. Mesh was started with a coarse mesh and gradually refined until it generated a mesh independent result. The grid-independent uniform mesh size is 0.85 mm for R-NCL and 0.7 mm for twin Tesla-NCL, respectively. With this grid size, the grid-independent number of elements found for R- NCL and twin Tesla-NCL are  $1.1 \times 10^5$  and  $1.2 \times 10^5$ , respectively. The sensitivity to the mesh results is reported in Fig. 5.2, which shows the evaluated temperature (in stable condition) as a function of the number of mesh elements.

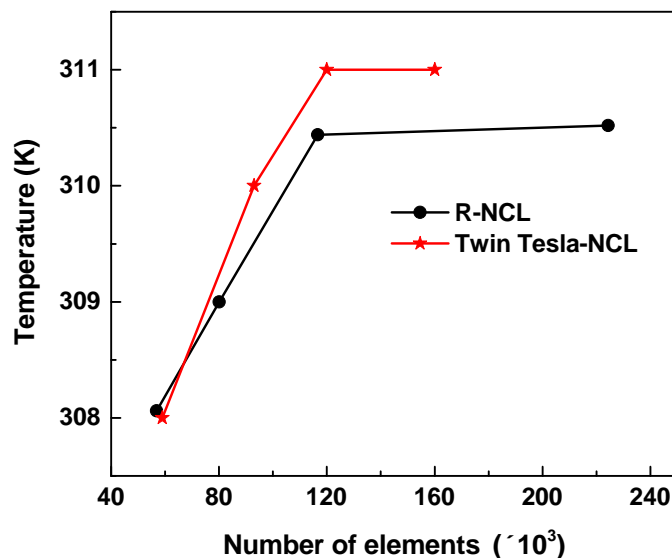


Figure 5.2: Grid independence study for supercritical CO<sub>2</sub> based Regular natural circulation loop and Twin Tesla natural circulation loop at 90 bar and sink temperature of 305 K at 1000 W heat input.

The results of the grid-independent study are compared with the grid convergence index (GCI) method proposed by Roache (1986). This method is based on the application of Richardson's extrapolation, in which as the grid is refined (grid cells become smaller



and the number of cells in the flow domain increases), the spatial and temporal (in unsteady numerical simulations) discretization errors approaches to zero asymptotically. The error estimated of R-NCL and T-NCL with the GCI method (Roache 1986, 1994) is 1.6 % and 1.7 %, respectively, with the mesh generated using 1,16672 and 1,20000 elements.

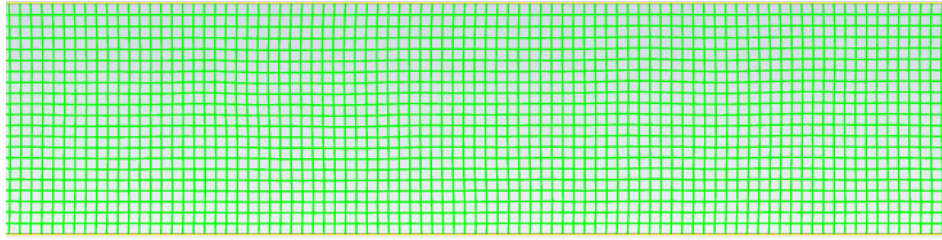


Figure 5.3: Mesh at heater section.

#### 5.4 Validation

For the validation of obtained CFD results, I have used two famous  $Re \sim Gr_m$  analytical correlations of (i) Swapnalee et al. (2012) correlation, which was developed based on the experimental studies, and (ii) a numerical correlation developed by Yadav et al. (2012b) with subcritical/supercritical CO<sub>2</sub>. A good agreement was found between the simulated results and existing correlations, as shown in Fig. 5.4. The maximum discrepancies are 14% and 8%, with experimental correlation and numerical correlation, respectively. The discrepancies may be due to the geometric dependence of NCL behaviours and the simplifications of the two-dimensional model over their three-dimensional effects.

Correlation suggested by Swapnalee et al. (2012),

$$Re = 1.907(Gr_m d/L_t)^{0.364} \quad (5.1)$$

Correlation suggested by Yadav et al. (2012b),

$$Re = 2.066(Gr_m d/L_t)^{1/2.77} \quad (5.2)$$

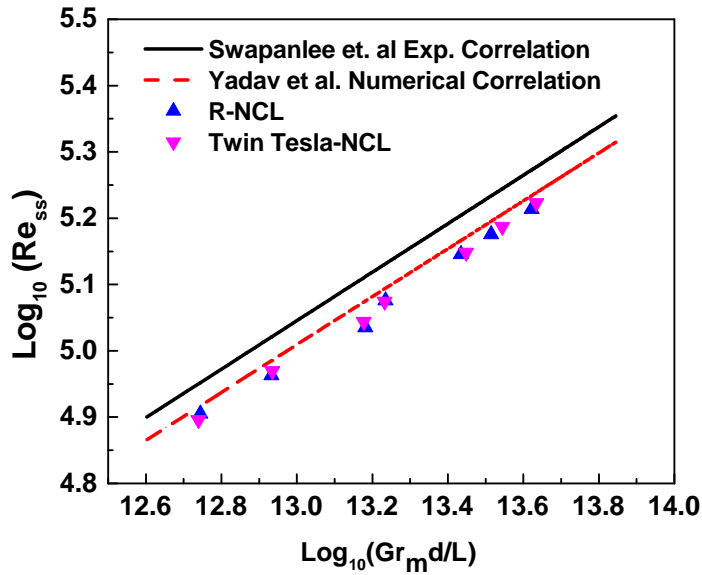


Figure 5.4: Validation plot of obtained results with steady-state Reynolds number ( $Re_{ss}$ ) and modified Grashof number ( $Gr_m d/L_t$ ) correlation for supercritical  $\text{CO}_2$  flow.

## 5.5 Results and discussion

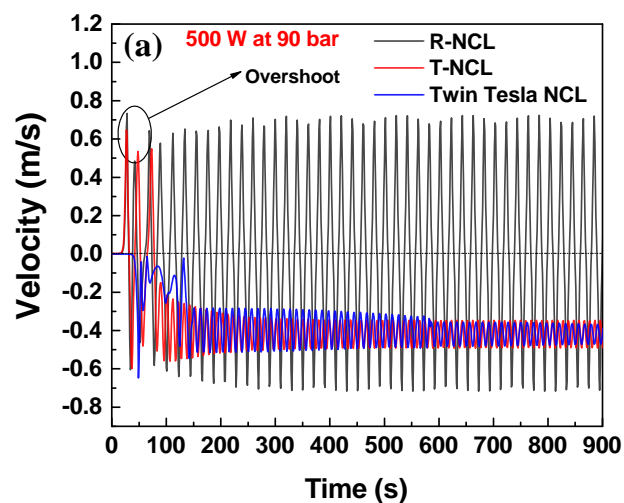
Results are obtained at the middle of the right leg (marked as ① in Fig. 5.1) by considering the area-weighted average across the cross-section of the loop. To minimize the effect of  $90^\circ$  bend at corners, semi-circular elbows are used. Initially, the entire loop is kept at a uniform temperature of 305 K to ensure ‘no flow condition’; this is the initial condition applied for unsteady simulation. The operating pressure of the loop is kept constant for each set of simulations carried out for the heat fluxes varied from 500 W to 2000 W. Effect of operating pressure on the transient behaviour of the loop is also studied in the supercritical region with the pressure variation form 80-100 bar. The transient flow behaviour of  $\text{scCO}_2$  in NCL is recorded from the initial time  $t = 0$  s to  $t = 500$  s until the repetitive behaviour is found.

### 5.5.1 Feasibility of twin Tesla in NCL

It was concluded from the previous chapter that the loop operating at low heat input and higher pressure shows higher instability. Thus, the present configuration of twin Tesla NCL is tested first for the most unstable operating conditions. Figure 5.5 shows

the transient velocity variation at an operating pressure of 90 bar at 500 W heat input and mass flow rate variation at an operating pressure of 100 bar at 500 W heat input for R-NCL, T-NCL and twin Tesla NCL. It is found that the velocity/mass stays at nearly zero value up to a certain time, and the temperature remains at 305 K, and after some time, the flow starts with overshoot. The initial overshoot in velocity is the sudden motion caused by buoyancy forces due to the beginning period of heat accumulation. This kind of typical overshoot found in the beginning without the help of any moving device shows the natural convection phenomenon (Zhang et al. 2010; Chen et al. 2010; Cao and Zhang 2012). The negative velocity value shows the flow is in a clock-wise direction and vice versa.

It is depicted from Fig. 5.5(a) that after initial overshoot in velocity, the flow of scCO<sub>2</sub> in R-NCL begins to fluctuate, and flow pattern changes with respect to time and attains a flow reversal phenomenon. However, in T-NCL, after the overshoot at the beginning, velocity experiences bidirectional fluctuation same as the R-NCL, but due to the influence of the Tesla valve in the loop after some time, a uni-directional flow is established.



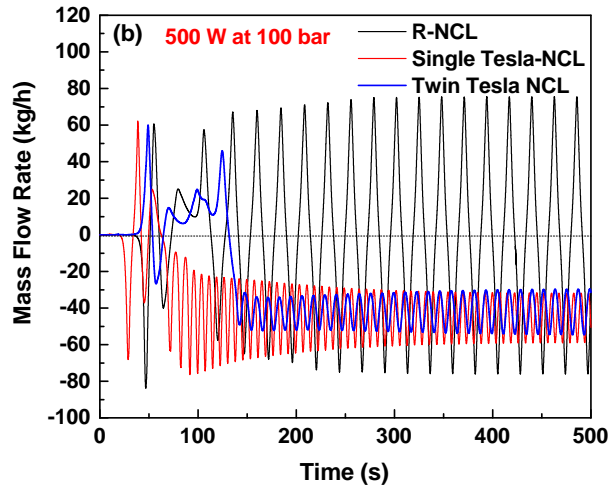


Figure 5.5: Transient variations of (a) velocity at 90 bar for a heat input of 500 W (b) mass flow rate at 100 bar for heat input of 500 W for R-NCL, T-NCL and Twin Tesla-NCL.

In twin Tesla NCL, the magnitude of velocity oscillation is comparatively less than T-NCL and R-NCL, and also establishes unidirectional flow without showing any flow reversal in the beginning. Thus, twin Tesla can be used as a viable option to curb instability for low heat inputs.

Similarly, a comparative analysis for the mass flow rate of R-NCL, single Tesla-NCL and twin Tesla-NCL at higher input of 500 W and at a higher pressure of 100 bar is shown in Fig. 5.5(b). It is found that the oscillation in R-NCL is maximum while in twin Tesla NCL it is minimum. Thus, the increase in the number of Tesla type valves mitigates the instabilities in the NCL.

### 5.5.2 Flow behaviour

The velocity and transient temperature variations are shown in Fig. 5.6 against time for an operating pressure of 100 bar at 500 W heat input for R-NCL and twin Tesla is obtained at the middle of the right leg (marked as ①) by considering the area-weighted average across the cross-section of the loop.

In the R-NCL case (as shown in Fig. 5.6(a)), the flow of scCO<sub>2</sub> in the loop begins

to fluctuate, and the flow pattern changes with the temperature (as shown in Fig. 5.6(b), near to 60 s it shows a flow reversal phenomenon.

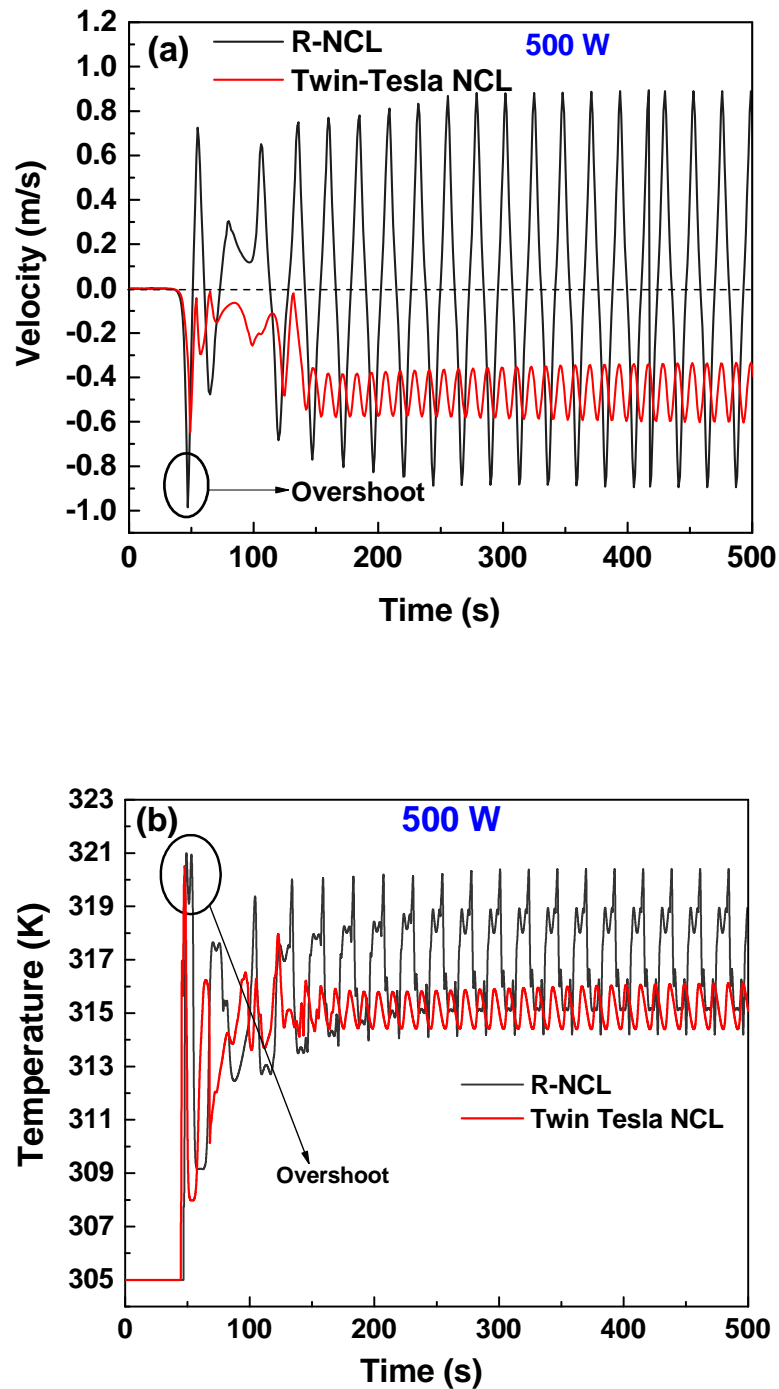


Figure 5.6: Variations of (a) velocity and (b) temperature at 100 bar at a heat input of 500 W for R-NCL and twin Tesla-NCL

This type of periodic flow reversal variation is common with previous NCL studies (Welander 1967; Chatoorgoon 2001; Chen et al. 2010; Archana et al. 2015a) supercritical CO<sub>2</sub> having smaller friction effect and more significant density differences. The pseudo-critical temperature at 100 bar is  $\sim 318$  K; at this temperature, specific heat capacity forms a high peak, whereas viscosity, thermal conductivity, and density decrease significantly.

While in the twin Tesla-NCL case (as shown in Fig. 5.6(b)), after the initial overshoot, temperature experiences the same change in the fluctuation amplitude as the R-NCL value, i.e., equal to 321 K. After the initial fluctuation, the temperature of the loop varies only  $\pm 1$  K from a mean value of 315 K due to the influence of the Tesla valve in the loop. The magnitude of temperature oscillation is comparatively less in twin Tesla-NCL ( $\pm 1$  K) than R-NCL ( $\pm 3$  K). Thus, incorporating the Tesla valve in the NCLs have a twin effect, first on temperature oscillation, i.e., it mitigates the magnitude of temperature oscillation and second, it also establishes unidirectional flow.

Due to the impedance created by the Tesla valve, the flow in the reverse direction experiences more resistance than the forward direction, which develops a pressure gradient along the vertical pipe. This pressure gradient creates a smooth movement of fluid in one direction only from the left leg to the right leg (i.e., a clock-wise direction). Owing to the fluidic diodicity of the Tesla valve, the magnitude of fluctuation is also less. This pressure gradient phenomenon is enlightened in Fig. 5.7.

Transient results for the velocity and the pressure difference vs time are reported in Fig. 5.7, over a time duration from 100 s to 375 s to understand a strong correlation between pressure difference and velocity clearly. The operating pressure of the loop is kept at 100 bar, and hence the values show the pressure variation considering 100 bar as the mean value (zero at the initial condition).

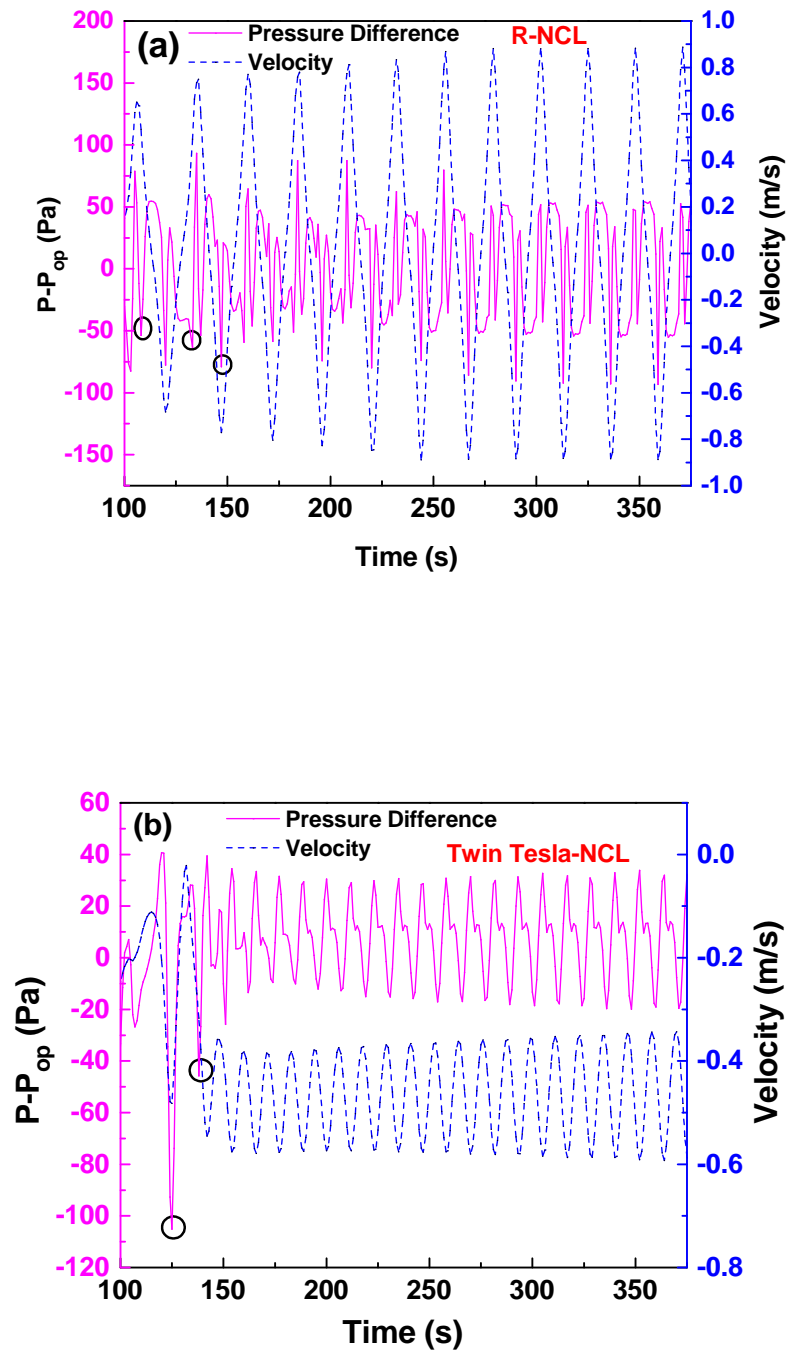


Figure 5.7: Velocity and pressure variation oscillations at 100 bar at a heat input of 500 W for (a) R-NCL and (b) Twin Tesla NCL.

In twin Tesla NCL, the Tesla valve generates potent pressure fluctuations ranging from 40 Pa to 110 Pa (as shown in Fig. 5.7(b)), which creates a pressure gradient along the vertical pipe, and this pressure fluctuation induces strong natural convection flow.

Whilst for R-NCL, the pressure fluctuations ranges from 25 Pa to -50 Pa (as shown in Fig. 5.7(a)), which is less than twin Tesla NCL pressure fluctuation. Due to this high-pressure gradient, a fluidic diodicity is developed along with the Tesla valve, and at this fluidic diodicity, flow reversal phenomena are difficult to occur, and hence a unidirectional flow is established. This high fluctuation in pressure gradient developed by the Tesla valve may be the probable reason for unidirectional flow developed in twin Tesla NCL.

### 5.5.3 Transient variation of temperature

Figures 5.8(a-d) compare temperature variation between R-NCL and twin Tesla NCL for various heat inputs at a pressure of 100 bar is obtained at the middle of the right leg (marked as ①) by considering the area-weighted average across the cross-section of the loop. A uniform initial temperature of 305 K is specified for the fluid, which is the same as that of sink wall temperature so that the complete loop will be in supercritical condition. Then heat inputs over a range of 500 W to 2000 W are provided on the heater to trigger the fluid flow from its quiescent state.

In both configurations, the temperature oscillates vigorously in the initial stage of imposing the heat input at the source, and later on, it increases with a consistent rate till neutral stability or steady-state establishes in the loop. Interestingly, the oscillation trends are somewhat analogous for both the loops at all heat input levels. However, the magnitude of temperature oscillation in the case of twin Tesla NCL is comparatively less due to the influence of the tesla valve in the loop. Further, the amplitude of temperature oscillation keeps decreasing in both cases, with an increase in heat input. For R-NCL, the fluid temperature continues to fluctuate abruptly, while for twin Tesla NCL, the fluid temperature slowly converges or vary with a constant magnitude always less than the R-NCL.



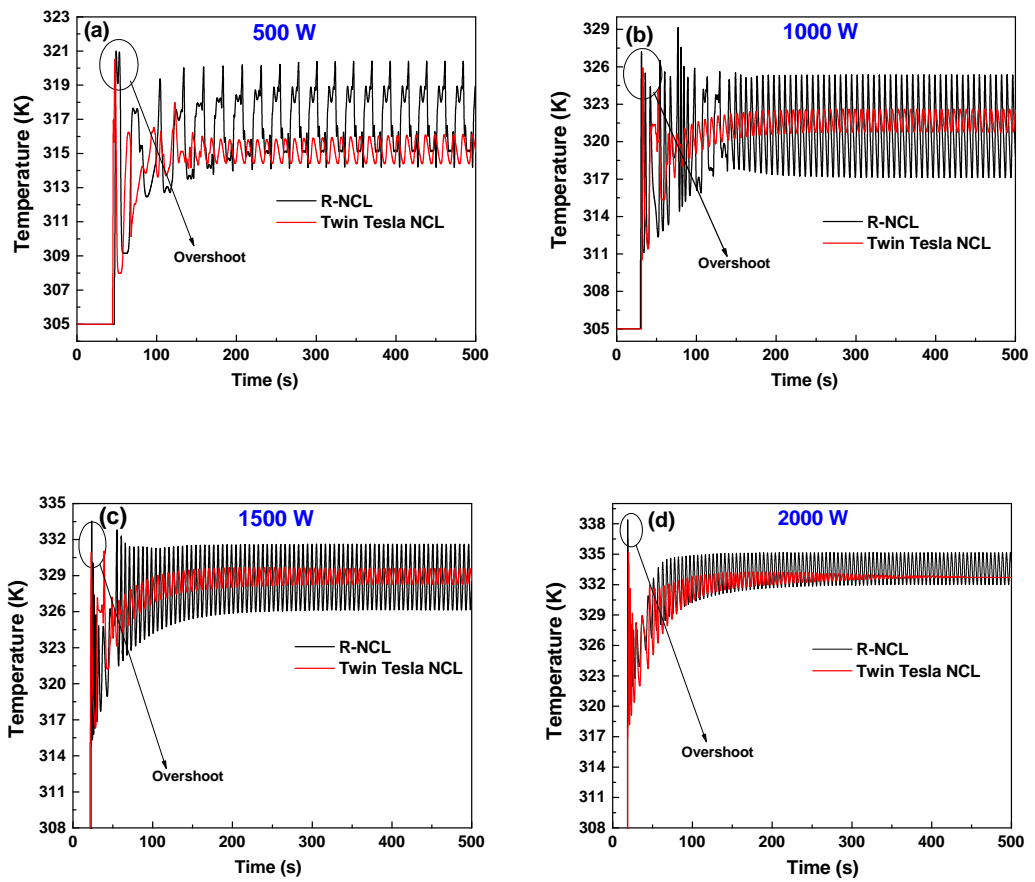


Figure 5.8: Variation of temperature at 100 bar for R-NCL and twin Tesla NCL cases with different heat fluxes of (a) 500 W, (b) 1000 W, (c) 1500 W and (d) 2000 W

At 2000 W heat input, the loop temperature in twin Tesla NCL gradually reaches a steady state without any fluctuations. Thus, incorporation of the tesla valve in the NCLs mitigates the magnitude of temperature oscillation, and it also establishes a steady state. The temperature of the loop also rises as the heat input increases, causing an increase in flow velocity. Due to the high momentum of fluid at high heat inputs, flow reversal is difficult.

#### 5.5.4 Transient variation of mass flow rate

Figures 5.9(a-f) show the transient variation of the mass flow rate of supercritical CO<sub>2</sub> at an operating pressure of 100 bar for different heat inputs.

Figures 5.9(a-b) for R-NCL show that the loop fluid is in the flow reversal stage

when the heat inputs range from 500 W to 750 W, and the oscillation frequency and peak flow of mass increases with an increase in heat input. For the low heat inputs, i.e., for 500 W and 750 W, the flow direction, instead of settling down in one direction, shows bidirectional oscillation (also called flow reversal phenomenon). However, Figs. 5.9(c-f) (for R-NCL) show that the flow pattern changes from flow reversal to single-direction flow when the heat input is  $\geq 1000$  W. Such kind of transition flow behaviour (i.e., from flow reversal to uni-direction) has been reported in many literatures (Vijayan et al. 1995; Cammarata et al. 2004; Chen et al. 2014).

An explanation for the results mentioned above is attempted (in the previous chapters) using the hot pocket theory (Welander 1967). When heat is applied to the loop, a hot pocket emerges from the heater. This hot pocket grows in length and eventually starts moving along one of the vertical legs. The length of the hot pocket can extend much larger than the length of the heater. Due to its relatively higher temperature induces a more significant flow rate due to the increase in buoyancy force. This explains the initial surge in velocity observed in most cases in Fig. 5.5(a).

In R-NCL, the buoyancy force generated is not sufficient enough to overcome friction force and inertia force, that is why flow direction changes quickly. Due to geometrical symmetry in R-NCL, even in a small fluctuation of temperature, it leads to the formation of hot (light) and cold (heavy) fluid packets and making it liable to periodic flows. However, it is also known that the stability of the scCO<sub>2</sub>-NCL depends on the geometrical parameters (diameter, aspect ratio etc.), heat inputs, loop inclination, operation procedures and their existing several transition parameters or stability threshold (Vijayan et al. 1995; Muscato and Xibilia 2003; Duffey and Pioro 2005). Results show that the prediction of flow direction in R-NCL is difficult. Hence, designing the loop for a particular application always needs design precision so that flow direction can be predicted easily.

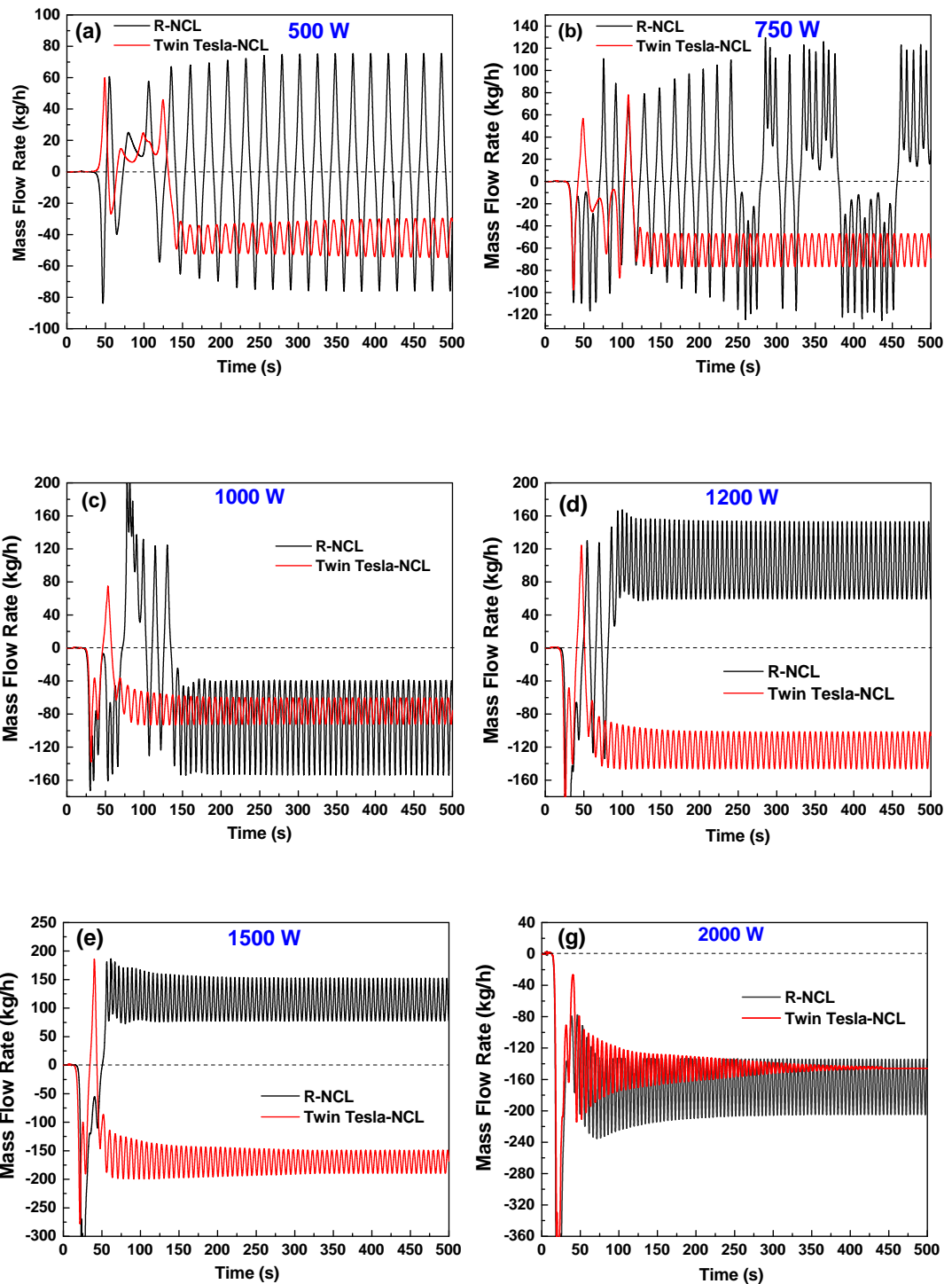


Figure 5.9: Mass flow rate of CO<sub>2</sub> for R-NCL and twin Tesla-NCL cases at 100 bar with different heat inputs of (a) 500 W, (b) 750 W, (c) 1000 W, (d) 1200 W, (e) 1500 W, and (f) 2000 W.

Whereas, in twin Tesla NCL, the direction of the flow can be decided by putting the Tesla valve in a particular direction. Results obtained for twin Tesla NCL show

the clock-wise flow (unidirectional) along the loop for all heat inputs considered in the study, as shown in Fig. 5.9(a-f). In twin Tesla NCL, the flow in a reverse direction for the Tesla valve experiences more resistance than the forward direction due to an adverse pressure gradient. Thus Tesla valve acts as a fluidic diode, and due to its diodicity, flow reversal phenomena is difficult to occur. In other words, the Tesla valve introduces differing flow impedance to circulation direction and causes unidirectional (clock-wise) oscillations in the loop. At heat input of 2000 W, in twin Tesla NCL, the flow sustains in a definite direction and eventually establishes a steady state. It is to be noted that at a higher heat input, in twin Tesla NCL, the flow direction never changes even during the initial stage of the flow. The diodicity developed on the loop establishes clock-wise flow, and it sustains the convection by continuous heating. So, it is recommended to use a Tesla valve with high heat inputs.

Table 5.1: Repetitive oscillation or unidirectional start time for regular natural circulation (R-NCL) and twin Tesla circulation loop (Twin Tesla-NCL).

<b>Heat Input</b> <b>W</b>	<b>Repetitive Oscillation or unidirectional flow</b> <b>flow start time of R-NCL</b>	<b>Unidirectional flow start</b> <b>time for Twin Tesla-NCL</b>
500 W	60 s (Reversal flow)	150 s
750 W	80 s (Reversal flow)	120 s
1000 W	140 s (Uni-directional flow)	80 s
1200 W	110 s (Uni-directional flow)	60 s
1500 W	60 s (Uni-directional flow)	52 s
2000 W	25 s (Uni-directional flow)	443 s (Reached steady-state)

Table 5.1 above, shows the repetitive oscillation or unidirectional flow start time for regular natural circulation (R-NCL) and twin Tesla natural circulation loop (twin Tesla NCL). It can be seen from Table 5.1 that with the increase of heat inputs, the flow time parameter is relatively shorter due to quick initiation. It is also observed that the flow pattern of CO<sub>2</sub> in the loop changes with the amount of heat input. Mass flow rate

is also found to be increased with heat input (Pegallapati et al. 2020).

### 5.5.5 Effect of operating pressure on flow instability

Figures 5.10(a-d) show the effect of loop fluid pressures (80, 90 and 100 bar) on the mass flow rate in twin Tesla NCL at different heat inputs (500, 1000, 1500 and 2000 W). The dynamics of the NCL significantly depend on the operating conditions (Saha et al. 2018). For this reason, proper analysis of the fluid flow dynamics in the NCL with operating pressure is very important. The pressure change concept behind this study is to check the feasibility of twin Tesla in the NCL. With this context, the following conclusions are inferred from the results obtained from the CFD simulation.

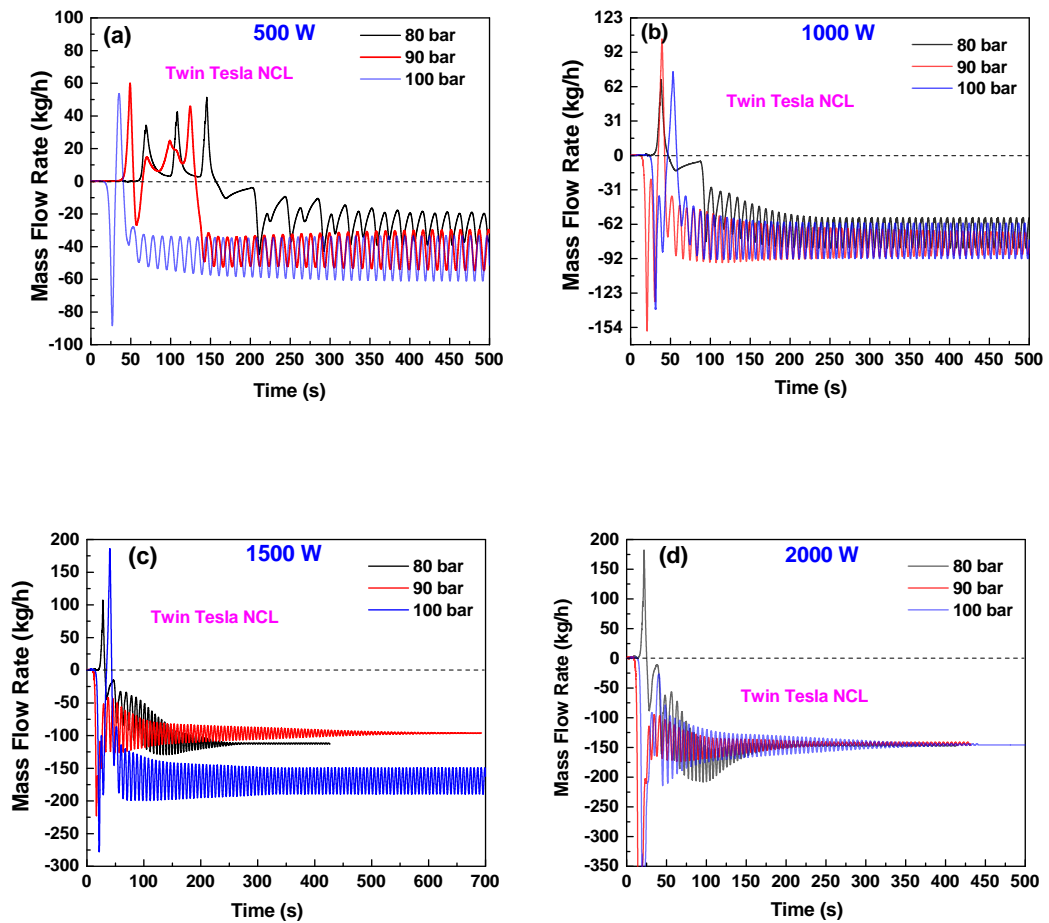


Figure 5.10: Variation of mass flow rate with different operating pressure at different heat inputs of (a) 500 W, (b) 1000 W, (c) 1500 W, and (d) 2000 W for twin Tesla NCL.

In twin Tesla NCL, irrespective of the operating pressure, the valve ensures directional stability, i.e., clockwise flow is found at all heat inputs considered in the study. It is found that the mass flow rate increases with an increase in the loop fluid pressure; the same phenomenon is observed by Archana et al. (2015b) on scCO<sub>2</sub> based NCL. From the Figs. 5.10(a-d), it can be inferred that with an increase in pressure, the magnitude of oscillation of mass flow rate or the degree of instability is more. In the considered range of heat inputs, the average temperature of the loop varies from 320 to 332 K, which is near to the pseudocritical region of 100 bar pressure (higher pressure). Near the pseudocritical region, variation in thermophysical properties is abrupt, and hence it causes instability in flow.

### 5.5.6 Nusselt number

Figure 5.11 depicts Nusselt number ( $Nu$ ) variation at an operating pressure of 90 bar for different heat inputs calculated at the sink section.

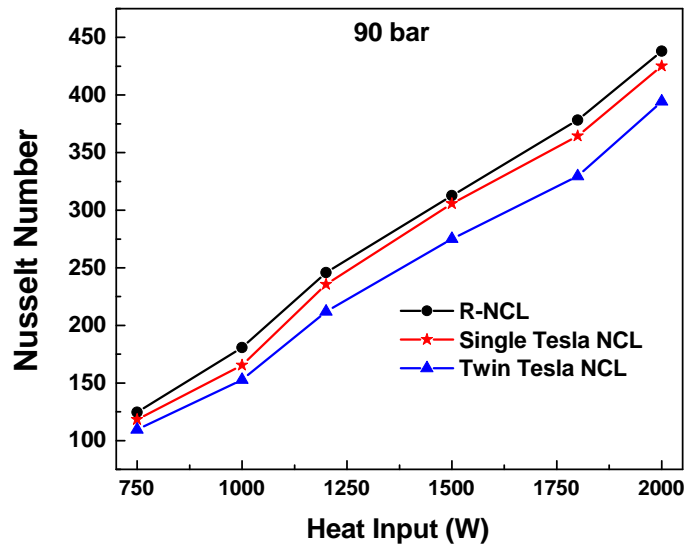


Figure 5.11: Variation of Nusselt number ( $Nu$ ) with different heat inputs at 90 bar of supercritical CO<sub>2</sub> for regular natural circulation loop (R-NCL), single Tesla NCL and twin Tesla NCL (twin Tesla NCL).

Results show the trend of an increase in  $Nu$  with an increase in heat inputs. R-NCL is

unstable in most of the transient simulation cases for the range of operating pressures chosen in the study. Thus, the heat transfer capacity (in terms of  $Nu$ ) of the loops was compared by considering the maximum absolute value of the parameters (such as heat transfer rate, mass flow rate, etc.) achieved in unidirectional constant fluctuation conditions.

Bidirectional fluctuation (like 500 W case) is referred to as a completely unstable case, and hence these cases are not considered for the comparison. While for Tesla NCL, unidirectional constant fluctuation conditions and steady-state cases are considered. It is found that the mass flow rate in R-NCL is maximum. High mass flow acts as additional incentive to increase  $Re$  and hence in increase in the  $h$ . Hence, maximum Nusselt number is found in R-NCL. Figure 5.11 indicates that the maximum drop in Nusselt number in twin Tesla NCL is 15%, whereas, for single T-NCL, it is 8% compared to R-NCL. Hence, it is advisable to use a single Tesla in the loop to better heat transfer capability and mitigate instability. However, for lower heat input, twin Tesla NCL can be used if a single Tesla valve cannot curb instability.

## 5.6 Summary

Computational fluid dynamics study is conducted to find a solution to the eternal problem of instability associated with the natural circulation loop (NCL). Results are obtained with supercritical  $CO_2$  based twin Tesla-NCL and compared with regular-NCL and single Tesla NCL at different heat inputs and operating pressures. Based on the simulation results, the following conclusions are made:

- i. Twin Tesla NCL is capable of mitigating oscillation even for low heat inputs.
- ii. Oscillation in twin Tesla is found to be minimum, while for R-NCL it is maximum.
- iii. Increase in the number of Tesla valves mitigates the instabilities in the NCL.
- iv. In twin Tesla NCL, steady-state reaches at a faster rate compared to R-NCL

- v. The maximum drop in Nusselt number in twin Tesla NCL is 15%, whereas, for single T-NCL, it is 8% compared to regular NCL. Hence, it is advisable to use a single Tesla in the loop to better heat transfer capability and mitigate instability. However, for lower heat input, twin Tesla NCL can be used if a single Tesla valve is not able to curb instability.



## CHAPTER 6

### An Experimental Study with Supercritical CO<sub>2</sub> based Natural Circulation Loops

This chapter discusses a set of experimental investigations with Regular NCL (R-NCL) and single Tesla NCL (T-NCL). A detailed methodology to develop a high-pressure experimental setup and the instruments used to perform experiments are also presented. The uncertainty analysis is included in the section.

#### 6.1 Design of regular natural circulation loop setup

A detailed schematic representation of a regular NCL (R-NCL) experimental facility used in this study is shown in Fig. 6.1. The setup consists of an electrical heater, a cold heat exchanger, a mass flow meter and two insulated legs (left and right leg). In addition to these main components, a CO<sub>2</sub> reservoir is also employed in the experimental setup.

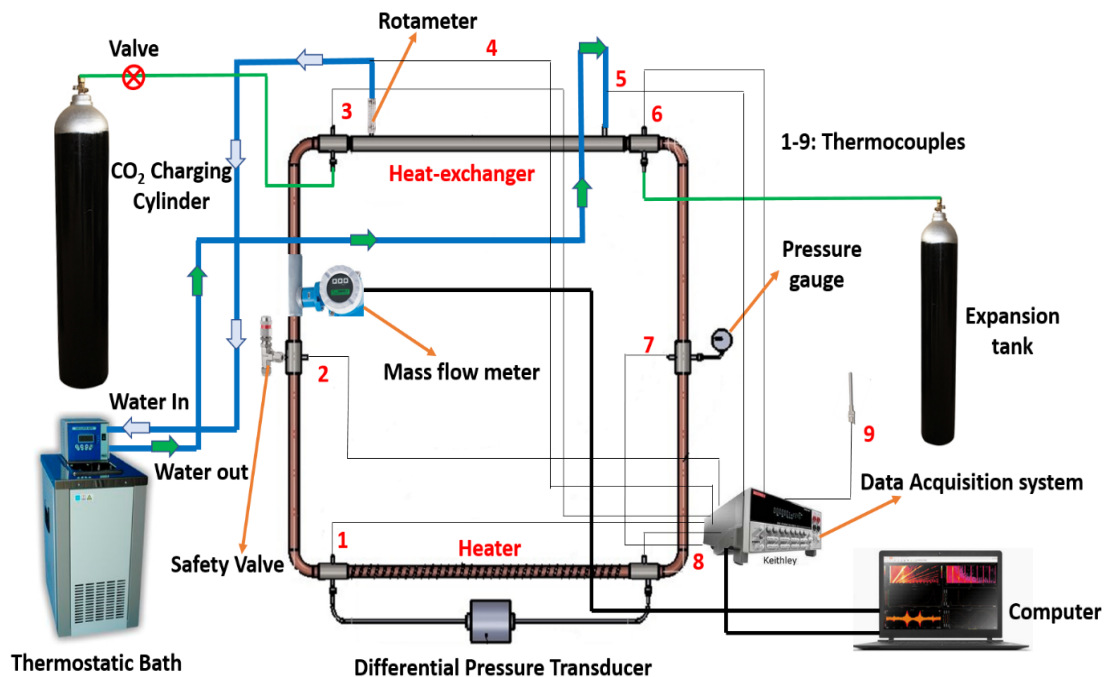


Figure 6.1: Schematic of the regular NCL (R-NCL) with instruments used in the experiment.

An NCL of  $1\text{ m} \times 1\text{ m}$  is consist of two horizontal circular pipes (heat transfer sections) and two vertical circular pipes (circulation driving sections) connected with four bends, as shown in Fig. 6.2.

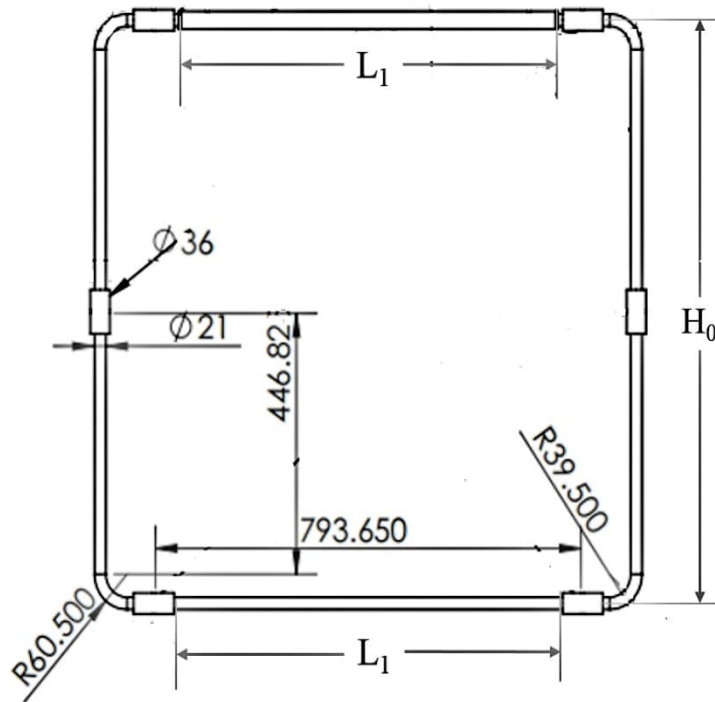


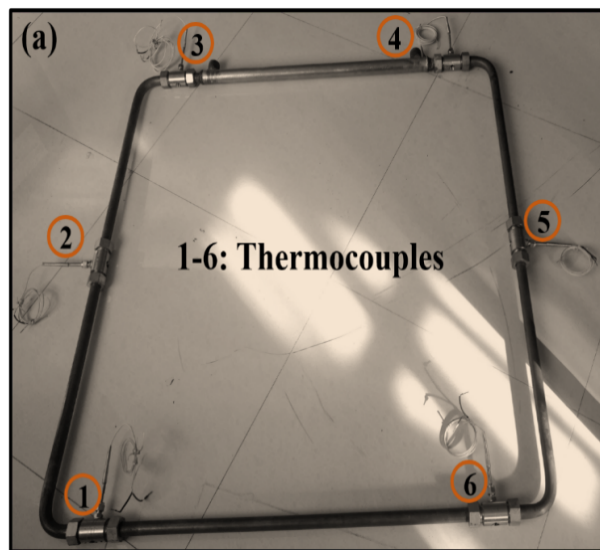
Figure 6.2: Design of fabricated regular natural circulation loop.

The geometrical detail of R-NCL is given in Table 6.1. All four pipes and the bends are made of stainless steel (SS-316) with a uniform inner diameter  $d = 15\text{ mm}$  throughout the circulation loop, having a thickness of  $3\text{ mm}$  and capacity to withstand pressure is up to  $210\text{ bar}$ . The entire loop is insulated with asbestos rope and foam tape insulation with a thickness of  $3\text{ mm}$ , each used to minimize heat transfer from the loop to the ambient. SS Grade 316 is a standard molybdenum-bearing grade austenitic stainless steel, which contains  $6\text{-}18.5\%$  Cr,  $10\text{-}14\%$  Ni,  $2\text{-}3\%$  Mo. The Molybdenum ( $^{93}\text{Mo}_{42}$ ) gives 316 better overall corrosion resistant properties and Chromium ( $^{52}\text{Cr}_{24}$ ) increases the oxidation resistance capacity. A tube in tube type of heat exchanger having  $660\text{ mm}$  length, the outer diameter of  $32\text{ mm}$  and thickness of  $3\text{ mm}$  is used.

Table 6.1: The geometrical dimensions of R-NCL.

Loop detail	Size (mm)
Inner diameter of the loop pipe	15
Outer diameter of the loop pipe	21
Thickness of the loop pipe	3
Length of heater and heat-exchanger ( $L_1$ )	660
Length of right leg and left leg ( $H_0$ )	1000
Radius of bend (outer)	60.5
Radius of bend (inner)	39.5
Outer diameter of heat-exchanger	32
Annulus distance (radial)	2.5

Figures 6.3(a) and (b) show the photographic view of the setup without insulation and with one-layer asbestos rope insulation, respectively. Six pre-calibrated T-type thermocouples are located at different locations along the loop to monitor the inside temperature of loop fluid, i.e., CO<sub>2</sub>.



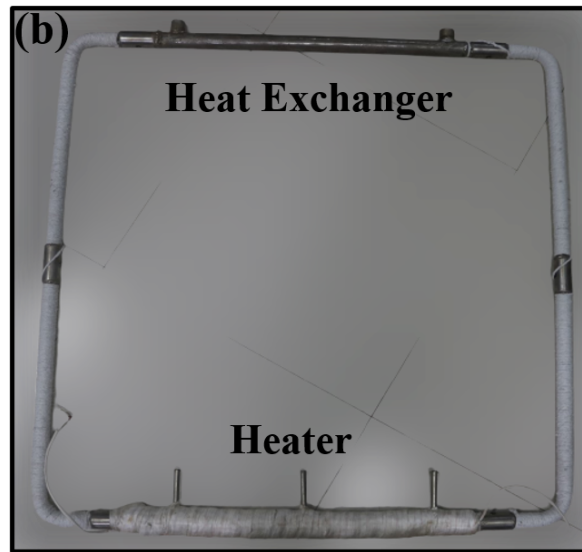


Figure 6.3: Photographic view of the experimental setup (a) Without insulation and (b) With one layer insulation (asbestos rope).

The thermocouples are directly connected to loop by using nut and ferrule arrangement, in such a way that its probe directly touches the the loop fluid. (shown in Fig. 6.3(a)).

## 6.2 Design of Tesla natural circulation loop setup

A detailed schematic representation of the Tesla NCL experimental setup used in this study is shown in Fig. 6.4. The experimental setup consists of an electrical heater, a cold heat exchanger, a mass flow meter, two insulated legs (left and right leg) and the attached instruments. In addition to these main components, a modified Tesla valve is integrated on the left leg of the loop to promote uni-directional flow, as shown in Fig. 6.5, and all the geometrical dimensions of T-NCL is given in Table 6.2.

Entire loop along with the Tesla valve is fabricated by using 316 grade stainless steel material. The inner diameter of the loop is 15 mm throughout the circulation loop with a thickness of 3 mm and having the capacity to withstand pressure is up to 210 bar. Similar to R-NCL, the entire loop is insulated with asbestos rope and foam tape. The length of the heat exchanger is 660 mm, outer diameter 32 mm and thickness of 3 mm.

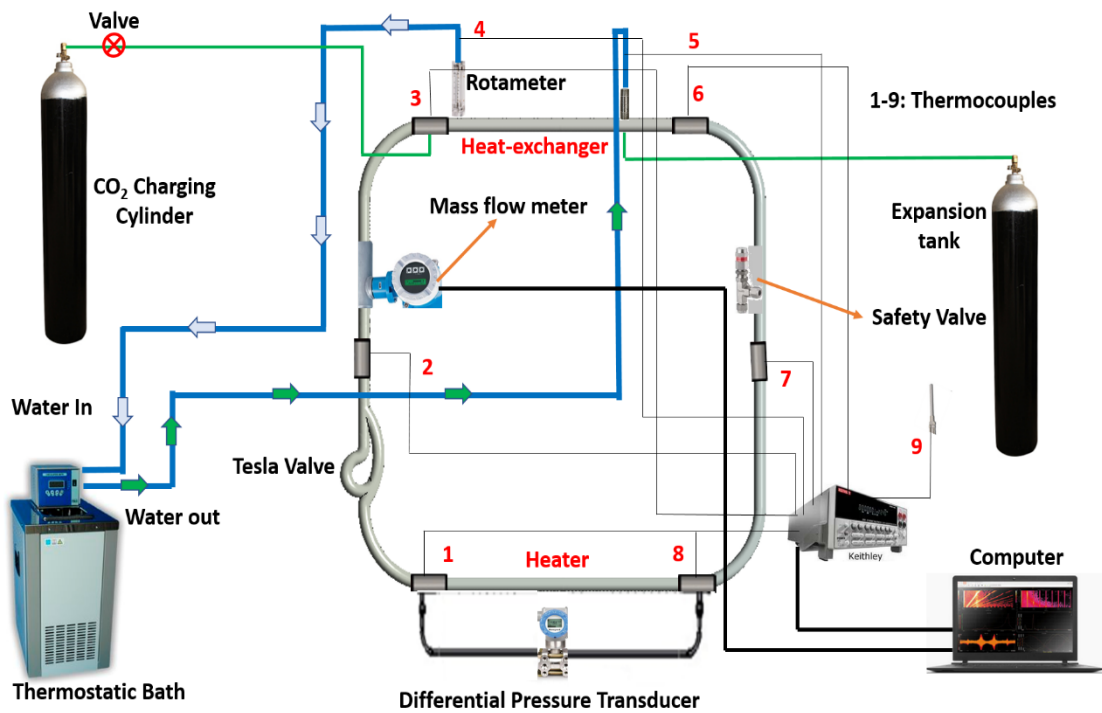


Figure 6.4: Schematic of the Tesla NCL with heater and heat exchanger.

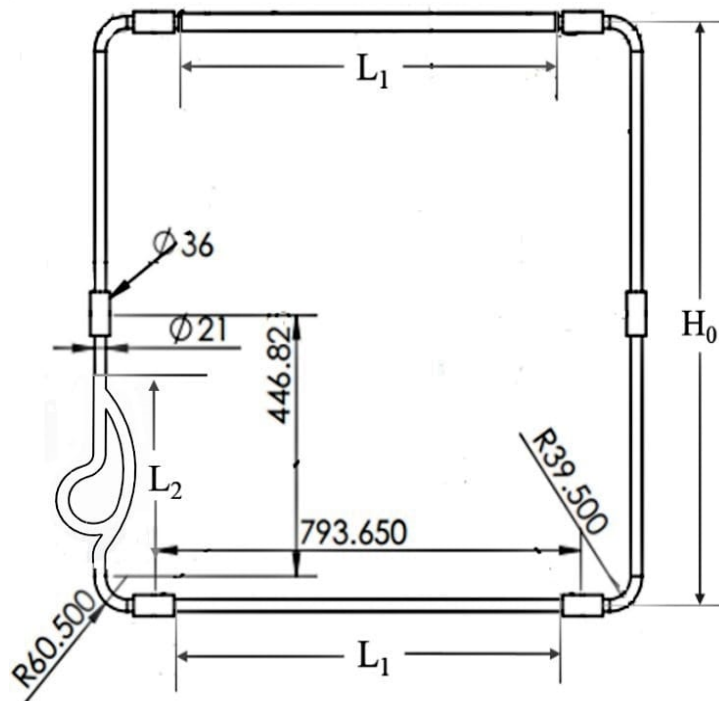


Figure 6.5: Design of fabricated Tesla natural circulation loop.

Figures 6.6 (a) and (b) show the photographic view of the setup without insulation and

the inner view of the modified Tesla valve, respectively. The design and dimensions of the Tesla valve are already indicated in Fig. 4.2 and Table 4.2 in section 4.2.

Table 6.2: The geometrical dimensions of T-NCL.

Loop detail	Size(mm)
Inner diameter of the loop pipe	15
Outer diameter of the loop pipe	21
Thickness of the loop pipe	3
Length of heater and heat-exchanger ( $L_1$ )	660
Length of right leg and left leg ( $H_0$ )	1000
Vertical length of Tesla valve ( $L_2$ )	200
Radius of bend (outer)	60.5
Radius of bend (inner)	39.5
Outer diameter of heat-exchanger	32
Annulus distance (radial)	2.5

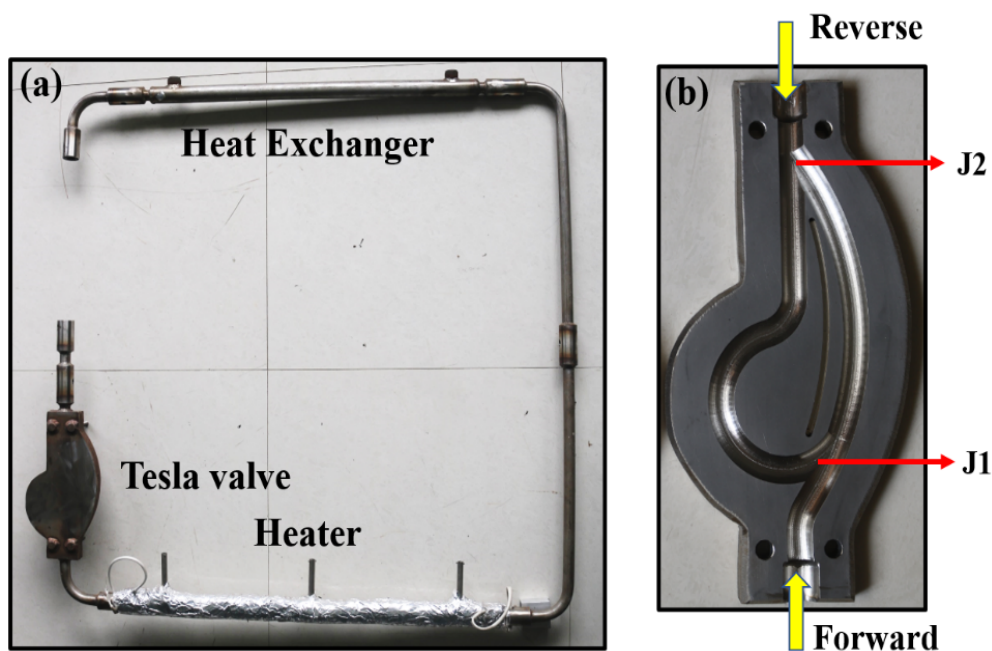


Figure 6.6: (a) Photographic view of the experimental setup (b) Modified Tesla valve inner view.

### 6.3 Fabrication of modified Tesla valve

The modified Tesla valve used in the current experimental study is indigenously fabricated by adopting a different technique, as it is a unique dual-veined flow path design, and this flow path comprises various curvatures of sharp radius. The accuracy of these curvatures and the flow path surface smoothness inside the tesla valve directly impacts the diodicity generation across the tesla valve and, in turn, affects the directional stability of the loop. Design and fabrication of a tesla valve for a laboratory-sized NCL using tube are challenging, requiring very high precision workmanship. The overall length of the modified tesla valve used in the experiment is 199.43 mm, and the fabrication of it by retaining required curvatures within such a short length using a 15 mm diameter tube is very intricate work, as the number of weld joints involved is more. These weld joints have to be located very close to each other, making fabrication activity much more difficult. Hence, it is difficult to ensure precise dimensions, which is mandatory to achieve the required diodicity, in such a small-sized prototype tesla valve with too many weld joints. Further, the very high temperature of welding distorts the shape of the tesla valve as the thickness of SS tube material is very less. Apart from the high precision requirement, the strength of the weld joint is also the main concern as the operating pressure of the loop fluid is significantly very high. Considering these complexities involved in fabricating the tesla valve using 3 mm thick SS tube material, a different technique has been adopted to address both accuracy and safety issues.

The innovative technique employed in fabricating the Tesla Valve: Instead of using a 3 mm thick stainless steel tube material, an innovative technique utilized a 16 mm thick stainless steel plates material to fabricate the modified Tesla valve using Computerized Numerical Control (CNC) machine. Using CNC machining technology, the tesla valve shaped flow path is machined in two rectangular SS 316 plates of  $250 \times 150 \times 16$  mm. In one of these plates, a half-circled groove of 15 mm diameter at inlet and outlet to join the loop pipe, and depth of 7.5 mm is machined, which resembles the shape of the Tesla valve flow path, as shown in Fig. 6.7.



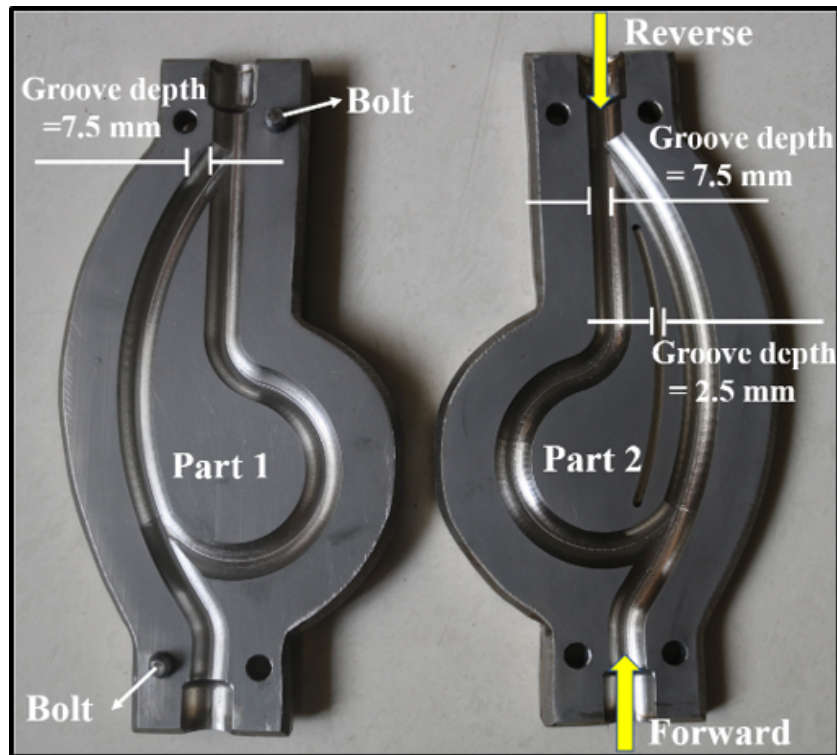


Figure 6.7: Photographic view of modified Tesla valve.

Similarly, in the second plate, the identical half-circled shaped groove is machined with a mirror image shape to the first plate, as shown in Fig. 6.7. To avoid ingress of loop fluid from the left channel to the right channel, one groove of 2.5 mm is machined in one of the plates, then a rubber gasket of 3 mm is inserted in this groove before bolting the plates. These two plates are welded together (TIG welding) at all four sides to make it a single block. Thus, a modified Tesla shaped flow path is formed using two plates and welded at the left leg of the natural circulation loop to form a T-NCL.

The modified Tesla valve is attached at the bottom of the left leg to create high impedance from the reverse side, allowing fluid to move in the forward direction only. The right-side channel of the valve is the primary channel, and the left side channel is secondary. The channels' intersections are marked as junctions J1 and J2 (shown in Fig. 6.6(b)). Due to the alignment of the secondary channels with the primary channel at junction J2, a substantial quantity of fluid enters the secondary channel for reverse flow, which improves the diodicity of the valve. When fluid moves in the forward di-



rection, the design of the valve forces most of the fluid to move in the right (primary) channel. However, fluid splits into both arms in the reverse direction, and fluid in the left channel opposes fluid moving in the right channel at junction J1. Hence, fluid experiences higher resistance (pressure drop) when moving in the reverse direction.

#### **6.4 Data collection and instrumentation for R-NCL and T-NCL**

A thermostatic bath (Thermo scientific PC200) having a heating/cooling capacity of 2 kW supplies external fluid (water) at a fixed temperature to the heat exchanger. The mass flow rate of external fluids is measured using a calibrated rotameter (0-5 LPM range) with a valve arrangement connected to a cold heat exchanger (CHX). A differential pressure transducer made by Honeywell (range 0-1000 mbar) is connected to either end of the heater. A safety valve cum pressure gauge (0-250 bar) is attached at the middle of the right leg, and it is set for 140 bar for the entire experiment. One Coriolis-type mass flow meter (Model: Rheonik RHE16) is placed at the right vertical leg to measure the mass flow rate of loop fluid (scCO<sub>2</sub>), capable of recording 0–500 kg/h. The Rheonik RHE16 Coriolis mass flow transmitter is a state-of-the-art multifunction DIN rail mount Coriolis transmitter. With full MODBUS capability, the RHE16 provides flow, density and temperature measurement to any supervisory control system. The heat input at the source is controlled by a dimmerstat (Make: Automatic electric, Model: 20D-1P) and measured by a power meter. Altogether, nine pre-calibrated T-type thermocouples (shown in Fig. 6.1) are placed on the experimental loop to monitor the temperatures throughout.

A computer integrated data acquisition system (Model: KEITHLEY-2700) having a Kickstart software (LabVIEW software) used for the in-time screening/monitoring (the reading error for the data collection is within  $\pm 0.1$  %) all the data for temperatures and pressure. Monitored data are stored in the computer.

Figure 6.8 and Fig.6.9 show the various equipment used in the experiment. Table 6.3 shows the equipment details, operating range and accuracy.

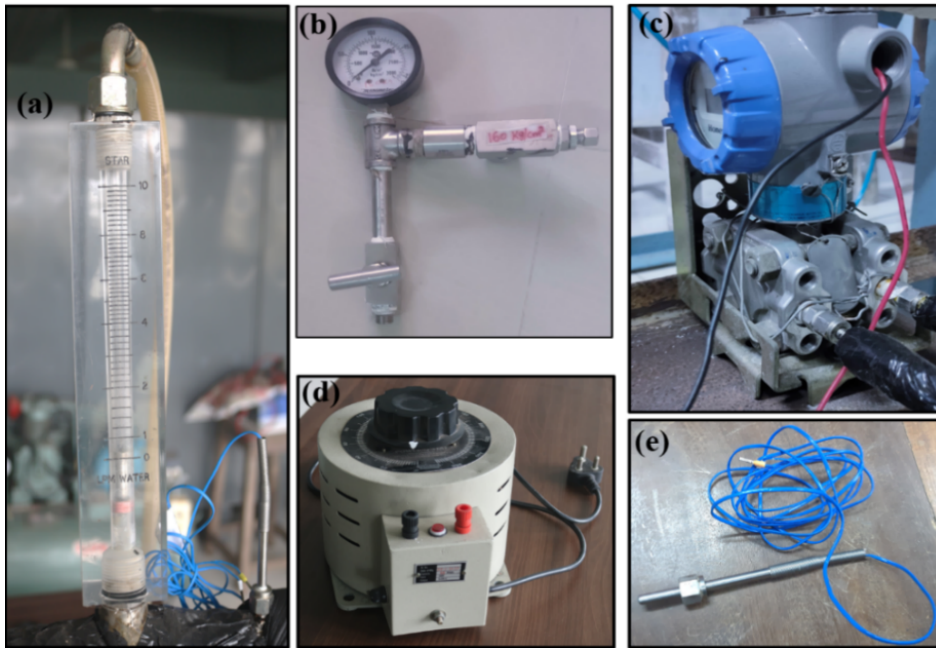


Figure 6.8: Equipment used for test facility (a) Rotameter (b) Safety valve (c) Differential Pressure transducer (d) Dimmerstat (e) Thermocouple.

The photographic view of the assembled test facility for R-NCL is shown in Fig. 6.10 and for T-NCL in Figure 6.11.



Figure 6.9: Equipment used for test facility (a) Thermostatic bath (b) Data acquisition system (c) Vacuum pump (d) Mass flow meter.

Table 6.3: Equipment details used for experimentation.

Equipment	Make/Type	Range	Accuracy
1. Thermostatic bath with inbuilt pump and heat exchanger	Thermo scientific PC200	-60 to 150 °C Heating /cooling capacity 2 kW	±0.01 °C
2. Thermocouple	T-type	-270°C -370 °C	±0.25 °C
3. Data Acquisition System	KEITHLY-2700	—	±0.01 °C
4. Differential Pressure transducer	Honeywell	0-1000 mbar	±0.1 mbar
5. Mass flow meter Rotameter	Rheonik, RHE 16 —	0-500 kg/h 0-10 LPM	±0.1 kg/min ±0.1 LPM
6. Watt Digital Meter	HTC PM-03	5-2200 W	±1 W
7. Pressure Gauge	Delta/Bourdon tube	0-150 bar	±1 bar

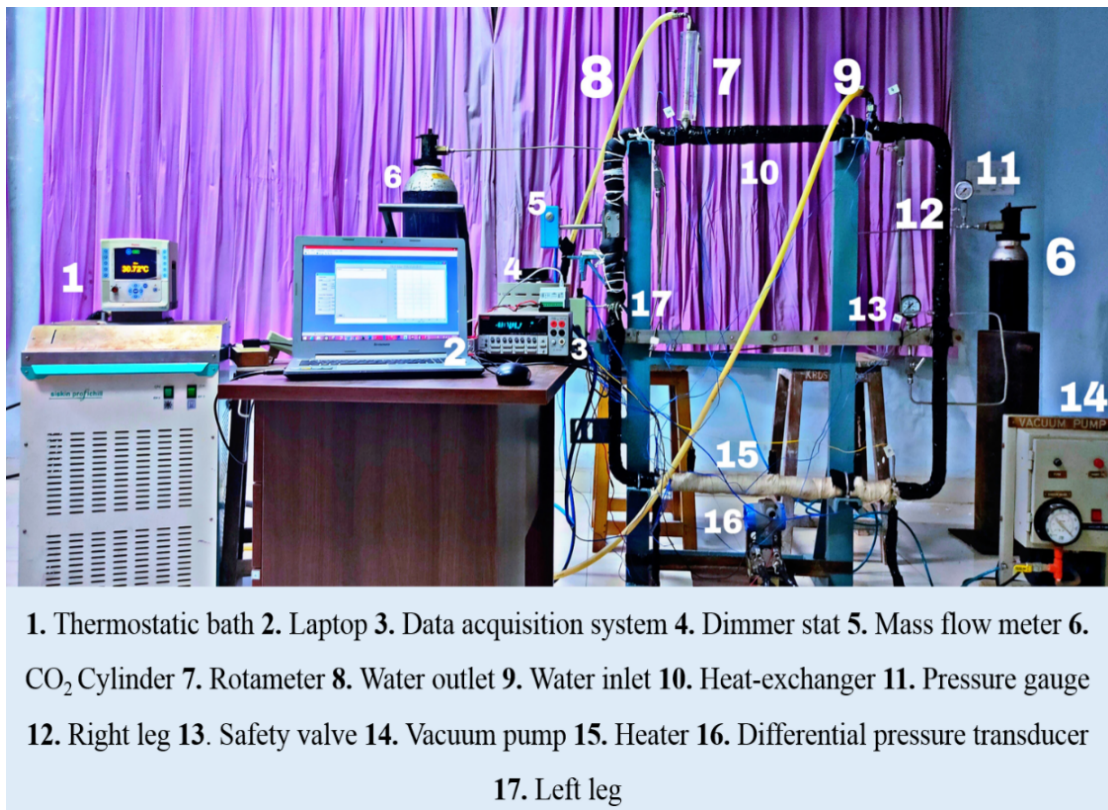


Figure 6.10: Experimental setup of regular natural circulation loop.



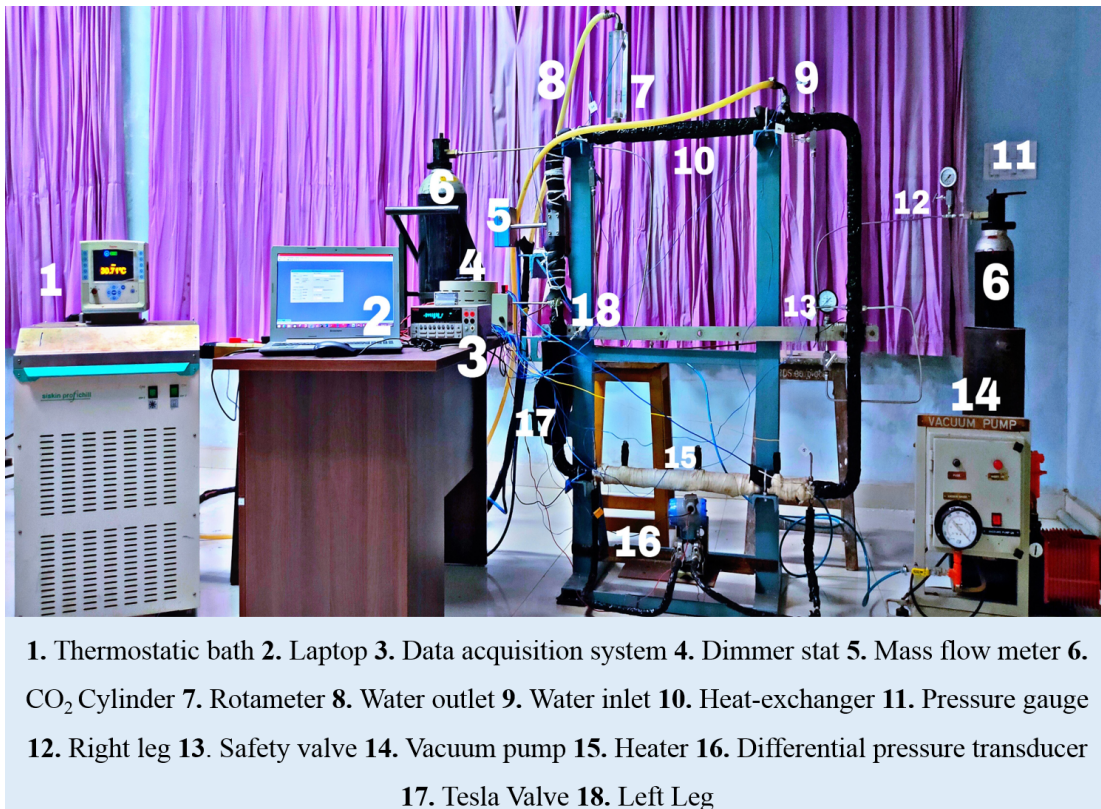


Figure 6.11: Experimental setup of Tesla natural circulation loop.

### 6.5 Experimental procedure

After fabrication, the loop is subjected to leakage test up to 150 bar i.e., one and half times the operating pressure. When no leakages were observed, then with the help of a vacuum pump, the loop was evacuated. After that, the loop was charged with CO<sub>2</sub> from the CO<sub>2</sub> cylinder (capacity: 65 bar). Based on the required initial condition (temperature and pressure), the loop along with the expansion tank were precooled to a certain temperature (calculated from [NIST \(2013\)](#) REFPROP software V 9.1) at a fixed charging pressure. The high-pressure operations are very dangerous, so special care was taken during the experiment. The precise temperature and pressure values are recorded during charging. External fluid (water) is made to flow inside an annular tube of the heat exchanger at a specified mass flow rate and temperature. As the loop reaches the initial operating condition, the heating system is initiated. When heating started, loop temperature starts varying with a small variation in loop pressure. The accumulator/expansion tank (cylinder) connected to the loop maintains almost a constant operating pressure in

the loop. The capacity of the expansion cylinder is kept 100 times more than the volume of the loop. In the current discussion, each experiment started at an initial temperature ( $T_0$ ) of 32°C and pressure ( $P_0$ ) of 90 bar for both the loops. The transient pressure, mass flow rate and temperatures are recorded throughout the experiment to observed the flow behaviour of the loop.

## 6.6 Uncertainty analysis

Every measurement is subject to some uncertainty. A measured result is only complete if it is accompanied by a statement of uncertainty in the measurement. Error is usually defined as the difference between the actual value and the calculated or measured value. Uncertainty refers to a possible value that the error may have. Measurement uncertainties can come from measuring instruments, ambient conditions or various parameters/variables considered during experiments. Such uncertainties can be estimated using statistical analysis of a set of measurements and other kinds of information about the measurement process.

In this study, the heat transfer rate is an important parameter that depends on the mass flow rate ( $\dot{m}$ ), temperature difference ( $\Delta T$ ), and specific heat of the external fluid. Since specific heat of external fluid is considered to be constant, the functional dependency of the various performance parameters relation formula is given as:

$$Q_{CHX} = f(\dot{m}_w, \Delta T_{CHX}) \quad (6.1)$$

Uncertainty in heat transfer rate:

Minimum mass flow rate (rotameter) measured in 3 LPM and least count is 0.1 LPM.

Hence maximum uncertainty in the case of mass flow rate measurement is

$$\frac{\Delta m_w}{m_w} = \frac{0.1}{3} = \pm 0.033 = \pm 3.3\% \quad (6.2)$$

For the Coriolis mass flow meter

$$\frac{\Delta m_l}{m_l} = \frac{0.1}{30} = \pm 0.0033 = \pm 0.33\% \quad (6.3)$$

The minimum temperature measured is 32 °C, and the least count is 0.25 °C. Hence, the maximum uncertainty in the case of temperature measurement with a data acquisition system is

$$\frac{\Delta T}{T} = \frac{0.25}{32} = \pm 0.0078125 = \pm 0.78125\% \quad (6.4)$$

Uncertainty in calculating heat transfer rate based on external fluid flow

$$\frac{\Delta Q}{Q} = \left[ \left( \frac{\Delta m_w}{m} \right)^2 + 2 \left( \frac{\Delta T}{T} \right)^2 \right]^{1/2} \quad (6.5)$$

$$\frac{\Delta Q}{Q} = [(0.033)^2 + 2(0.0078125)^2]^{1/2} = 0.034 = 3.4\%$$

Uncertainty in calculating heat transfer rate based on internal fluid flow

$$\frac{\Delta Q}{Q} = \left[ \left( \frac{\Delta m_w}{m} \right)^2 + 2 \left( \frac{\Delta T}{T} \right)^2 \right]^{1/2} \quad (6.6)$$

$$\frac{\Delta Q}{Q} = [(0.0033)^2 + 2(0.0078125)^2]^{1/2} = 0.0034 = 0.34\%$$

However, the heat transfer rate is an input in the experiment and measured using Wattmeter having uncertainty,

$$\frac{\Delta W}{W} = \frac{1}{250} = \pm 0.004 = \pm 0.4\% \quad (6.7)$$

Uncertainty of correlation used for validation:

Correlation by [Chen and Zhang \(2011\)](#),

$$Re = 1.129(Gr_m d/L_t)^{0.3924} \quad (6.8)$$

This correlation consists of mass flow rate and heat input as main variables, considering other thermophysical properties and geometrical parameters constant. Hence, total uncertainty ( $X$ ) involved in the correlation,

$$X = \left[ \left( \frac{\Delta m}{m} \right)^2 + \left( \frac{\Delta Q}{Q} \right)^2 \right]^{1/2} = \pm 0.00518 = \pm 0.5\% \quad (6.9)$$

## 6.7 Results and discussion

Experimental investigations with Regular NCL (R-NCL) and Single Tesla NCL (TNCL) have been done at a pressure of 90 bar over a heat input ranges from 250 W-1000 W. Mass flow rate, differential pressure and temperatures at varies locations are recorded during experiments. Obtained experimental data is also used to validate simulation results.

### 6.7.1 Mass flow rate variations

Figures 6.12(a-d) show the transient variation of the mass flow rate of supercritical CO<sub>2</sub> at an operating pressure of 90 bar at various levels of heat input ranging from 250 W to 1000 W.

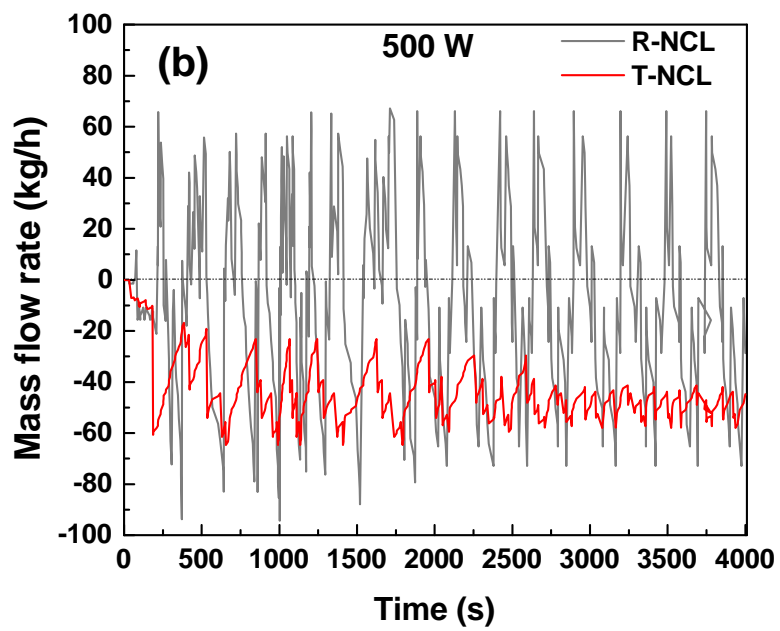
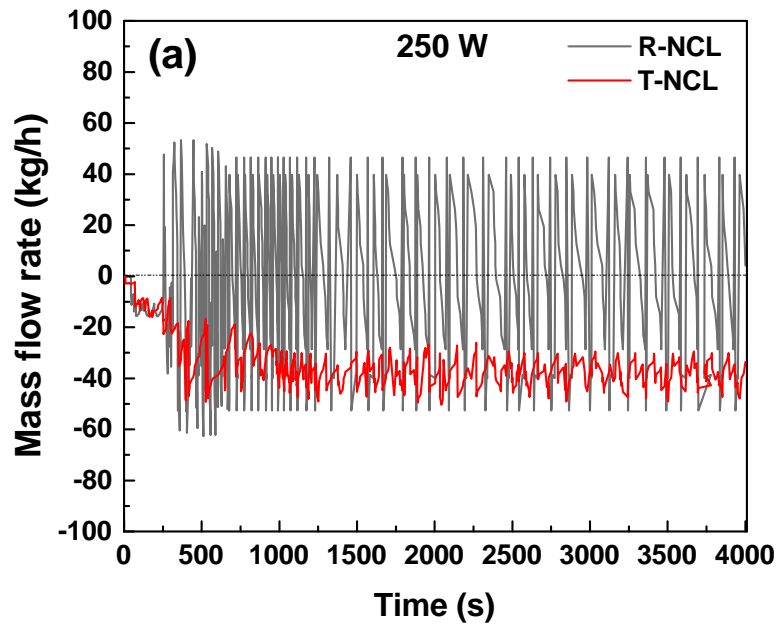
In R-NCL, at a lower level of heat input (250 W and 500 W), in the beginning, the flow undergoes a relatively low flow rate, and after that, the fluid circulates with flow oscillation, and flow reversal emerges, while that the flow pattern changes from flow reversal to uni-directional flow when the heat input is  $\geq 750$  W. At low heat input, the driving force/buoyancy force and inertia developed are not sufficient enough to provide a uni-directional flow. However, at a higher level of heat input, the fluid responds more sensitively to the changes in the heat input and takes a uni-directional path due to a higher inertial effect. At a higher level of heat input, the differential temperature at the inlet and outlet of the heater, i.e., at the bottom of the left and right legs, will be high and enhance the flow velocity. This increased velocity overcomes all the resistive forces in the loop, and flow follows a unidirectional path. Due to the high momentum

of fluid at high heat inputs, flow reversal is difficult.

In T-NCL, even at lower heat input, the flow takes a unidirectional path due to the favourable differential pressure gradient developed in the forward direction across the Tesla valve. Because of the impedance developed by the Tesla valve, the flow in the reverse direction encounters more resistance than the flow in the forward direction, resulting in a pressure gradient along the vertical pipe. This pressure gradient causes fluid to flow smoothly in only one direction, from the left leg to the right leg (i.e., a clockwise direction). The negative mass flow rate value shows the flow is in a clockwise direction and vice versa. At all levels of heat inputs, because of diodicity in T-NCL, the frequency and amplitude of mass flow oscillation consistently decrease with time for a given heat input, and at 750 W and 1000 W, the loop reaches to steady-state. It is very interesting to note that incorporating the Tesla valve in the loop effectively mitigates the inherent instability behaviour of the natural circulation loop without sacrificing (maximum 7% reduction) the performance of the loop to the mass flow rate.

The measured time required to reach steady state for the experimental study is found to be longer than the simulation study. It occurs due to the assumptions of adiabatic walls considered in the simulation. In experiments, heat transfer from the loop to the surrounding cannot be made zero, and it also varies as the temperature of the loop changes. Additionally, the heat loss to the ambient puts the loop to behave as the case of lower heat input. It is to be noted that the loop at lower heat input takes more time to reach steady state in the case of supercritical CO<sub>2</sub>.





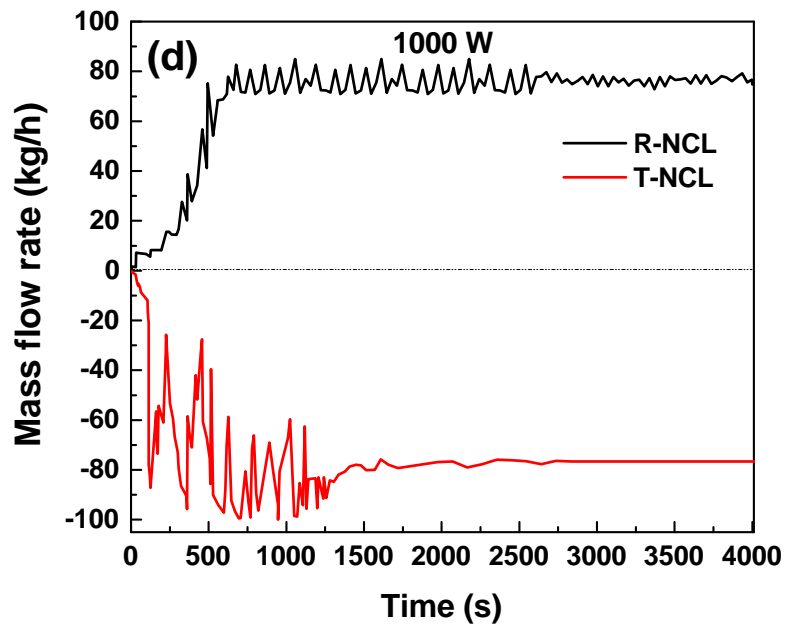
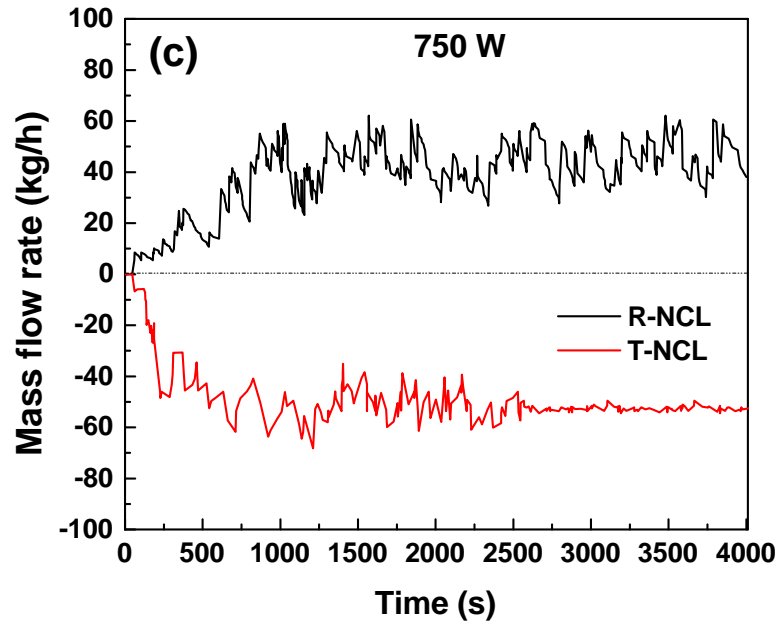
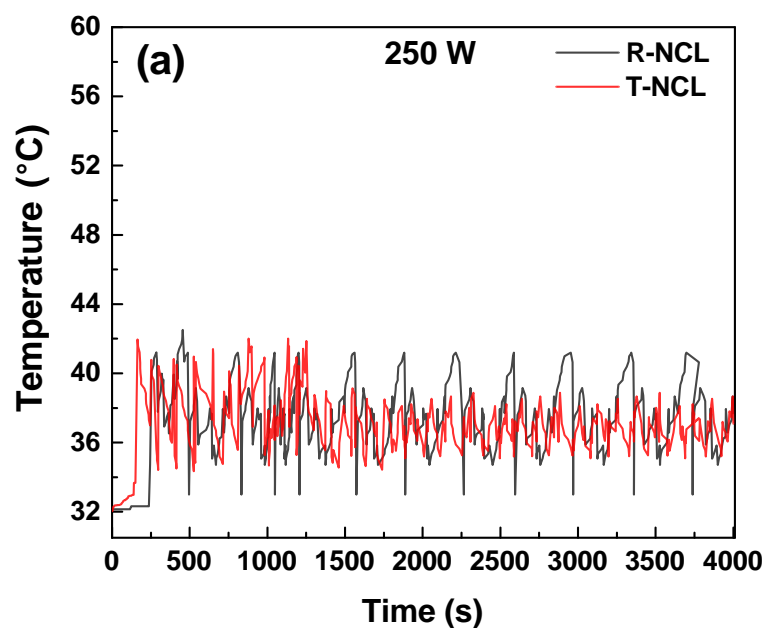


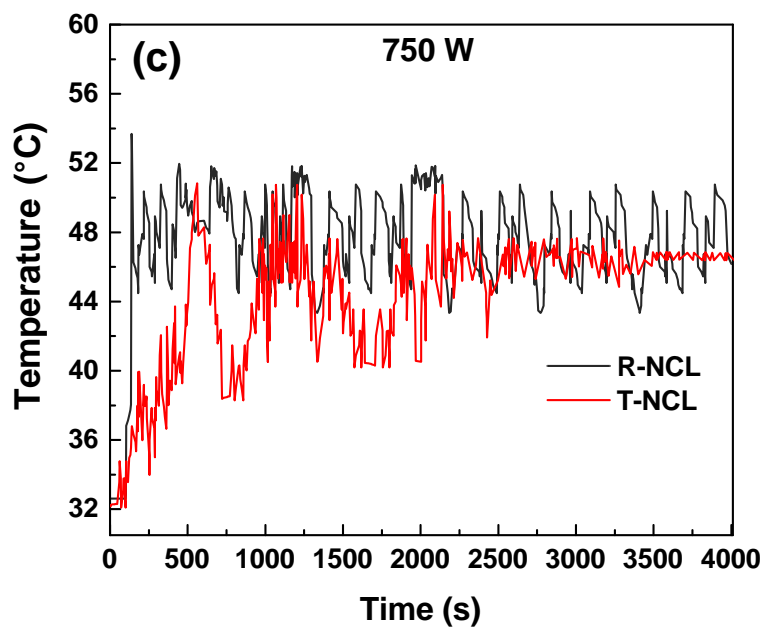
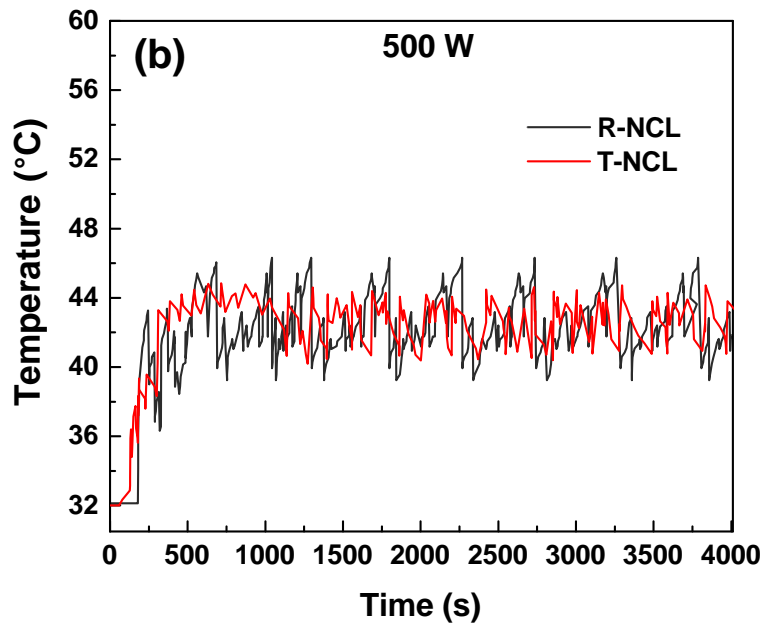
Figure 6.12: Mass flow rate variation at 90 bar with different heat inputs at (a) 250 W, (b) 500 W, (c) 750 W and (d) 1000 W.

### 6.7.2 Temperature variations

A comparative transient temperature variation of R-NCL and T-NCL for various heat inputs at a pressure of 90 bar are shown in Fig. 6.13(a-d) is calculated at the center of right leg. In CHX, water is used as a coolant fluid at a temperature of 32°C with a mass flow rate of 3 LPM to sensibly remove the heat from the loop. The heat inputs over a range of 250 W to 1000 W are applied to the heater to trigger the fluid flow from its quiescent state. Circulation of the loop fluid is maintained due to the buoyancy effect caused by heating at the bottom and cooling at the top.

It is proven that the heat exchanger efficiency deteriorates if its nature switches from counter-flow to parallel flow. Similarly, the heat transfer performance at the heater also gets affected if the temperature difference between the heating section and the loop fluid keeps on changing with time.





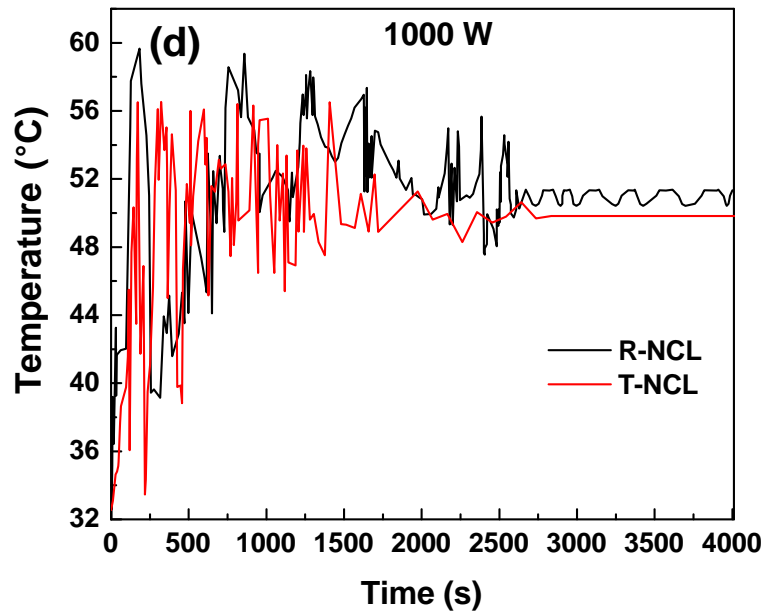


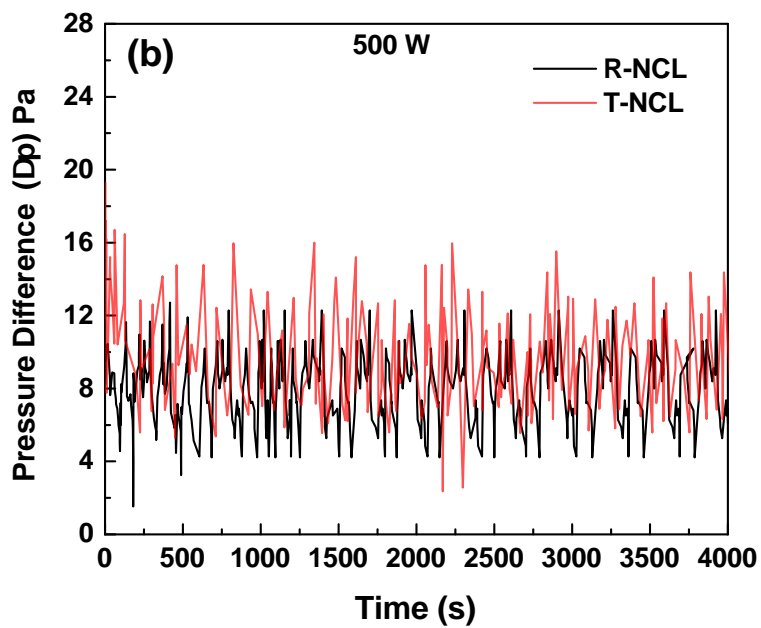
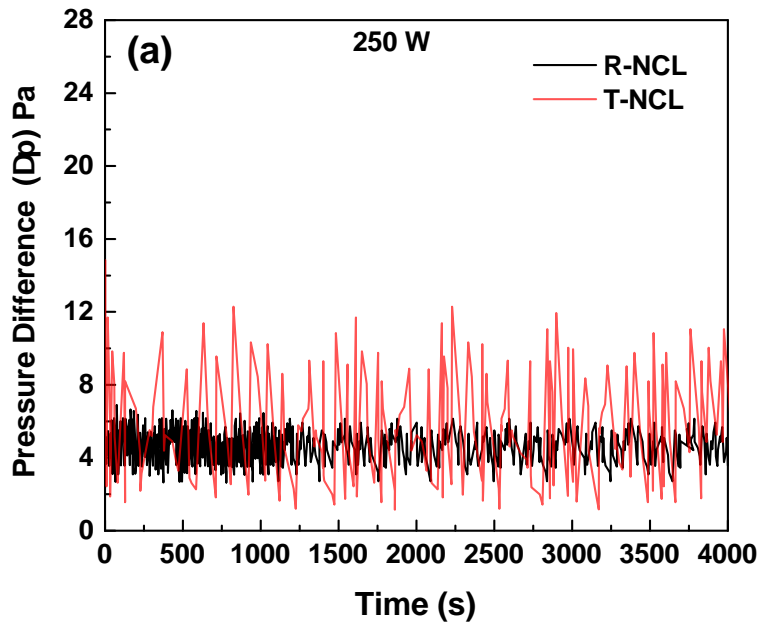
Figure 6.13: Variation of temperature at 90 bar for R-NCL and T-NCL cases with different heat inputs at (a) 250 W, (b) 500 W, (c) 750 W and (d) 1000 W.

So, the temperature distribution in the loop fluid adversely affects the overall heat transport capacity of the loop and eventually amplifies instability in the loop. Hence, by providing a uni-directional flow, the oscillatory behaviour of the loop gets reduced to the maximum extent and enhances the heat transport capability.

From Fig. 6.13, it is observed that fluid temperature oscillation is appreciably reduced with Tesla valve integration in the loop. The effect of Tesla in mitigating the oscillatory nature of the loop fluid keeps on improving with an increase in the heat input at the source. The amplitude of temperature oscillation of loop fluid in T-NCL is less than R-NCL, and at a higher level of heat input, its reduction is very noticeable. It is interesting to note that the time duration required to reach a stable state or a steady state in T-NCL is less than R-NCL at all levels of heat input. In T-NCL, the temperature reaches a steady state at a faster rate than R-NCL at higher heat input considered in the experimental study.

### 6.7.3 Pressure variation

Figures 6.14(a-d) depict the variation of differential pressure across the heater in the R-NCL and T-NCL at various heat input levels ranging from 250 W to 1000 W.



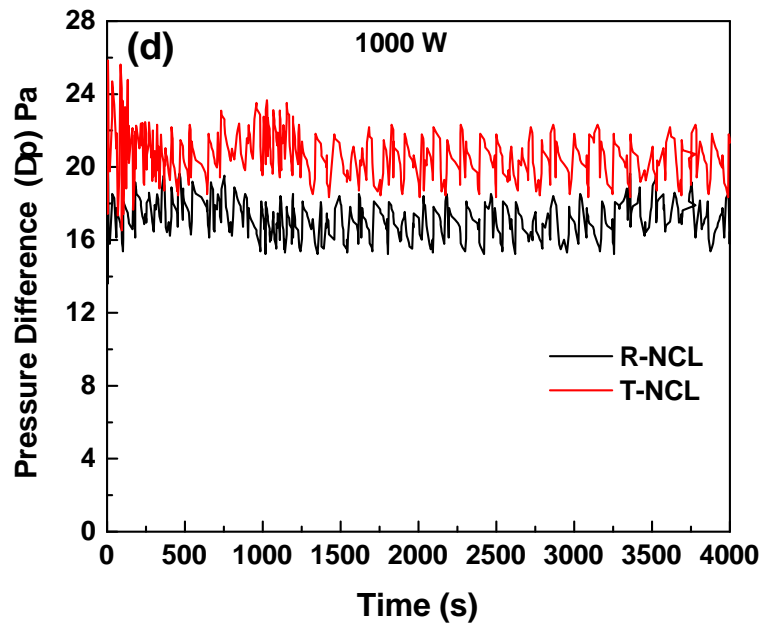
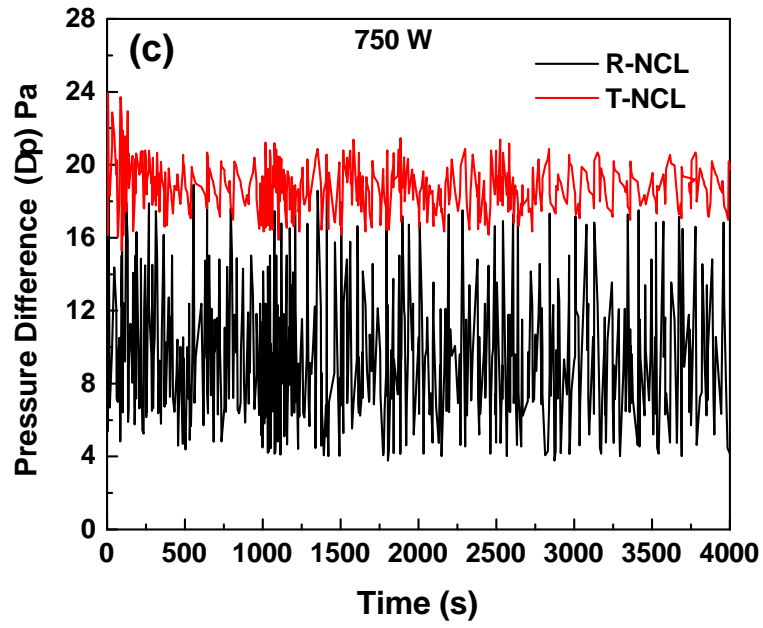


Figure 6.14: Variation of differential pressure across heater at 90 bar for R-NCL and T-NCL cases with different heat inputs at (a) 250 W, (b) 500 W, (c) 750 W and (d) 1000 W.

The differential pressure gradient across the heater is the one that decides the flow behaviour of the loop. At higher heat input, the mass flow rate increases due to higher buoyancy force cause a higher pressure drop across the heater. Also, as the heat input increases, the density of the loop fluid decreases and thus, flow velocity in the loop increases. An increase in the fluid velocity along the Tesla valve increases the pressure drop across it, as shown in Fig 6.14. The pressure drop in the T-NCL is high compared to R-NCL at all heat inputs due to additional length of curved part in the Tesla valve.

## 6.8 Validation

Validation of obtained simulation results are done with the experimental data and available correlation given by [Chen and Zhang \(2011\)](#) in terms of non-dimensional parameters (shown in Fig. 6.15), a good agreement is found between them.

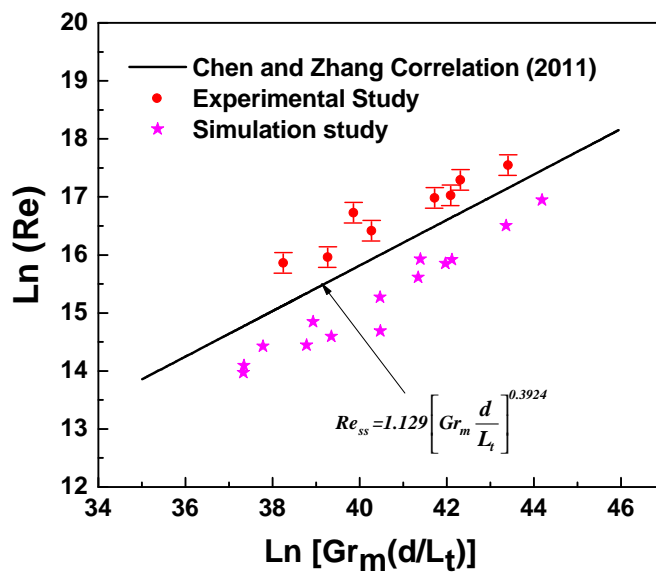


Figure 6.15: Validation of simulation data with experimental results and available correlation.

Reynolds number is calculated on the basis of below formulae:

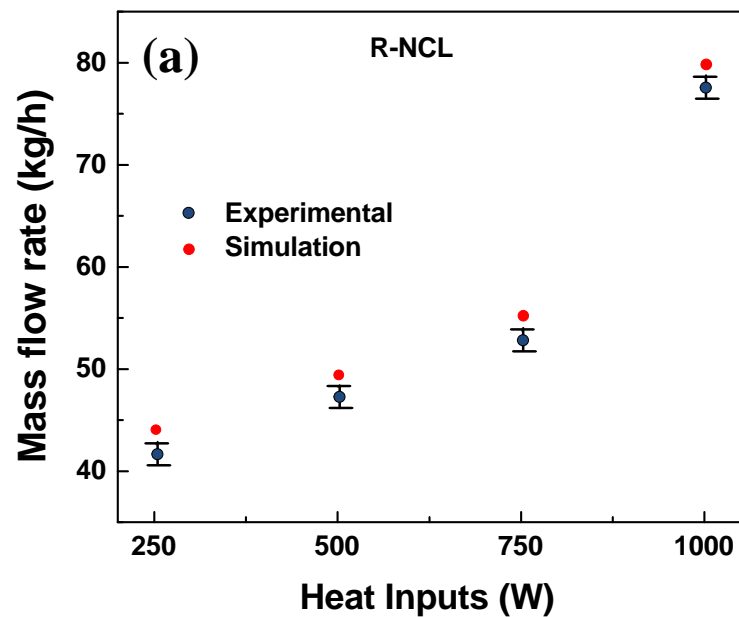
$$Re = \frac{4m}{\pi\mu d}$$



Where,  $m$  i.e., mass flow rate is obtained from Coriolis flow meter and thermophysical properties are calculated from [NIST \(2013\)](#) data, based on the loop temperature taken from thermocouples. The maximum deviation of simulation results from experimental data is 12% and from correlation is 4%.

Simulation results obtained from CFD analysis are also validated with the experimental data in terms of mass flow rate (as shown in Fig. 6.16), and the comparison reflects a good match.

The maximum difference is found to be 6% between the experimental and the numerical data. The deviations are due to the three-dimensional (experimental) analysis and two-dimensional CFD simulation.



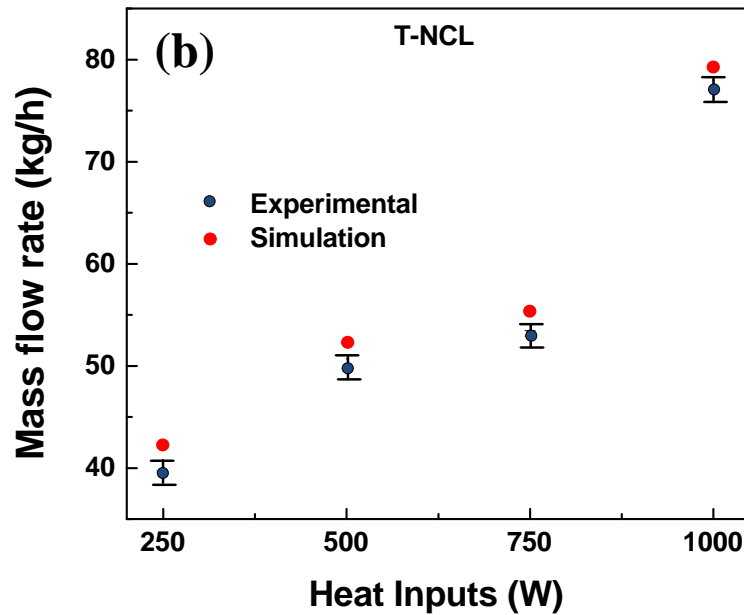


Figure 6.16: Validation of simulation data with experimental results in terms of mass flow rate.

## 6.9 Summary

Conclusions from experimental results can be summarized as follows:

- i. Experimentally it is also found that Modified Tesla valve is found to be an effective tool to curb instability in NCLs.
- ii. For the accuracy of the curvatures, flow path surface smoothness inside the Tesla valve and capability to withstand the supercritical pressure, it is advisable to use sufficiently thick SS plates with proper CNC machining procedure to fabricate the modified Tesla valve.
- iii. A reasonably good agreement is exhibited between the simulation predictions and the test data.
- iv. The reported time required to reach steady-state in study is longer in the experimental study than the simulations.

## CHAPTER 7

### Conclusions and Scope of Future Work

#### 7.1 Conclusions

The present dissertation analyzes several aspects of supercritical CO<sub>2</sub> based NCL with and without Tesla valve in both numerical and experimental points of view. To provide a comprehensive overview of the dissertation, all the investigations are briefly summarized, and the salient observations are reiterated in the following sections.

##### 7.1.1 Supercritical CO<sub>2</sub> flow instability in natural circulation loop

Three-dimensional computational fluid dynamics (CFD) simulation on a supercritical CO<sub>2</sub> based natural circulation loop (scCO<sub>2</sub>-NCL) with heater as a source and heat-exchanger as a sink is carried out by varying the operating pressure from 80 to 100 bar and heat input from 250 W to 2500 W. The following conclusions are drawn from the study:

- i. For supercritical CO<sub>2</sub> based NCL, a threshold heat input value exists at which the loop switches from an unstable bi-directional or unstable unidirectional fluctuation to a stable flow.
- ii. In the range of operating pressure (80-100 bar) considered in the study, it is advisable to operate scCO<sub>2</sub>-NCL near pseudo-critical region to get minimum instability. The study noticed that operation at pseudo-critical pressure (also lower pressure in this study) led to unidirectional pulsations, whereas bidirectional oscillations were observed at pressures away from pseudocritical region.
- iii. Unidirectional flow shows better heat transfer in the loop.

### **7.1.2 Instability mitigation by integrating modified Tesla type valve**

As observed in the previous section, NCL can undergo continuous fluctuations and flow reversals. Therefore, an effort has been made to identify suitable options for suppressing instability. Thus, the possibility of implementing a modified Tesla valve in the loop has been used to curb instability by promoting a unidirectional flow. A two-dimensional comparative computational fluid dynamics simulation with and without a modified Tesla type valve for supercritical CO<sub>2</sub> based NCL having heater as a source and isothermal wall as a sink over a range of pressures (80 to 100 bar) and heat inputs (500 to 2000 W) have been carried out to determine the fluid flow behaviour and performance of both the loops. The following conclusions are drawn based on the obtained CFD simulation:

- i. By inserting a modified Tesla valve in the loop, directional instability of natural circulation loop can be avoided.
- ii. Modified Tesla valve in NCLs is capable of mitigating the magnitude of velocity oscillation to a greater extent and eventually establishes a steady-state in the loop.
- iii. Oscillation in temperature and the thermal shocks in the NCL can be reduced with the help of modified Tesla valve.
- iv. Modified Tesla valve can reduce flow reversal in low heat input condition (or lower down the reversal limit) and prescribe flow direction, ensuring a steady-state at relatively higher heat input conditions.
- v. This design of the Tesla valve is found to be highly effective for mitigating instability in supercritical CO<sub>2</sub> based NCL.

### **7.1.3 Instability mitigation by integrating twin Tesla type valves in NCL**

In the previous section, it was observed that the use of a single Tesla type valve in NCL is not capable of mitigating the instability at low heat input (500 W). Hence, twin Tesla type of valves is chosen for the study. 2-D CFD simulations have been carried out for

a range of supercritical pressures (80 to 100 bar) and heat inputs (500 to 2000 W) to do the comparative investigation of instability phenomenon in supercritical CO<sub>2</sub> based regular natural circulation loop, single Tesla NCL and twin Tesla NCL. The following conclusions are drawn from this study:

- i. For low heat inputs, twin Tesla valve can be used as a viable option to curb instability.
- ii. Oscillation in regular NCL is maximum, while in twin Tesla NCL it is minimum. Thus, an increase in the number of Tesla type valve mitigates the instabilities in the NCL.
- iii. Twin Tesla valve is capable of providing steady state at a faster rate.
- iv. The maximum drop in Nusselt number in Twin Tesla NCL is 15%, whereas, for single T-NCL it is 8% compared to regular NCL. Hence, it is advisable to use single Tesla in the loop for better heat transfer capability and to mitigate instability. However, for lower heat input, twin Tesla NCL can be used if a single Tesla valve is not able to curb instability.

#### **7.1.4 Experimental investigation**

Experimental investigations with regular NCL (R-NCL) and single Tesla NCL (TNCL) have been done at a pressure of 90 bar for the various heat inputs 250 W, 500 W, 750 W, and 1000 W. Mass flow rate, differential pressure, and temperatures at various locations are recorded during experiments. Obtained experimental data is also used to validate simulation results. Conclusions from experimental results are summarized as follows:

- i. Experimentally, it is proved that the modified Tesla valve is found to be an effective tool to curb instability in NCLs.
- ii. The measured time required to reach a steady-state for the experimental study is found to be longer than the simulation study.

- iii. Simulation results show a higher amplitude of instability than experimental data.
- iv. A reasonably good agreement is exhibited between the simulation predictions and the test data.

## **7.2 Scope for future work**

In the course of the present study, a few areas were set aside that need to be addressed in the near future. Some are enumerated below:

- i. More experiments with and without Tesla valve with precisely controlled instrumentation system and image-sensing technologies are needed to understand the effect of the operating parameters on fluid behaviour.
- ii. Experiments with different geometrical modification (like change in diameter, height and orientation etc.) with greater precision and accuracy are required.
- iii. Due to the dearth of any direct controlling mechanism in supercritical fluid-based NCLs, intense analysis at the design level is needed to ensure proper performance prior to real-time operation.
- iv. A fully dedicated study on the factors affecting the stability behaviour needs to be investigated numerically and experimentally.

## REFERENCES

- Acosta, R., Sen, M. and Ramos, E. (1987). "Single-phase natural circulation in a tilted square loop." *Wärme-und Stoffübertragung*, 21(5), 269–275.
- Archana, V., Vaidya, A. and Vijayan, P. (2015a). "Flow transients in supercritical  $CO_2$  natural circulation loop." *Procedia Engineering*, 127, 1189–1196.
- Archana, V., Vaidya, A. and Vijayan, P. (2015b). "Numerical modeling of supercritical  $CO_2$  natural circulation loop." *Nuclear Engineering and Design*, 293, 330–345.
- Basu, D. N., Bhattacharyya, S. and Das, P. (2012). "Performance comparison of rectangular and toroidal natural circulation loops under steady and transient conditions." *International Journal of Thermal Sciences*, 57, 142–151.
- Bau, H. H. and Torrance, K. (1981). "Transient and steady behavior of an open, symmetrically-heated, free convection loop." *International Journal of Heat and Mass Transfer*, 24(4), 597–609.
- Bernier, M. and Baliga, B. (1992). "A 1-d/2-d model and experimental results for a closed-loop thermosyphon with vertical heat transfer sections." *International journal of heat and mass transfer*, 35(11), 2969–2982.
- Blackburn, J. M., Long, D. P., Cabanas, A. and Watkins, J. J. (2001). "Deposition of conformal copper and nickel films from supercritical carbon dioxide." *Science*, 294(5540), 141–145.
- Bodkha, K., Kumar, N., Vijayan, P. and Saha, D. (2010). "Investigations on role of mechanical gadgets in controlling flow instability in single-phase natural circulation loops." In *Proceedings of the 20th National and 9th International ISHMT-ASME Heat and Mass Transfer Conference, Mumbai, India*.

- Bondioli, P., Mariani, C., Lanzani, A., Fedeli, E., Mossa, A. and Muller, A. (1992). “Lampante olive oil refining with supercritical carbon dioxide.” *Journal of the American Oil Chemists’ Society*, 69(5), 477–480.
- Bošković, D. M. and Krstić, M. (2001). “Nonlinear stabilization of a thermal convection loop by state feedback.” *Automatica*, 37(12), 2033–2040.
- Cammarata, L., Fichera, A., Guglielmino, I. and Pagano, A. (2004). “On the effect of gravity on the bifurcation of rectangular closed-loop thermosyphon.” *Heat and mass transfer*, 40(10), 801–808.
- Cao, Y. and Zhang, X.-R. (2012). “Flow and heat transfer characteristics of supercritical  $CO_2$  in a natural circulation loop.” *International Journal of Thermal Sciences*, 58, 52–60.
- Chato, J. (1963). “Natural convection flows in parallel-channel systems.” *Journal of Heat Transfer*, 85, 339–345.
- Chatoorgoon, V. (1986). “Sports-a simple non-linear thermalhydraulic stability code.” *Nuclear Engineering and Design*, 93(1), 51–67.
- Chatoorgoon, V. (2001). “Stability of supercritical fluid flow in a single-channel natural-convection loop.” *International Journal of Heat and Mass Transfer*, 44(10), 1963–1972.
- Chatoorgoon, V., Voodi, A. and Fraser, D. (2005). “The stability boundary for supercritical flow in natural convection loops: Part i:  $H_2O$  studies.” *Nuclear Engineering and Design*, 235(24), 2570–2580.
- Chauhan, A. and Kandlikar, S. G. (2019). “Characterization of a dual taper thermosiphon loop for cpu cooling in data centers.” *Applied Thermal Engineering*, 146, 450–458.



- Chen, K. (1985a). “On the oscillatory instability of closed-loop thermosyphons.” *Journal of Heat Transfer*, 107, 826–832.
- Chen, K. (1985b). “The optimum configuration of natural convection loops.” *Solar Energy*, 34(4-5), 407–416.
- Chen, L., Deng, B.-L., Jiang, B. and Zhang, X.-R. (2013a). “Thermal and hydrodynamic characteristics of supercritical  $CO_2$  natural circulation in closed loops.” *Nuclear Engineering and Design*, 257, 21–30.
- Chen, L., Deng, B.-L. and Zhang, X.-R. (2013b). “Experimental investigation of  $CO_2$  thermosyphon flow and heat transfer in the supercritical region.” *International Journal of Heat and Mass Transfer*, 64, 202–211.
- Chen, L., Deng, B.-L. and Zhang, X.-R. (2013c). “Experimental study of trans-critical and supercritical  $CO_2$  natural circulation flow in a closed loop.” *Applied Thermal Engineering*, 59(1-2), 1–13.
- Chen, L. and Zhang, X.-R. (2011). “Simulation of heat transfer and system behavior in a supercritical  $CO_2$  based thermosyphon: effect of pipe diameter.” *Journal of Heat Transfer*, 133(12), 122–505.
- Chen, L., Zhang, X.-R., Deng, B.-L. and Jiang, B. (2013d). “Effects of inclination angle and operation parameters on supercritical  $CO_2$  natural circulation loop.” *Nuclear Engineering and Design*, 265, 895–908.
- Chen, L., Zhang, X.-R. and Jiang, B. (2014). “Effects of Heater Orientations on the Natural Circulation and Heat Transfer in a Supercritical  $CO_2$  Rectangular Loop.” *Journal of Heat Transfer*, 136(5). 052501.
- Chen, L., Zhang, X.-R., Yamaguchi, H. and Liu, Z.-S. S. (2010). “Effect of heat transfer on the instabilities and transitions of supercritical  $CO_2$  flow in a natural circulation loop.” *International journal of heat and mass transfer*, 53(19-20), 4101–4111.

- Creveling, F. H., F. De Paz, J., Y. Baladi, J. and J. Schoenhals, R. (1975). “Stability characteristics of a single-phase free convection loop.” *Journal of Fluid Mechanics*, 67.
- Deng, B., Chen, L., Zhang, X. and Jin, L. (2019). “The flow transition characteristics of supercritical  $CO_2$  based closed natural circulation loop (ncl) system.” *Annals of Nuclear Energy*, 132, 134–148.
- Devia, F. and Misale, M. (2012). “Analysis of the effects of heat sink temperature on single-phase natural circulation loops behaviour.” *International journal of thermal sciences*, 59, 195–202.
- Dostal, V., Hejzlar, P. and Driscoll, M. J. (2006). “The supercritical carbon dioxide power cycle: comparison to other advanced power cycles.” *Nuclear Technology*, 154(3), 283–301.
- Duffey, R. B. and Pioro, I. L. (2005). “Experimental heat transfer of supercritical carbon dioxide flowing inside channels (survey).” *Nuclear Engineering and Design*, 235(8), 913–924.
- Fichera, A. and Pagano, A. (2003). “Modelling and control of rectangular natural circulation loops.” *International journal of heat and mass transfer*, 46(13), 2425–2444.
- Filonenko, G. (1954). “Hydraulic resistance in pipes.” *Heat exchanger design handbook*, 1, 40–44.
- Forster, F. K., Bardell, R. L., Afromowitz, M. A., Sharma, N. R. and Blanchard, A. (1995). “Design, fabrication and testing of fixed-valve micro-pumps.” *ASME-PUBLICATIONS-FED*, 234, 39–44.
- Gamble, R. E., Hinds, D. H., Hucik, S. A. and Maslak, C. E. (2006). “Esbwr... an evolutionary reactor design.” In *Proceedings of the 2006 International Congress on Advances in Nuclear Power Plants-ICAPP’06*.

- Gamboa, A. R., Morris, C. J. and Forster, F. K. (2005). “Improvements in fixed-valve micropump performance through shape optimization of valves.” *Journal of Fluids Engineering*, 127, 339–346.
- Goudarzi, N. and Talebi, S. (2015). “An approach to stability analysis and entropy generation minimization in the single-phase natural circulation loops.” *Energy*, 80, 213–226.
- Goudarzi, N. and Talebi, S. (2018). “Heat removal ability for different orientations of single-phase natural circulation loops using the entransy method.” *Annals of Nuclear Energy*, 111, 509–522.
- Greif, R. (1988). “Natural circulation loops.” *Journal of Heat Transfer*, 110(1243-1259).
- Hagen, V. T. and Stekelenburg, A. (1997). “The low-power low-pressure flow resonance in a natural circulation cooled boiling water reactor.” *Nuclear Engineering and Design*, 177(1-3), 229–238.
- Hallinan, K. P. and Viskanta, R. (1986). “Dynamics of a natural circulation loop: analysis and experiments.” *Heat Transfer Engineering*, 7(3-4), 43–52.
- Hitt, D. L., Danforth, C. M. et al. (2011). “A numerical investigation of 3-d flow regimes in a toroidal natural convection loop.” *International journal of heat and mass transfer*, 54(25-26), 5253–5261.
- Holman, J. and Boggs, J. (1960). “Heat transfer to freon 12 near the critical state in a natural-circulation loop.” *Journal of Heat Transfer*, 82(3), 221–226.
- Inampudi, S. T., Marthi, B. and Sahoo, S. (2018). “Entropy generation in water-based natural circulation loop.” *Journal of Heat Transfer*, 140(9).
- Jain, P. K. et al. (2008). “Numerical analysis of supercritical flow instabilities in a natural circulation loop.” *Nuclear Engineering and Design*, 238(8), 1947–1957.

- Jain, R. and Corradini, M. (2006). "A linear stability analysis for natural-circulation loops under supercritical conditions." *Nuclear technology*, 155(3), 312–323.
- Japikse, D. (1973). "Advances in thermosyphon technology." 9, 1–111.
- Jiang, Y. and Shoji, M. (2003). "Flow stability in a natural circulation loop: influences of wall thermal conductivity." *Nuclear Engineering and design*, 222(1), 16–28.
- Keller, J. B. (1966). "Periodic oscillations in a model of thermal convection." *Journal of Fluid Mechanics*, 26(3), 599–606.
- Kondoh, E. (2004). "Deposition of cu and ru thin films in deep nanotrenches/holes using supercritical carbon dioxide." *Japanese journal of applied physics*, 43(6S), 28–39.
- Kreitlow, D., Reistad, G., Miles, C. and Culver, G. (1978). "Thermosyphon models for downhole heat exchanger applications in shallow geothermal systems." *Journal of Heat Transfer*, 100(713-719).
- Krishnani, M. and Basu, D. N. (2017). "Computational stability appraisal of rectangular natural circulation loop: Effect of loop inclination." *Annals of Nuclear Energy*, 107, 17–30.
- Kudariyawar, J. Y., Vaidya, A. M., Maheshwari, N. K. and Satyamurthy, P. (2016). "Computational study of instabilities in a rectangular natural circulation loop using 3d cfd simulation." *International Journal of Thermal Sciences*, 101, 193–206.
- Kumar, K. K. and Gopal, M. R. (2009a). "Carbon dioxide as a secondary fluid in natural circulation loops." *Proceedings of the Institution of Mechanical Engineers, Part E: Journal of Process Mechanical Engineering*, 223(3), 189–194.
- Kumar, K. K. and Gopal, M. R. (2009b). "Steady-state analysis of  $CO_2$  based natural circulation loops with end heat exchangers." *Applied Thermal Engineering*, 29(10), 1893–1903.

- Lavine, A. S., G. R. and Humphrey, J. A. (1987). “A three-dimensional analysis of natural convection in a toroidal loop—the effect of grashof number.” *International Journal of Heat and Mass Transfer*, 30(2), 251—262.
- Liu, G., Huang, Y., Wang, J. and Leung, L. H. (2016). “Heat transfer of supercritical carbon dioxide flowing in a rectangular circulation loop.” *Applied Thermal Engineering*, 98, 39–48.
- Liu, G., Huang, Y., Wang, J., Lv, F. and Liu, S. (2017). “Experimental research and theoretical analysis of flow instability in supercritical carbon dioxide natural circulation loop.” *Applied Energy*, 205, 813–821.
- Luzzi, L., Misale, M., Devia, F., Pini, A., Cauzzi, M. T., Fanale, F. and Cammi, A. (2017). “Assessment of analytical and numerical models on experimental data for the study of single-phase natural circulation dynamics in a vertical loop.” *Chemical Engineering Science*, 162, 262–283.
- Madejski, J. and Mikielewicz, J. (1971). “Liquid fin—a new device for heat-transfer equipment.” *International Journal of Heat and Mass Transfer*, 14(3), 357–363.
- Mertol, A., Greif, R. and Zvirin, Y. (1982). “Two-dimensional study of heat transfer and fluid flow in a natural convection loop.” *Journal of Heat Transfer*, 104(3), 508–514.
- Misale, M. (2016). “Experimental study on the influence of power steps on the thermo-hydraulic behavior of a natural circulation loop.” *International Journal of Heat and Mass Transfer*, 99, 782–791.
- Misale, M., Devia, F. and Garibaldi, P. (2012). “Experiments with  $Al_2O_3$  nanofluid in a single-phase natural circulation mini-loop: Preliminary results.” *Applied Thermal Engineering*, 40, 64–70.
- Misale, M. and Froggeri, M. (2001). “Stabilization of a single-phase natural circulation loop by pressure drops.” *Experimental Thermal and Fluid Science*, 25(5), 277–282.

- Misale, M., Frogheri, M., D'Auria, F., Fontani, E. and Garcia, A. (1999). "Analysis of single-phase natural circulation experiments by system codes." *International Journal of Thermal Sciences*, 38(11), 977–983.
- Misale, M., Garibaldi, P., Tarozzi, L. and Barozzi, G. S. (2011). "Influence of thermal boundary conditions on the dynamic behaviour of a rectangular single-phase natural circulation loop." *International Journal of Heat and Fluid Flow*, 32(2), 413–423.
- Mochizuki, H. (1994). "Flow instabilities in boiling channels of pressure-tube-type reactor." *Nuclear Engineering and Design*, 149(1-3), 269–277.
- Mousavian, S. K., Misale, M., D'Auria, F. and Salehi, M. A. (2004). "Transient and stability analysis in single-phase natural circulation." *Annals of Nuclear Energy*, 31(10), 1177–1198.
- Muscato, G. and Xibilia, M. (2003). "Modeling and control of a natural circulation loop." *Journal of Process Control*, 13(3), 239–251.
- Nayak, A., Gartia, M. and Vijayan, P. (2008). "An experimental investigation of single-phase natural circulation behavior in a rectangular loop with  $Al_2O_3$  nanofluids." *Experimental thermal and fluid science*, 33(1), 184–189.
- Nayak, A., Kulkarni, P. and Vijayan, P. (2011). "Study on the transient and stability behaviour of a boiling two-phase natural circulation loop with  $Al_2O_3$  nanofluids." *Applied thermal engineering*, 31(10), 1673–1681.
- Nayak, A., Vijayan, P., Saha, D. and Raj, V. V. (1995). "Mathematical modelling of the stability characteristics of a natural circulation loop." *Mathematical and computer modelling*, 22(9), 77–87.
- Nayak, A., Vijayan, P., Saha, D., Raj, V. V. and Aritomi, M. (2000). "Analytical study of nuclear-coupled density-wave instability in a natural circulation pressure tube type boiling water reactor." *Nuclear Engineering and Design*, 195(1), 27–44.

- Nekså, P., Rekstad, H., Zakeri, G. R. and Schiefloe, P. A. (1998). “CO<sub>2</sub>-heat pump water heater: characteristics, system design and experimental results.” *International Journal of refrigeration*, 21(3), 172–179.
- Nikola, T. (1920). “Valvular conduit.” )US Patent 1,329,559.
- NIST (2013). “Standard reference database-refprop version 9.1.” *National Institute of Standards and Technology*.
- Nobakht, A., Shahsavan, M. and Paykani, A. (2013). “Numerical study of diodicity mechanism in different tesla-type microvalves.” *Journal of Applied Research and Technology*, 11(6), 876–885.
- Ong, K. (1974). “A finite-difference method to evaluate the thermal performance of a solar water heater.” *Solar Energy*, 16(3-4), 137–147.
- Pegallapati, A. S., Banoth, P. and Maddali, R. (2020). “Dynamic model of supercritical CO<sub>2</sub> based natural circulation loops with fixed charge.” *Applied Thermal Engineering*, 169, 114906.
- Peng, S., Podowski, M. and Lahey Jr, R. (1986). “Bwr linear stability analysis.” *Nuclear Engineering and Design*, 93(1), 25–37.
- Pilkhwal, D., Ambrosini, W., Forgione, N., Vijayan, P., Saha, D. and Ferreri, J. (2007). “Analysis of the unstable behaviour of a single-phase natural circulation loop with one-dimensional and computational fluid-dynamic models.” *Annals of Nuclear Energy*, 34(5), 339–355.
- Pini, A., Cammi, A. and Luzzi, L. (2016). “Analytical and numerical investigation of the heat exchange effect on the dynamic behaviour of natural circulation with internally heated fluids.” *Chemical Engineering Science*, 145, 108–125.

- Ramos, E., Sen, M. and Treviño, C. (1985). “A steady-state analysis for variable area one-and two-phase thermosyphon loops.” *International Journal of Heat and Mass Transfer*, 28(9), 1711–1719.
- Rao, N., Maiti, B. and Das, P. (2005). “Dynamic performance of a natural circulation loop with end heat exchangers under different excitations.” *International journal of heat and mass transfer*, 48(15), 3185–3196.
- Rayleigh, L. (1916). “Lix. on convection currents in a horizontal layer of fluid, when the higher temperature is on the under side.” *The London, Edinburgh, and Dublin Philosophical Magazine and Journal of Science*, 32(192), 529–546.
- Roache, P.J., G. K. W. F. (1986). “Editorial policy statement on the control of numerical accuracy.” *Journal of Fluids Engineering*, 108(3), 1–2.
- Roache, P. (1994). “Perspective: a method for uniform reporting of grid refinement studies.” *Journal of Fluids Engineering*, 116(3), 405–413.
- Rohatgi, U., Neymotin, L. and Wulff, W. (1993). “Assessment of ramona-3b methodology with oscillatory flow tests.” *Nuclear Engineering and Design*, 143(1), 69–82.
- Ruiz, D., Cammi, A. and Luzzi, L. (2015). “Dynamic stability of natural circulation loops for single phase fluids with internal heat generation.” *Chemical Engineering Science*, 126, 573–583.
- Sadhu, S., Ramgopal, M. and Bhattacharyya, S. (2018). “Experimental studies on an air-cooled natural circulation loop based on supercritical carbon dioxide–part b: Transient operation.” *Applied Thermal Engineering*, 133, 819–827.
- Saha, R., Ghosh, K., Mukhopadhyay, A. and Sen, S. (2018). “Dynamic characterization of a single phase square natural circulation loop.” *Applied Thermal Engineering*, 128, 1126–1138.



- Sahu, M. and Sarkar, J. (2019). “Steady-state energetic and exergetic performances of single-phase natural circulation loop with hybrid nanofluids.” *Journal of Heat Transfer*, 141(8).
- Samba, A., Louahlia-Gualous, H., Le Masson, S. and Nörterhäuser, D. (2013). “Two-phase thermosyphon loop for cooling outdoor telecommunication equipments.” *Applied Thermal Engineering*, 50(1), 1351–1360.
- Sarkar, M. K. S. and Basu, D. N. (2017). “Numerical comparison of thermalhydraulic aspects of supercritical carbon dioxide and subcritical water-based natural circulation loop.” *Nuclear Engineering and Technology*, 49(1), 103–112.
- Sekulicá, D. (1986). “Entropy generation in a heat exchanger.” *Heat Transfer Engineering*, 7(1-2), 83–88.
- Sharma, M., Vijayan, P., Pilkhwal, D. and Asako, Y. (2013). “Steady state and stability characteristics of natural circulation loops operating with carbon dioxide at supercritical pressures for open and closed loop boundary conditions.” *Nuclear Engineering and Design*, 265, 737–754.
- Shitzer, A., Kalmanoviz, D., Zvirin, Y. and Grossman, G. (1979). “Experiments with a flat plate solar water heating system in thermosyphonic flow.” *Solar Energy*, 22(1), 27–35.
- Sinha, R. K. and Kakodkar, A. (2006). “Design and development of the ahwr—the indian thorium fuelled innovative nuclear reactor.” *Nuclear Engineering and Design*, 236(7-8), 683–700.
- Swapnalee, B., Vijayan, P., Sharma, M. and Pilkhwal, D. (2012). “Steady state flow and static instability of supercritical natural circulation loops.” *Nuclear Engineering and Design*, 245, 99–112.

- Thippeswamy, L. and Yadav, A. K. (2020). “Heat transfer enhancement using  $CO_2$  in a natural circulation loop.” *Scientific Reports*, 10(1), 1–10.
- Thompson, S. M., Paudel, B., Jamal, T. and Walters, D. (2014). “Numerical investigation of multistaged tesla valves.” *Journal of Fluids Engineering*, 136(8).
- Torrance, K. (1979). “Open-loop thermosyphons with geological applications.” *Journal of Heat Transfer*, 101, 677–683.
- Truong, T. and Nguyen, N. (2003). “Simulation and optimization of tesla valves.” *Nanotech*, 1, 178–181.
- Vijayan, P. (2002). “Experimental observations on the general trends of the steady state and stability behaviour of single-phase natural circulation loops.” *Nuclear Engineering and Design*, 215(1-2), 139–152.
- Vijayan, P., Austregesilo, H. and Teschendorff, V. (1995). “Simulation of the unstable oscillatory behavior of single-phase natural circulation with repetitive flow reversals in a rectangular loop using the computer code athlet.” *Nuclear Engineering and Design*, 155(3), 623–641.
- Vijayan, P. and Date, A. (1992). “The limits of conditional stability for single-phase natural circulation with throughflow in a figure-of-eight loop.” *Nuclear Engineering and Design*, 136(3), 361–380.
- Vijayan, P. and Nayak, A. (2005). “Introduction to instabilities in natural circulation systems.” *Natural Circulation in Water Cooled Power Plants*, 2152–22.
- Vijayan, P. and Nayak, A. (2010). “Natural circulation systems: advantages and challenges.” *Natural Circulation in Water Cooled Power Plants*, 2152–21.
- Vijayan, P., Nayak, A., Saha, D. and Gartia, M. (2008). “Effect of loop diameter on the steady state and stability behaviour of single-phase and two-phase natural circulation loops.” *Science and Technology of Nuclear Installations*, 2008.

- Vijayan, P., Sharma, M. and Saha, D. (2007). “Steady state and stability characteristics of single-phase natural circulation in a rectangular loop with different heater and cooler orientations.” *Experimental Thermal and Fluid Science*, 31(8), 925–945.
- Vries, S., Florea, D., Homburg, F. and Frijns, A. (2017). “Design and operation of a tesla-type valve for pulsating heat pipes.” *International Journal of Heat and Mass Transfer*, 105, 1–11.
- Wang, L., Maxey, M., Burton, T. and Stock, D. (1992a). “Chaotic dynamics of particle dispersion in fluids.” *Physics of Fluids A: Fluid Dynamics*, 4(8), 1789–1804.
- Wang, Y., Singer, J. and Bau, H. H. (1992b). “Controlling chaos in a thermal convection loop.” *Journal of Fluid Mechanics*, 237, 479–498.
- Welander, P. (1967). “On the oscillatory instability of a differentially heated fluid loop.” *Journal of Fluid Mechanics*, 29(1), 17–30.
- Xiao, M., Chen, X., Zhang, M., Veziroglu, T. and Kakac, S. (1993). “A multivariable linear investigation of two-phase flow instabilities in parallel boiling channels under high pressure.” *International Journal of Multiphase Flow*, 19(1), 65–77.
- Yadav, A. K., Gopal, M. R. and Bhattacharyya, S. (2012a). “Cfd analysis of a  $CO_2$  based natural circulation loop with end heat exchangers.” *Applied Thermal Engineering*, 36, 288–295.
- Yadav, A. K., Gopal, M. R. and Bhattacharyya, S. (2012b). “ $CO_2$  based natural circulation loops: new correlations for friction and heat transfer.” *International Journal of Heat and Mass Transfer*, 55(17-18), 4621–4630.
- Yadav, A. K., Gopal, M. R. and Bhattacharyya, S. (2014). “Transient analysis of sub-critical/supercritical carbon dioxide based natural circulation loops with end heat exchangers: Numerical studies.” *International Journal of Heat and Mass Transfer*, 79, 24–33.

- Yadav, A. K., Gopal, M. R. and Bhattacharyya, S. (2016). “Effect of tilt angle on subcritical/supercritical carbon dioxide-based natural circulation loop with isothermal source and sink.” *Journal of Thermal Science and Engineering Applications*, 8(1).
- Yadav, A. K., Ramgopal, M. and Bhattacharyya, S. (2017). “Transient analysis of subcritical/supercritical carbon dioxide based natural circulation loop with end heat exchangers: experimental study.” *Heat and Mass Transfer*, 53(9), 2951–2960.
- Yamaguchi, H., Sawada, N., Suzuki, H., Ueda, H. and Zhang, X. (2010). “Preliminary study on a solar water heater using supercritical carbon dioxide as working fluid.” *Journal of Solar Energy Engineering*, 132(1).
- Yamaguchi, H., Zhang, X.-R. and Fujima, K. (2008). “Basic study on new cryogenic refrigeration using  $CO_2$  solid–gas two phase flow.” *International Journal of Refrigeration*, 31(3), 404–410.
- Yoshikawa, S., Smith Jr, R. L., Inomata, H., Matsumura, Y. and Arai, K. (2005). “Performance of a natural convection circulation system for supercritical fluids.” *The Journal of Supercritical Fluids*, 36(1), 70–80.
- Zhang, S., Winoto, S. and Low, H. (2007). “Performance simulations of tesla microfluidic valves.” In *International Conference on Integration and Commercialization of Micro and Nanosystems*, volume 42657, 15–19.
- Zhang, X.-R., Chen, L. and Yamaguchi, H. (2010). “Natural convective flow and heat transfer of supercritical  $CO_2$  in a rectangular circulation loop.” *International Journal of Heat and Mass Transfer*, 53(19-20), 4112–4122.
- Zhu, G., Yang, X. and Zhu, H. (2019). “Reduction of flow oscillation of natural circulation in non-inertial system.” *International Journal of Heat and Mass Transfer*, 139, 720–724.

Zvirin, Y. (1982). "A review of natural circulation loops in pressurized water reactors and other systems." *Nuclear Engineering and Design*, 67(2), 203–225.

Zvirin, Y. and Greif, R. (1979). "Transient behavior of natural circulation loops: two vertical branches with point heat source and sink." *International Journal of Heat and Mass Transfer*, 22(4), 499–504.

Zvirin, Y., Jeuck III, P., Sullivan, C. and Duffey, R. (1981). "Experimental and analytical investigation of a natural circulation system with parallel loops." *Journal of Heat Transfer*, 103, 645–652.



**List of Publications based on PhD Research Work**

<b>S. No.</b>	<b>Title of the paper</b>	<b>Authors</b>	<b>Name of the Journal/ Conference, Vol., No., Pages</b>	<b>Month, Year of Publication</b>	<b>Category*</b>
1.	Instability mitigation by integrating twin Tesla type valves in supercritical carbon dioxide based natural circulation loop	<b><u>Tabish Wahidi</u></b> and Ajay Kumar Yadav	Applied Thermal Engineering journal, Vol. 182, 116087. <a href="https://doi.org/10.1016/j.applthermaleng.2020.116087">https://doi.org/10.1016/j.applthermaleng.2020.116087</a> (SCI IF= 4.725)	5 January 2021	1
2.	Supercritical CO <sub>2</sub> flow instability in natural circulation loop: CFD analysis	<b><u>Tabish Wahidi,</u></b> R.A Chandavar & A. K. Yadav	Annals of Nuclear Energy, Vol. 160, 108374. <a href="https://doi.org/10.1016/j.anucene.2021.108374">https://doi.org/10.1016/j.anucene.2021.108374</a> (SCI IF= 1.378)	29 May 2021	1
3.	Stability enhancement of supercritical CO <sub>2</sub> based natural circulation loop using a modified Tesla valve	<b><u>Tabish Wahidi,</u></b> R.A Chandavar & A. K. Yadav	The Journal of Supercritical Fluids, Vol. 166, 105020 <a href="https://doi.org/10.1016/j.supflu.2020.105020">https://doi.org/10.1016/j.supflu.2020.105020</a> (SCI IF= 3.744)	01 December 2020	1
4.	Comparative computational appraisal of supercritical CO <sub>2</sub> -based natural circulation loop: effect of heat-exchanger and isothermal wall	Srivatsa Thimmaiah, <b><u>Tabish Wahidi,</u></b> A. K. Yadav & Arun M.	Journal of Thermal Analysis and Calorimetry, vol. 141, 2219–2229 <a href="https://doi.org/10.1007/s10973-020-09854-x">https://doi.org/10.1007/s10973-020-09854-x</a>  (SCI IF= 2.471)	14 September 2020	1
5.	Effect of Subcritical and Supercritical Phase on The Steady State Behavior of CO <sub>2</sub> based Natural Circulation Loop	<b><u>Tabish Wahidi,</u></b> & A. K. Yadav	International Journal of Mechanical and Production Engineering Research and Development, Trans Stellar ISSN (P): 2249–6890; ISSN (E): 2249–8001 Vol. 9, Special Issue  (Scopus)	December 2019	1
6.	Comparative Numerical Appraisal of Subcritical and Supercritical CO <sub>2</sub> based Natural Circulation Loop	<b><u>Tabish Wahidi,</u></b> & A. K. Yadav	Springer Book publication	2021	5
7.	Numerical Instability Assessment of Natural Circulation Loop Subjected to Different Heating Conditions	Srivatsa Thimmaiah, <b><u>Tabish Wahidi,</u></b> A. K. Yadav & Arun M.	Springer Book publication	2021	5

8.	CFD Study on the Steady State Behaviour of 3-D Supercritical CO <sub>2</sub> based Natural Circulation Loop	<b><u>Tabish Wahidi,</u></b> & A. K. Yadav	7 <sup>th</sup> International and 45 <sup>th</sup> National Conference on Fluid Mechanics and Fluid Power (FMFP) IIT Bombay, Mumbai, India	December 10-12, 2018.	3
9.	CFD Study on the Steady State Behaviour of 3-D Subcritical/Supercritical CO <sub>2</sub> based Natural Circulation Loop	<b><u>Tabish Wahidi,</u></b> & A. K. Yadav	International Conference on Recent Advances in Materials, Manufacturing & Energy Systems, (VRESC) Vijayawada, India	January 3-4, 2019.	3
10.	Effect of supercritical carbon dioxide based natural circulation loop for low temperature applications: CFD analysis	<b><u>Tabish Wahidi,</u></b> P. P. Nagrani & A. K. Yadav	12 <sup>th</sup> International Conference on Thermal Engineering: Theory and Applications (ICTEA 19) Gandhinagar, Gujarat, India.	February 23-26, 2019.	3
11.	Fluid Flow and Heat Transfer Characteristics of Subcritical and Supercritical CO <sub>2</sub> based Natural Convection Loop.	<b><u>Tabish Wahidi,</u></b> & A. K. Yadav	11 <sup>th</sup> International Exergy, Energy and Environment Symposium (IEEEES-11), SRM University, Chennai, India.	July 14-18, 2019.	3
12.	Heat transfer performance of CO <sub>2</sub> based NCL with and without tilting: An experimental study	Thippeswamy L. R., A. K. Yadav & <b><u>Tabish Wahidi</u></b>	11 <sup>th</sup> International Exergy, Energy and Environment Symposium (IEEEES-11), SRM University, Chennai, India.	July 14-18, 2019.	3
13.	Comparative Computational Appraisal of Supercritical CO <sub>2</sub> based Natural Circulation Loop: Effect of Heat-Exchanger and Isothermal Wall	Srivatsa Thimmaiah, <b><u>Tabish Wahidi,</u></b> A. K. Yadav & Arun M.	Proceedings of IMEC 2019 International Mechanical Engineering Congress (IMEC-2019), NIT Tiruchirappalli, India.	29th Nov-1st December 2019.	3
14.	Supercritical CO <sub>2</sub> Flow Instability in Natural Circulation Loop: CFD Analysis	<b><u>Tabish Wahidi,</u></b> & A. K. Yadav	Proceedings of 25th National and 3rd International ISHMT-ASTFE Heat and Mass Transfer Conference (IHMTTC-2019), IIT Roorkee, Roorkee, India.	December 28-31, 2019.	3
15.	Numerical assessment of transient and stability behaviour of Supercritical CO <sub>2</sub> based NCLs configured with Heat exchanger and Isothermal wall as heat sources	Srivatsa Thimmaiah, <b><u>Tabish Wahidi,</u></b> A. K. Yadav & Arun M.	2 <sup>nd</sup> International Conference on Numerical Heat Transfer and Fluid Flow (NHTFF-2020), NIT Warangal	January 17-19, 2020.	3



16.	Numerical Instability Assessment of Natural Circulation Loop Subjected to Different Heating Conditions.	Srivatsa Thimmaiah, <b><u>Tabish Wahidi</u></b> , A. K. Yadav & Arun M.	A Recent Trends in Fluid Dynamics Research (RTFDR-21), NIT Rourkela, India	April 2-4, 2021.	3
17.	Comparative Numerical Appraisal of Subcritical and Supercritical CO <sub>2</sub> based Natural Circulation Loop.	<b><u>Tabish Wahidi</u></b> , & A. K. Yadav	A Recent Trends in Fluid Dynamics Research (RTFDR-21), NIT Rourkela, India	April 2-4, 2021.	3
18.	Numerical assessment of stability behaviour in Supercritical CO <sub>2</sub> based NCLs configured with Heater, Heat exchanger and Isothermal wall as heat sources	Srivatsa Thimmaiah, <b><u>Tabish Wahidi</u></b> , A. K. Yadav & Arun M.	Journal of Thermal Engineering <b>(Accepted)</b>	2021	1

\*Category: 1: Journal paper, the full paper reviewed

2: Journal paper, Abstract reviewed

3: Conference/Symposium paper, the full paper reviewed

4: Conference/Symposium paper, abstract reviewed

5: others (Book chapter, NITK Research Bulletins, Short notes, etc.)

Tabish Wahidi

**Research Scholar**

Name & Signature, with Date

Dr. Ajay Kumar Yadav

**Research Guide**

Name & Signature, with Date

## BIODATA

**Name:** TABISH WAHIDI

**Date of Birth:** 17/08/1986

**Mobile Number:** +91-9030796649

**E-mail ID:** tabishwahidi@gmail.com



**Residential Address:** Tabish Wahidi

S/o: Sarware Islam

Vill: Wahid Nagar (Hakka)

P.O.: Baraidgah, P.S. Amour

Dist: Purnia

Bihar, 854315

**Qualification:**

Examination	Institute	University	Year	Percentage /CGPA
B.Tech. (Mechanical Engineering)	Nimra College of Engineering and Technology, Vijayawada, Andhra Pradesh	JNTU, Kakinada	2011	75.8%
M.Tech (Thermal Engineering)	Lords Institute of Engineering and Technology, Hyderabad, Telangana	JNTU, Hyderabad	2015	80.81%

**Research Interests:** Supercritical fluid, Instability analysis, CFD, Natural convection, Heat and mass transfer, Fluid mechanics.